To Monica

Friendship has arms long enough to hold and join from one end of the world to the other.

M. de Montaigne

University of Tor Vergata

Consiglio Nazionale delle Ricerche

UNIVERSITY OF ROME

"TOR VERGATA"

Dr. Alessandro Stassi

Ph.D. course in "Materials for Environment and Energy"

(XXII cycle)

Preparation and Characterization of Electrocatalysts for High Temperature Polymer Electrolyte Fuel Cells

A.A. 2008/2009

Tutor

Dr. Antonino S. Aricò

Coordinator

Prof. Silvia Licoccia

TABLE OF CONTENTS

SUMMARY

Large scale application of polymer electrolyte fuel cell (PEFC) system technology requires a reduction of its high cost as well as improvement of performance and stability. The catalysts employed for operation in the present PEFC are nanosized platinum particles supported on carbon. The reduction of the noble metal content and enhancement of catalytic stability are significant challenges for this fuel cell technology on the way to become cost competitive. High temperature PEFC operation (130°C) requires the development of catalyst with proper resistance to sintering and corrosion under working conditions.

In order to reach these goals, the aim of this Ph.D. activity was the development of practical carbon supported Pt anode and cathode catalysts with high metal surface area capable of operation at high temperature (130°C) and with suitable resistance to corrosion, Pt dissolution, thermal and electrochemical sintering. Another aspect was the development of new alloyed electrocatalysts. Our attention was focused on the development of practical carbon supported Pt-Co alloyed catalysts

The aim was focused on the achievement of a proper crystalline structure with face-centered-cubic phase and a high degree of alloying for the catalysts with small mean particle size (< 3 nm). The synthesis method was optimized to obtain a suitable dispersion of the metal particles on the support for high metal concentration catalysts (50 wt.%) with a mean particle size smaller than 3 nm for both Pt and Pt-Co alloyed electrocatalysts. Moreover, further studied were addressed to different pre-leaching methods of synthesized Pt-Co alloy catalysts supported on carbon.

To understand electrocatalysts behaviour in terms of resistance to corrosion and electrochemical sintering, different analyses were carried out before and after various accelerated degradation tests performed in a gas-fed sulfuric acid electrolyte half-cell and in a PEM single cell in a temperature range of 75 – 130°C.

1

POLYMER ELECTROLYTE MEMBRANE FUEL CELL

1.1 Introduction

Nowadays the worldwide energy demand is based widely on fossil fuels economy. It is common knowledge that fossil fuels had been leading to an increase of environmental pollution and global warming. It is also well-known that renewable energy based on solar, wind and other "green" systems could help to alleviate these problems. Unfortunately, the green sources (solar, wind, etc.) are unsteady and thus they cannot satisfy all energy demand, in particular the energy request for transportation. In this contest, fuel cell (FC) technology, in synergy with the renewable energies represents one of the potential solutions to minimize the effect of global warming and environmental pollution. Low or zero emission, low or zero noise pollution associated with a high efficiency are the main characteristics of an FC. These latter are the reason of the high appealing of this technology. In addition, the possibility to adopt FC systems to supply power and heat could make fuel cell as the technology of the next future [1-8]. Obviously, it must be reinforced by a high diffusion of so called "hydrogen economy" [9].

FCs are an important technology for a potentially wide variety of applications including micropower, auxiliary power, transportation power, stationary power for buildings and other distributed generation applications. Their potential applications may concern with a large number of industries worldwide [10]. Moreover, the possibility to use a large variety of fuels (i.e. hydrogen, methane, methanol, etc.) makes these systems highly flexible as a function of local available energy sources.

1.2 Polymer electrolyte membrane fuel cell

An FC is a device that converts chemical energy into electrical energy. It is composed of an electrolyte layer in contact with a porous anode and cathode on either side (see Fig. 1.1). There are various types of FCs that are classified in function of different electrolytes or in function of the operating temperature. For what concern polymer electrolyte membrane fuel cells (PEMFCs), hydrogen (as fuel) is fed continuously to the anode compartment (-) and oxygen/air (as oxidant) to the cathode compartment (+).

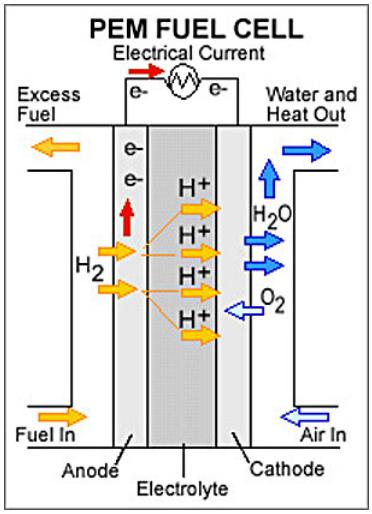

Fig. 1.1 A simple scheme of a PEMFC.

The overall reaction (see below) corresponds to the catalytic combustion of hydrogen with oxygen with a production of an electric current:

Anode reaction:	$H_2 \Rightarrow 2\ H^+ + 2\ e^-$	(1)
Cathode reaction:	$½\ O_2 + 2\ H^+ + 2\ e^- \Rightarrow H_2O$	(2)
Overall reaction:	$H_2 + ½\ O_2 \Rightarrow H_2O$	(3)

The electrons flow (electric current) from the anode electrode inside the cell up to the load and then return to the cathode electrode. To close the circuit it is necessary that positive ions flow through the electrolyte from the anode to the cathode side. The electrolyte in this FC is an proton exchange membrane (perfluorinated sulfonic acid polymer or other similar polymers). The only liquid in this FC is water; thus, corrosion problems are minimal.

Water management in the membrane is critical for efficient performance; the fuel cell must operate under conditions where the by-product water does not evaporate faster than it is produced because the membrane must be hydrated. Because of the limitation on the operating temperature imposed by the polymer, usually less than 100 °C, and because of problems with water balance, a H_2-rich gas with minimal or no CO (a poison at low temperature) is used. Porous carbon supported platinum electrocatalysts are usually required for both the anode and cathode [10]. The choice of platinum as catalyst is due to the high activity of this element towards hydrogen oxidation and oxygen reduction reactions.

1.3 Thermodynamic and performance of a PEMFC

The maximum electrical work (W_{el}) obtainable in a fuel cell operating at constant temperature and pressure is given by the change in Gibbs free energy (ΔG) of the electrochemical reaction:

$$W_{el} = \Delta G^0 = -nFE^0 \tag{1.1}$$

where n is the number of electrons participating in the reaction, F is Faraday's constant (96,487 coulombs/g-mole electron), and E^0 is the ideal potential of the cell.

The Gibbs free energy change is also given by the following state function:

$$\Delta G = \Delta H - T\Delta S \tag{1.2}$$

where ΔH is the enthalpy change and ΔS is the entropy change.

The total thermal energy available is ΔH. The available free energy is equal to the enthalpy change less the quantity TΔS which represents the unavailable energy resulting from the entropy change within the system.

For the overall cell reaction (3) if the reactants and products are gaseous the free energy change can be expressed by the equation:

$$\Delta G = \Delta G^0 + RT \ln \frac{[P_{H_2O}]}{[P_{H_2}][P_{O_2}]} \tag{1.3}$$

where P_x are the partial gasses pressure. When Equations (1.1) and (1.2) are substituted in Equation (1.3),

$$E_{rev} = E^0 + \frac{RT}{nF} \ln \frac{[P_{H_2O}]}{[P_{H_2}][P_{O_2}]} \tag{1.4}$$

which is the general form of the Nernst equation. The Nernst equation provides a relationship between the ideal standard potential (E^0) for the cell reaction and the ideal equilibrium potential (E_{rev}) at other partial pressures of reactants and products. The ideal standard potential (E^0) at 298K for a fuel cell in which H_2 and O_2 react is 1.229 V with liquid water product, or 1.180 V with gaseous water product [11]. The potential is the change in Gibbs free energy resulting from the reaction between hydrogen and oxygen.

Concerning with performance the thermal efficiency of a fuel conversion device is defined as the amount of useful energy produced relative to the change in enthalpy, ΔH, between the product and feed streams.

$$\varepsilon = \frac{Useful\ Energy}{\Delta H} \tag{1.5}$$

Conventionally, for example in the internal combustion engine (ICE) chemical (fuel) energy is first converted to heat, which is then converted to mechanical energy, which can then be converted to electrical energy. For the thermal to mechanical conversion, a heat engine is conventionally used. Carnot showed that the maximum efficiency of such an engine is limited by the ratio of the absolute temperatures at which heat is rejected and absorbed, respectively.

Fuel cells convert chemical energy directly into electrical energy. In the ideal case of an electrochemical converter, such as a fuel cell, the change in Gibbs free energy, ΔG, of the reaction is available as useful electric energy at the temperature of the conversion. The ideal efficiency of a fuel cell, operating reversibly, is then

$$\varepsilon_{ideal} = \frac{\Delta G}{\Delta H} \tag{1.6}$$

At standard conditions of 25°C (298°K) and 1 atmosphere, the thermal efficiency of an ideal fuel cell operating reversibly on pure hydrogen and oxygen at standard conditions is:

$$\varepsilon_{ideal} = \frac{237.1}{285.8} = 0.83 \tag{1.7}$$

For convenience, the efficiency of an actual fuel cell is often expressed in terms of the ratio of the operating cell voltage to the ideal cell voltage. The thermal efficiency of a hydrogen/oxygen fuel cell can then be written in terms of the actual cell voltage:

$$\varepsilon = \frac{Useful\ Energy}{\Delta H} = \frac{Useful\ Energy}{(\Delta G / 0.83)} = \frac{E_{cell} \times I}{E_{ideal} \times I} = \frac{(0.83 \times E_{cell})}{E_{ideal}} \tag{1.8}$$

Thus, the thermal efficiency of an actual fuel cell operating at a voltage of E_{cell}, based on the higher heating value of hydrogen, is given by

$$\varepsilon = 0.83 \times E_{cell} / E_{ideal} = 0.83 \times E_{cell} / 1.229 = 0.675 \times E_{cell} \tag{1.9}$$

The foregoing has assumed that the fuel is completely converted in the fuel cell, as is common in most types of heat engines. This efficiency is also referred to as the voltage efficiency. However, in fuel cells, the fuel is typically not completely converted. To arrive at the net cell efficiency, the voltage efficiency must be multiplied by the fuel utilization [10].

1.4 Effective fuel cell voltages

When a fuel cell work under real conditions the recorded voltage is less than the theoretical value reported in the equation (1.4). The difference between the ideal and real voltage is due to some overpotential (or polarization loss) which are called: activation overpotential (η_{act}), ohmic overpotential (η_{ohm}) and concentration overpotential (η_{conc}). It is possible to see clearly these overpotential in Figure 1.2 that represent a typical FC polarization curve.

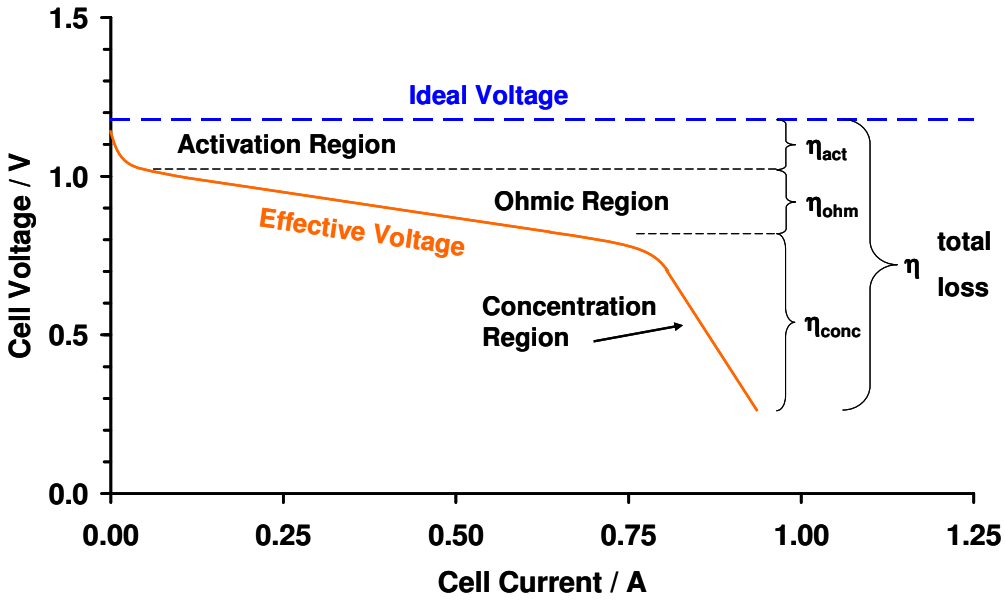

Fig. 1.2 A typical PEMFC polarization curve.

The activation overpotential is dominant at low current density. At this point, electronic barriers have to be overcome prior to current and ion flow. Activation losses show some increase as current increases. Ohmic overpotential varies directly with

current, increasing over the whole range of current because cell resistance remains essentially constant. Gas transport losses occur over the entire range of current density, but these losses become prominent at high limiting currents where it becomes difficult to provide enough reactant flow to the cell reaction sites [10].

Activation overpotential. Activation polarization is present when the rate of an electrochemical reaction at an electrode surface is controlled by sluggish electrode kinetics. In other words, this region is directly related to the rates of electrochemical reactions. Thus, reactants have to overcome an activation barrier. The η_{act} is described by the general form of the Tafel equation:

$$\eta_{act} = \frac{RT}{\alpha n F} \ln \frac{i}{i_0} \tag{1.10}$$

or

$$\eta_{act} = a + b \log i \tag{1.11}$$

where, a = (-2.3 RT/αnF) log i_0 and b = -2.3 RT/αnF.

i_0 is an important kinetic characteristic of an electron transfer process, called exchange current density.

Ohmic overpotential. The resistance to flow of ions in the electrolyte and resistance to flow of electrons through the electrode materials determine ohmic losses. The dominant ohmic losses, through the electrolyte, are reduced by decreasing the electrode separation and enhancing the ionic conductivity of the electrolyte. Because both the electrolyte and fuel cell electrodes obey to Ohm's law, the ohmic losses can be expressed by the equation:

$$\eta_{ohm} = i R \tag{1.12}$$

where i is the current flowing through the cell, and R is the total cell resistance.

Concentration overpotential. When the reaction is running the reactants react immediately on the electrodes surface (C_s=0). It is important to have a good diffusion rate of the reactants (from bulk = C_b, to surface = C_s) on the catalyst pores and, a good diffusion rate of the products from internal pores. Otherwise, a significant concentration gradient will form, whit C_s<C_b.

The reaction rate in this case will be a function of reactants/products flow from reaction sites. There is an inside and outside diffusional control. This concentration gradient causes an over potential (ΔE) that is recorded as a potential drop:

$$\eta_{conc} = \frac{RT}{nF} \ln \frac{[C_s]}{[C_b]} \tag{1.13}$$

It is well know that the current is function of the reactants concentration, then:

$$\frac{C_s}{C_b} = \left(\frac{i_l - i}{i_l} \right) \tag{1.14}$$

Upon substituting Equation (1.14) in (1.13), the concentration polarization is given by the equation

$$\eta_{conc} = \frac{RT}{nF} \ln \left(\frac{i_l - i}{i_l} \right) \tag{1.15}$$

where i_l is the limiting current that is a measure of the maximum rate at which a reactant can be supplied to an electrode, and it occurs when C_s = 0 [10].

Considering the overpotential the effective cell potential (E_{cell}) is:

$$E_{cell} = E_{rev} - \eta_{act} - \eta_{ohm} - \eta_{conc} \tag{1.16}$$

The irreversible losses in fuel cells lead to waste heat generation ($\dot{Q}$), which may be expressed by:

$$\dot{Q} = -\frac{4.18T(\Delta S)i}{nF} + i\eta_{act} + i\eta_{conc} + i^2R \qquad (1.17)$$

In this equation the first term represents the entropic loss, which cannot be overcome due to thermodynamic considerations (see section 1.3), the second and the third terms are due to activation and mass transport overpotentials, respectively, and the fourth is due to ohmic heating effects [12].

Due to the heat generation in fuel cells, it is necessary to incorporate cooling subsystem in the fuel cell system. Yet, the heat could be used to produce hot water, ambient heating or cogeneration that increase total system efficiency.

References

1. J.M..M. Amouroux, IEPE, Grenoble, France, (2003); BP Statistical Review of World Energy 2004.
2. Hydrogen report Switzerland (2008/09). Download from: http://www.empa.ch/plugin/template/empa/*/73305.
3. G. Cacciola, "Low environmental impact energy sources: fuel cells", CNR report (2000). Donload from: http://www.cnr.it/documenti/Istituzionali/Consuntivo/Report/Report2000_file/pdf/focus/focus00.pdf
4. S.H. Wu, D.B. Kotak, M.S. Fleetwood, Renew. Energy 30 (2005) 1525.
5. B.D. McNicol, D.A.J. Rand, K.R. Williams, J. Power Sources, 100 (2001) 47.
6. M.R. von Spakovsky, B. Olsommer, Energy Convers. Manag., 43 (2002) 1249.
7. B.D. Solomon, A. Banerjee, Energy Policy, 34 (2006) 781.
8. A.M. Shipley, R.N. Elliott, report n° IE041, (2004). Download from: http://www.aceee.org.
9. J. Rifkin in: "The Hydrogen Economy", Ed. Tarcher, New York, (2003).
10. Fuel Cell Handbook, 7th ed., Report prepared by EG&G Services, for the DOE, (2004).
11. P.W. Atkins, "Physical Chemistry," 3rd Edition, W.H. Freeman and Company, New York,(1986).
12. S.Srinivasan, B.B. Davè, K.A. Murugesamoorthi, A. Parthasarathy in: "Fuel Cell Systems", Ed. L.J.M.J. Blomen, M.N. Murgewa, Plenum, New York, (1993).

2

HIGH TEMPERATURE PEM FUEL CELLS FOR AUTOMOTIVE APPLICATIONS

2.1 Introduction

In the last few years, due to potential oil crises and stringent government pollution regulations, automotive companies were attracted by FC technologies for a possible replacement of ICEs with PEMFCs [1-5]. Obviously, it is necessary to solve some drawbacks to make competitive PEMFCs with respect to ICEs for automotive market [1-5]. These problems will be discussed in the following paragraphs and are summarized below:

- PEMFCs working temperature;
- lifetime of different components of membrane electrode assembly (MEA);
- cost of membrane and precious metals;
- sluggish kinetic of oxygen reduction reaction (ORR) at the cathode.

2.2 PEMFC working temperature

For automotive market application one of the main problems for PEMFCs is the working temperature. In contrast to ICE, which rejects almost half of the heat through the exhaust, a fuel cell has to reject most of the heat through the radiator (Fig. 2.1) [6,7]. Due to its operation temperature, which even for the most recent perfluorosulfonic acid based membranes is limited to a permanent operation temperature of less than 90°C, additional cooling efforts are necessary to keep the operating temperature at a reasonable temperature level.

The waste heat has to be rejected at a much lower temperature level which translates into the need for significantly larger radiators and thermal subsystems. Figure 2.2 shows that a fuel cell system radiator has to be significantly larger than a current mass production radiator at elevated ambient temperatures. This, from a fuel cell system point of view, means that the front area of a fuel cell powered car has to be changed completely ending in not very streamlined solutions. Increasing the operating temperature to ~130 °C, however, would help to reduce the size of the thermal subsystem to dimensions that are compatible with existing automotive dimensions [6,7].

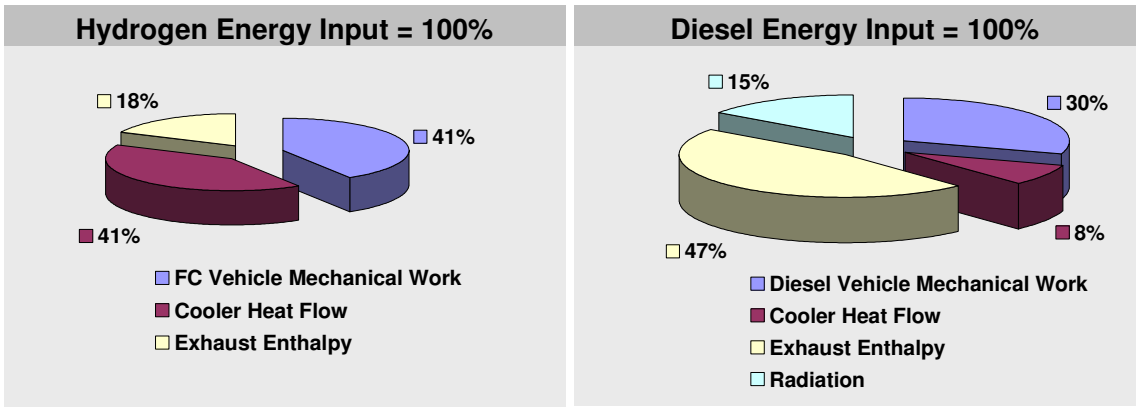

Fig. 2.1 Enthalpy flow in fuel cell systems and ICEs for representative load.

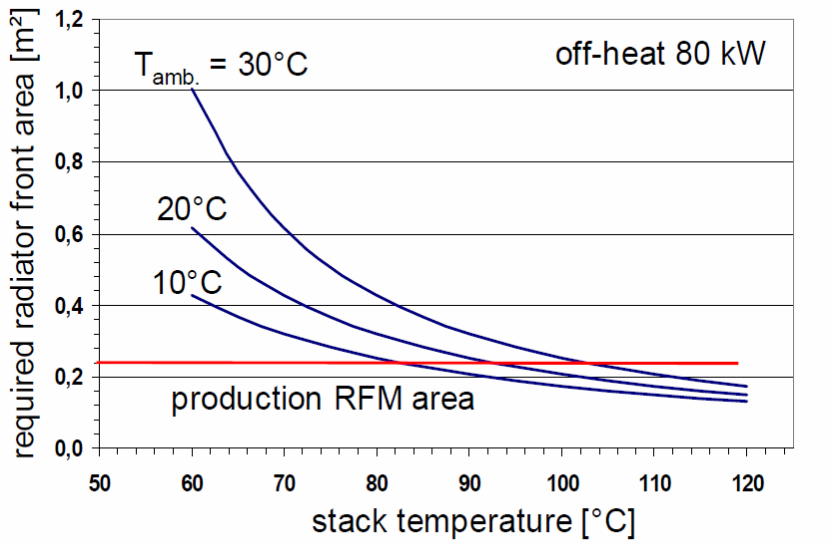

Fig. 2.2 Radiator size requirements vs. stack temperature and ambient conditions.

Moreover, for stationary purpose, the heat produced by a PEMFC at higher temperature (i.e. 130 °C) could be used to produce hot water, ambient heating or cogeneration that increase total system efficiency.

2.3 Lifetime of different components of membrane electrode assembly

Another problem regarding a possible replacement of ICEs with PEMFCs is the membrane electrode assembly (MEA) lifetime. For example the Department of Energy (DOE) considered as a target for 2010 an FC lifetime of 5.000 h and 40.000 h for automotive and stationary application, respectively [8-10].

The MEA is the heart of a FC (Fig. 2.3). One of the most used configurations consists of a macroporous layer, which is a carbon cloth or paper; this is the conductive support onto which the microporous gas diffusion layer and, thereafter, the catalytic layer are deposited. In most electrode configurations, the gas diffusion layer is formed by polytetrafluoroetylene (PTFE) and carbon black, whereas the composite catalytic layer consists of carbon supported Pt or Pt alloy catalysts and Nafion ionomer. The membrane is placed between the two electrodes and then all components are pressed together at high temperature and pressure.

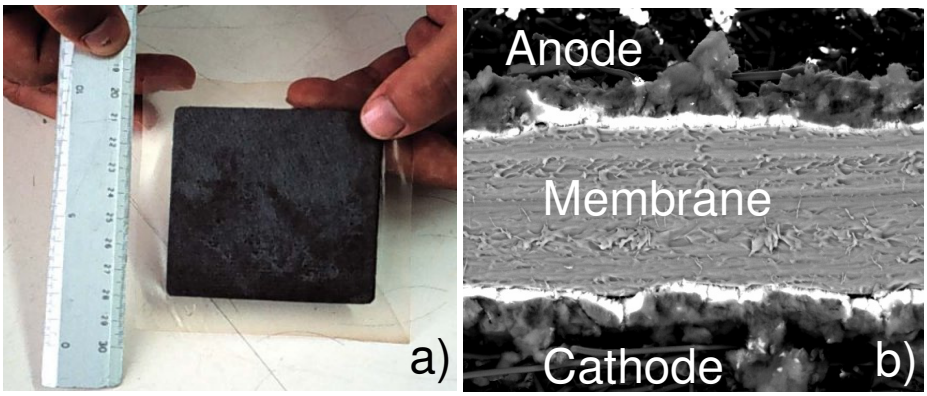

Fig. 2.3 a) The heart of an FC, MEA; b) SEM micrograph section of a MEA.

The degradation of MEA is due to different factors [10-12]. They could be resumed as follow:

- membrane degradation;
- electrocatalyst degradation;
- support degradation.

The degradation of each MEA component frequently has a high influence towards the degradation of other components. For example, the dissolution of platinum from electrocatalyst often lead to a poisoning of the membrane due to a diffusion of platinum particles into the membrane.

Membrane degradation. Perfluorosulfonic acid (PFSA) membranes, in particular Nafion, have been the material of choice and the technology standard in PEMFC for many years. They have excellent proton conduction and chemical stability when operated in a water-swollen state. However, such perfluorosulfonic acid membranes have several critical limitations: proton conductivity of standard Nafion at 30 % of relative humidity (R.H.) is less than 10 % of the value at 80 % R.H. (see Fig. 2.4) [13]. This means that in order to ensure high performance of a fuel cell, large amounts of water have to be provided and handled by a complex water-management subsystem. Although the mechanical and thermal stability of the commercial perfluorsulfonic acid based membranes has considerably improved during the last years [14-17] . From a fuel cell system point of view the dependence on a constant level of humidification of the feed gases is still a permanent cause of instability and a main reason for the reduced long term stability of the existing PEM fuel cell stacks in field tests at automotive companies all over the world. The considerable volume shrinking of the membranes (thickness and area) which is observed once the membranes are dried locally can cause high mechanical stresses and an irreversible rupture of the membrane and the membrane electrode interface, causing failure of the whole fuel cell stack [18].

Moreover, PFSA-based membranes lose mechanical strength at temperatures above 80 °C particularly under the plasticizing influence of water on the polymer, thereby seriously reducing the durability of the membrane and the fuel cell far below the automotive industries target of approximately 5000 h fuel cell operation within 10 years

of vehicle operation. This is similarly true for the chemical degradation of the polymer, e.g. by peroxyl-radical attack. However, mechanical as well as chemical failure mechanisms are still poorly understood and in consequence also require investigation.

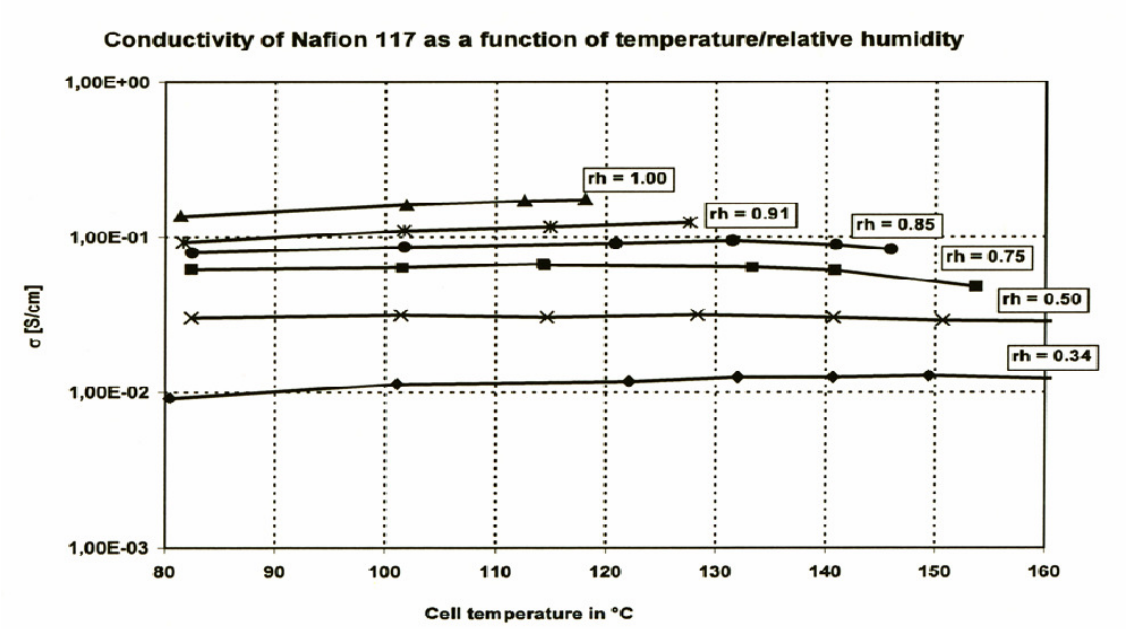

Fig. 2.4 Conductivity dependence of Nafion on relative humidity.

Electrocatalyst degradation. The main drawback that affects these electrocatalysts is their durability. This latter is one of the main objectives that are necessary to solve in the next future for a real introduction of PEMFCs into the market [19]. The relative short life of electrocatalysts is mainly due to the corrosive environment where these MEA components must operate. In the cathode side (O_2 feed) the catalysts work under strong oxidizing conditions, whereas in the anode side hydrogen fed creates strong reducing ambient. The high temperature (> 70 °C), the presence of water and a very low pH contribute to increase the corrosive conditions. In addition, to obtain high efficiency (see eq. 1.9) it is necessary that cathode electrodes are working at a potential above 0.6 V. Finally, especially for automotive applications, PEMFCs are exposed to a high number of start-up and shut-down cycles [19-22].

In PEMFCs, as well as in direct alcohol fuel cells (DAFCs), electrodes are commonly based on carbon-supported Pt (Pt/C) and Pt-alloy (Pt-M/C, with M = Ru, Co, Fe, Cu and etc.) electrocatalysts with nanometric dimensions [23-30]. Update, researchers have developed various types of non noble metal based electrocatalysts

[31], but Pt and its alloys remain the most active ones towards oxygen reduction and hydrogen oxidation. These reactions occur on electrochemical active Pt sites. Accordingly, higher is the number of the Pt active sites, also considered as the electrochemical surface area (ECSA), higher is the overall cell performance [21,22]. This justifies the necessity to develop electrocatalysts with a nanoscale dimension. On the other hand, nanometric particles increase the electrocatalyst degradation effects.

Catalysts performance losses are principally caused by sintering, corrosion and dissolution of metal particles. These drawbacks are boosted in stressing environment as above described. The sintering process consists in an agglomeration of the metal particles. The growth of particles, in the case of PEM electrocatalysts, could be due to different mechanisms, such as Ostwald ripening (metal dissolution and reprecipitation) and surface migration [22]. The mentioned mechanism can participate singly or simultaneously depending on PEMFC operating conditions. Cathode potential above 0.6 V caused a Pt surface oxidation that can lead to a successive Pt dissolution or metal surface corrosion. Then, Pt particles could migrate in water, membrane or reprecipitate on the support, but in sites that are not electrochemical active. Moreover, Pt particles could reprecipitate over other Pt particles leading to a growth of these latter (sintering).

Another aspect regard the poison of active Pt sites due to the presence of carbon monoxide. Carbon monoxide is a by-product present in the H_2 stream if this latter derived for example from the reforming process. The CO molecules are strongly adsorbed onto the Pt surface and lead to a significantly loss of ECSA [32] (see also section 2.5).

One of the main problems that regards carbon supported Pt-M alloy catalysts is the leaching of alloyed metals from the surface of the particles. This is due to the fact that most of Pt alloyed metals are thermodynamically unstable under PEMFC conditions. Pourbaix diagrams indicate that most of the metals used such as Co, Cu, Fe, Ni, etc. are soluble at a potential between 0.3 and 1 V versus standard hydrogen electrode (SHE) and at low pH values [33]. The corrosion of alloyed metals generally leads to a increase of ohmic resistance and in addition gives rise to a poisoning of membrane or ionomer.

Support degradation. In PEMFCs, the main function of the support is to increase the ECSA and reduce the load of the active phase (Pt particles) to get low the cost of the catalyst. As a consequence, support needs to be a good electric conductor with high surface area to maximize Pt particles dispersion and an appropriate pores distribution and dimension to minimize the mass transport constraints. Due to their characteristics, carbon-blacks are the most common used supports for this purpose. Update, a high variety of carbon-blacks was studied and developed but Vulcan XC-72 results the most widely used carbon support employed in the synthesis of the electrocatalysts for PEM applications. In fact, it is the best support for Pt catalyst because of its suitable compromise about the characteristics above mentioned [34,35].

Similarly to what happens for Pt particles, the main problem for Vulcan and other carbon supports is the surface oxidation that occurs under PEM working condition. Therefore, high temperature, water content, low pH and, especially for the cathode side, high potential contributed to the oxidation of the carbon surface, yielding the following reactions [12]:

$$C + 2\,H_2O \Rightarrow CO_2 + 4\,H^+ + 4\,e^- \quad (4)$$

$$C + H_2O \Rightarrow CO + 2\,H^+ + 2\,e^- \quad (5)$$

$$CO + H_2O \Rightarrow CO_2 + 2\,H^+ + 2\,e^- \quad (6)$$

where reaction (4) can happen directly or by (5) and (6) reaction steps.

Carbon corrosion could give rise to: a modification of carbon morphology (surface and pores); a loss of carbon; a decrease in terms of performance due to an increase of the mass transport constraints and decrease of carbon conductivity [10].

In addition, the carbon oxidation could lead to a loss of metal particles anchored onto the surface or to a poison of the active Pt sites that can occur due to the production of carbon monoxide (see reaction 5). Moreover, as clearly reported by Siroma et al. [36], the presence of platinum onto the carbon surface increases significantly the degradation of this latter.

2.4 Cost of membrane and precious metals

As European Commission reported in Strategic Research Agenda (2005) [8] the short-term target cost (2015) for a FC propulsion system for transport application is down to 100 €/kW whereas, today, the cost of a 1 kW FC system is about 6.000 €/kW. Moreover, cost analysis carried out by TIAX for DOE in the 2008 Annual Progress Report [37] for a hypothetical large scale FCs (500.000 units) production conclude that the stack FC cost is around to 54% with respect to the total system cost (see fig. 2.5.a). Futhermore, as reported by TIAX in a previous analysis [37] with respect to the total stack price the cost of electrocatalysts (anode and cathode) and membrane is about 31% and 22%, respectively (see fig. 2.5.b).

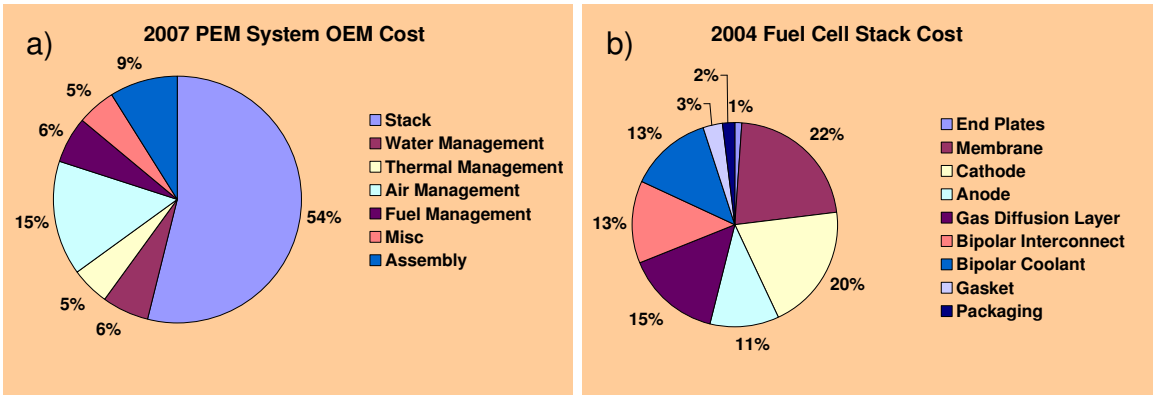

Fig. 2.5 a) 2007 FC system cost analysis (TIAX); b) 2004 FC stack cost analysis (TIAX).

So it is evident that the MEA cost reduction within its durability are the major challenges to FC commercialization. Different work were addressed to minimize the cost of membrane or electrocatalysts and to increase both durability and performance [19].

As discussed before, if on one hand the request to operate at higher temperature and low humidification simplified the system, on the other hand these conditions are heavy critical for membrane lifetime. Different type of solid polymer electrolyte such as: perfluorinated, partially fluorinated; non-fluorinated membranes with aromatic

backbone; non-fluorinated hydrocarbons and acid-base blend [16,17]. They were developed with the aim to increase stability, performance and try to reduce production cost for high temperature applications [16,17]. Unfortunately, in spite of many efforts addressed to this problem no significant improvement are achieved up today. So, it is evident that many research must be addressed to this target.

With regard to electrocatalysts many researcher are in agreement that the only way to reduce the cost of catalysts is to decrease noticeably the Pt metal content [19]. Nowadays, different research team have been working on electrocatalysts with no noble metal content but, in spite of everything Pt remain the most active metal for both anode and cathode reactions. Other research team try to develop Pt supported catalysts with higher activity able to generate a power density of 1 W/cm^2 with a total metal loading smaller than 0.2 mg/cm^2. This represent the target for reasonable electrocatalysts cost that can make competitive PEMFCs towards of the ICEs [19].

2.5 Sluggish kinetic of oxygen reduction reaction at the cathode

In the overall PEM reaction (see reaction 3) the rate determining step (RDS) is the ORR (see reaction 2). In fact, in the cathode side the activation overpotential losses are higher than in the anode side where the hydrogen oxidation on Pt is very fast [12]. These losses are mainly due to the slow ORR kinetic. To improve significantly the ORR it was demonstrate that it is necessary to increase the operating temperature at least up to 130 °C [19]. Moreover, on the anode side, the adsorption of CO on the Pt sites decrease proportionally with the increase of temperature. In fact, the CO tolerance pass from 10-20 ppm at 80 °C up to 1000 ppm at 130 °C [32]. Afterwards, another goal to rise a marketable of PEMFCs is to enhance the ORR kinetic.

To reach this aim, for PEMFCs and DAFCs applications, in the last years several papers address to the development of binary Pt-alloys with numerous metals [23-30]. In fact, results show more active and less expensive Pt-alloy for oxygen reduction reaction (ORR) catalysts with better stability than pure Pt based catalysts. Unfortunately, as said before the main

problem that afflict these catalysts is the leaching of the alloyed metal that lead to an increase of the membrane degradation [19].

2.6 Electrocatalyst development for high temperature PEM fuel cell

As discussed before high temperature PEMFC operation (130 °C) requires the development of catalysts with proper resistance to sintering and corrosion under working conditions. This represent the aim of this Ph.D study.

It is general opinion that corrosion resistant catalyst supports need to be selected for high temperature operation as well as proper anchoring of the metal phase on the support is necessary to improve stability [38-41]. Yet, no systematic study has been carried out to investigate the degradation properties of conventional fuel cell catalysts in PEM fuel cells under high temperature operation (e.g. 130 °C). This is mainly due to the scarce availability of polymer electrolyte membranes that can operate under such conditions. Since a wide number of research groups is actively involved to search for high temperature solid polymer electrolytes [42-46], it appears appropriate to analyse the catalysts behaviour under conditions similar to the target application for electrotraction [19]. Some information can be derived from corrosion studies carried out in phosphoric acid fuel cells using similar catalysts [47]. This is appropriate to evaluate the catalysts stability for phosphoric acid doped polybenzoimidazole (PBI) fuel cell [4]; but, it seems less useful for classical PEMFCs based on perfluorosulfonic membranes being the reaction environment quite different in these two fuel cell technologies.

The scope of this work was try to develop electrocatalysts suitable for automotive application and to evaluate the high temperature performance and stability of the catalysts. Electrochemical studies were carried out in both liquid electrolyte (sulphuric acid) gas-fed half cell and in single cell PEM configuration. The tests were performed to correlate catalysts performance and stability with the physico-chemical

characteristics both in terms of electrocatalytic activity for oxygen reduction and resistance to degradation under high temperature conditions.

References

1. S. Srinivasan, R.Dillon, L. Krishnan, A. S. Aricò, V. Antonucci, A.B. Bocarsly, W.J. Lee, K.L. Hsueh, C.C. Lai, A. Peng, Proceedings of the Fuel Cell Science, Engineering and Technology, Rochester, (2003) 529.
2. J. Zhang, S. Holdcroft et al., J. Power Sources, 160 (2006) 872.
3. Y. Shao, G. Yin, Z. Wang, Y. Gao, J. Power Sources, 167 (2007) 235.
4. Q. Li, R. He, J.O. Jensen, N.J. Bjerrum, Chem. Mater.**,** 15 (2003) 4896.
5. B.D. McNicola, D.A.J. Randb, K.R. Williams, J. Power Sources, 100 (2001) 47.
6. D.A. Masten, A.D. Bosco. in: Wolf Vielstich, Hubert, A. Gasteiger, Arnold Lamm (Eds.), Handbook of Fuel Cells-Fundamentals, Technology and Applications: Fuel Cell technology and Application, vol. 4, John Wiley and Sons, Ltd., (2003).
7. R.K. Ahluwalia, X. Wang, J. Power Sources, 177 (2008) 167.
8. EU (JTI) Strategic Research Agenda 2005 from: http://ec.europa.eu
9. U.S. DOE, http://www1.eere.energy.gov/hydrogenandfuelcells/mypp/, 2007.
10. R.Borup et al., Chem. Rev., 107 (2007) 3904.
11. J. Wu, X.Z. Yuan, J.J. Martin, H. Wang, J. Zhang, J. Shen, S. Wu,W. Merida, J. Power Sources, 184 (2008) 104.
12. F.A. de Bruijn, V.A.T. Dam, G.J.M. Janssen, Fuel Cells, 08 (1) (2008) 3.
13. G. Alberti, M. Casciola, Solid State Ionics, 145 (2001) 3.
14. C. Yang, P. Costamagna, S. Srinivasan, J. Benziger, A.B. Bocarsly, J. Power Sources 103 (2001) 1.
15. S. Licoccia, E. Traversa, J. Power Sources 159 (2006) 12.
16. D. Jones, Fuel Cells, 5 (2) (2005) 169.
17. D. Jones, Fuel Cells, 5 (3) (2005) 315.
18. Collier, H. Wang, X.Z. Yuan, J. Zhang, D.P. Wilkinson, Int. J. Hydrogen Energy 31 (2006) 1838.
19. H.A. Gasteiger, S.S. Kocha, B. Sompalli, F.T. Wagner, Appl. Catal. B: Environ. 2005, 56, 9.
20. S. Zhang, X. Yuan, H. Wang, W. Merida, H. Zhu, J. Shen, S. Wu, J. Zhang, Int. J. Hydrogen Energy, 34 (2009) 388.
21. Y. Shao, G. Yin, Z. Wang, Y. Gao, J. Power Sources, 167 (2007) 235.
22. Y. Shao, G. Yin, Y. Gao, J. Power Sources, 171 (2007) 558.
23. D.A. Landsman, F.J. Luczak, in: W. Vielstich, A. Lamm, H. Gasteiger (Eds.), Handbook of Fuel Cells-Fundamentals, Technology and Applications, vol. 3, Wiley, Chichester, UK, 2003 (Chapter 65).
24. S. Mukerjee, S. Srinivasan, J. Electroanal. Chem., 357 (1993) 201.
25. P. Yu, M. Pemberton, P. Plasse, J. Power Sources, 144 (2005) 11.
26. A. Stassi, C. D'Urso, V. Baglio, A. Di Blasi, V. Antonucci, A.S. Aricò, A.M. Castro Luna, A. Bonesi, W.E. Triaca, J. Appl. Electroch., 36 (2006) 1143.
27. S.Song, Y. Wang, P. Tsiakaras, P.K. Shen, Appl. Catal., B Environ., 78 (2008) 381.
28. L. Xiong and A. Manthiram, J. Electrochem. Soc., 152 (2005) A697.
29. H. Uchida, H. Ozuka and M. Watanabe, Electrochim. Acta, 47 (2002) 3629.
30. T. Toda, H. Igarashi and M. Watanabe, J. Electroanal. Chem., 460 (1999) 258.
31. B. Wang, J. Power Sources 152 (2005) 1.

32. X. Gang, L. Qingfeng, H.A. Hjuler, N.J. Bjerrum, J. Electrochem. Soc., 142 (9) (1995) 2890.
33. M. Pourbaix, Altas of Electrochemical Equilibrium in Aqueous Solutions, Pergamon Press, New York, 1966.
34. Y. Shao, G. Yin, J. Zhang, Y. Gao, Electrochim. Acta, 51 (2006) 5853.
35. K. Wikander, H. Ekström, A.E.C. Palmqvist, A. Lundblad, K. Holmberg, G. Lindbergh, Fuel Cells, 6 (2006) 21–25.
36. Z. Siroma, K. Ishii, K. Yasuda, Y. Miyazaki, M. Inaba, A. Tasaka, Electroch. Commun. 7 (2005) 1153.
37. Documents download from: http://www.hydrogen.energy.gov.
38. T. Tada, in:W. Vielstich, A. Lamm, H. Gasteiger (Eds.), Handbook of Fuel Cells—Fundamentals, Technology and Applications, vol. 3, Wiley, 2003.
39. R. Atanasoski, Proceedings of the 4th International Conference on Applications of Conducting Polymers, ICCP-4, Como, Italy, February 18–20, (2004).
40. J. Scholta, N. Berg, P. Wilde, L. J¨orissen, J. Garche, J. Power Sources, 127 (2004) 206.
41. A.S. Aricò, P.L. Antonucci, V. Antonucci, in: A. Wieckowski, E.R. Savinova, C.G. Vayenas (Eds.), Catalysis and Electrocatalysis at Nanoparticle Surfaces, Marcel Dekker, Inc., New York, 2003.
42. G. Alberti, M. Casciola, Annu. Rev. Mater. Res., 33 (2003) 129.
43. A.S. Aricò, V. Baglio, A. Di Blasi, P. Cretì, P.L. Antonucci, V. Antonucci, Solid State Ionics, 161 (2003) 251.
44. K.D. Kreuer, Solid State Ionics, 97 (1997) 1.
45. S. Reichman, T. Duvdevani, A. Aharon, M. Philosoph, D. Golodnitsky, E. Peled, J. Power Sources, 153 (2006) 228.
46. O. Savadogo, J. New Mater. Electrochem. Syst., 1 (1998) 47.
47. N. Giordano, P.L. Antonucci, E. Passalacqua, L. Pino, A.S. Aricò, K. Kinoshita, Electrochim. Acta, 36 (1991) 1931.

3

EXPERIMENTAL AND METHODS

3.1 Introduction

The different catalysts, electrodes and MEA developed during this thesis have been characterized by different techniques. The structural and morphological characterization and electrochemical methods used during this thesis in order to study the electrocatalysts and MEA behaviour will be discusses in this chapter. The physical-chemical analysis were carried out by the following techniques:

- X-Ray Diffraction (XRD);
- X-Ray Fluorescence (XRF);
- Transmission Electron Microscopy (TEM);
- Scanning Electron Microscopy (SEM);
- Thermal Gravimetric Analysis (TGA);
- Elementary analysis (CHNS-O).

Whereas, electrochemical characterization was carried out adopting a gas-fed half cell and a single cell configurations connected with different instruments and test stations that will be described in the next paragraphs.

3.2 Physical-chemical analysis

All physical-chemical characterization were carried out on catalysts, electrodes and MEA (before and after electrochemical experiments) by ex situ methodology.

XRD for powder catalysts and electrodes were recorded with a Philips X'Pert X-Ray diffractometer (see Fig. 3.1 b) using a Cu-Kα source operating at 40 kV and 30 mA. The two-theta scale was calibrated by using a standard silicon reference (Panalytical). The catalyst powders and the catalyst layers scratched from the electrodes after the electrochemical tests were deposited on a silicon support. A thin-film analysis methods was used. The peak profiles of the (2 2 0) reflection for the face-centred-cubic (fcc) structure of Pt and Pt–Co phase were obtained by applying the Marquardt algorithm [1]. The crystallographic parameters have been calculated from 220 peak by the formula [2,3]:

$$A_{220} = \frac{\sqrt{2} \cdot \lambda_{K\alpha 1}}{\sin \theta_{max}} \tag{3.1}$$

where A_{220} is the lattice dimension of the fcc structure, λ is the wavelength of the Cu X-ray source, θmax is the Bragg angle. The percentage of Pt in the Pt/Co atomic ratio for the alloy was determined by using the Vegard's law according to the follow empirical relationship:

$$X_{Pt} = \frac{A_{220} - A_{fccCo}}{A_{fccPt} - A_{fccCo}} \tag{3.2}$$

where X_{Pt} is the atomic fraction of platinum in the Pt–Co alloy.

The mean particle size (L) was determined by the Debye-Sherrer equation 3.3:

$$L = \frac{0.9 \cdot \lambda_{K\alpha 1}}{B_{2\theta} \cdot \cos \theta_{max}} \tag{3.3}$$

where B is the true particle size broadening as determined from the 220 reflection full width at half maximum corrected by the instrumental broadening (standard Pt sample) [2]:

$$B_{2\theta} = \sqrt{B_{2\theta measured} - B_{2\theta instrument}} \tag{3.4}$$

XRF analysis of the catalysts was carried out to confirm the Pt/Co atomic ratio for the alloy electrocatalysts and to verify the absence of pollutants. The analysis were conducted by a Bruker AXS S4 Explorer spectrometer (see Fig. 3.2 a-b) operating at a power of 1 kW and equipped with a Rh X-ray source, a LiF 220 crystal analyzer and a 0.12° divergence collimator. Transmission electron-micrographs for the catalyst samples were obtained using a Philips CM12 transmission electron microscope (see Fig. 3.3 a-b) with spatial resolution of 0.2 nm. To obtain the electron micrographs the catalyst samples were finely grinded and ultrasonically dispersed in isopropyl alcohol. A drop of the resultant dispersion was deposited and dried on to a standard copper-grid coated with carbon. SEM-EDX analyses of electrode-polymer membrane electrolyte interface were carried out by a FEI XL-30 FEG instrument. The total metal content in the catalysts was determined by thermal gravimetric analysis up to 950 °C in air by using an STA TGA-DSC NETZSCH 409C instrument. Quantitative analysis of light elements was carried out with Carlo Erba CHNS-O instrument. Some of the instrument used for the physical-chemical investigations are reported in Figures 3.1-3.3. The figures also reported drawing that explain their working mechanism.

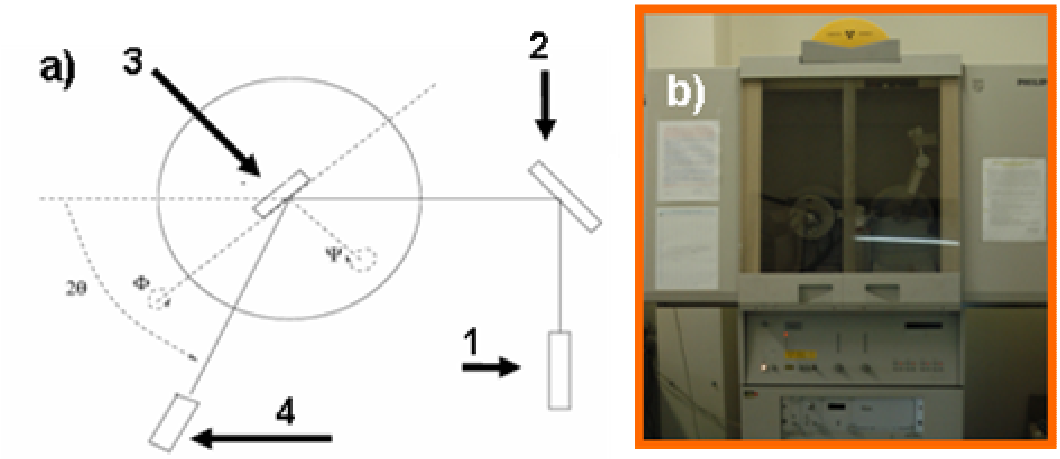

Fig. 3.1 a-b X-ray diffractometer. a) analyser system: 1. X-ray source; 2. monocromator; 3. sample; 4. detector; b) Philips X'Pert X-Ray diffractometer.

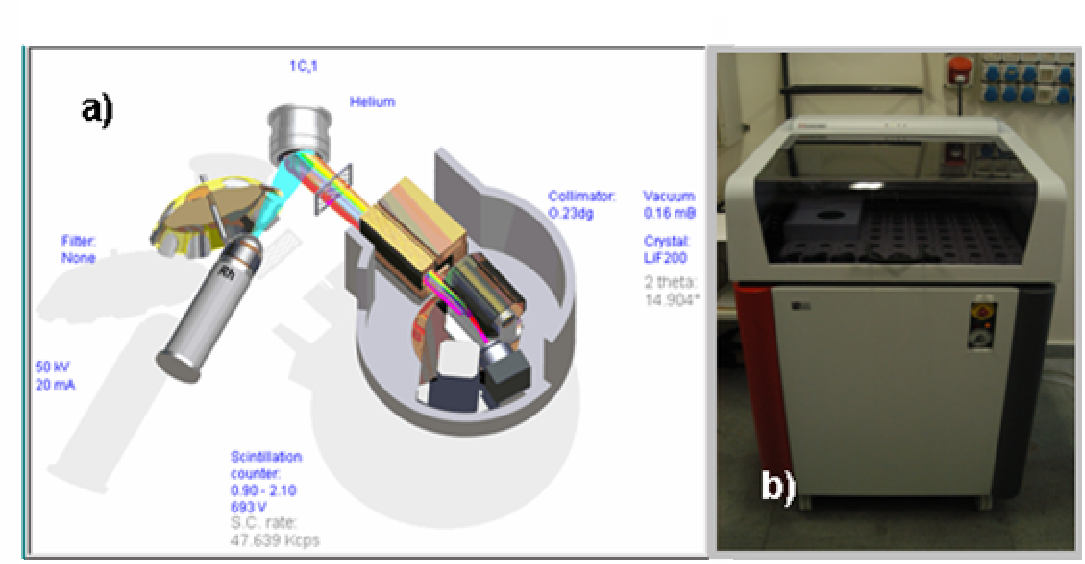

Fig. 3.2 a-b X-ray fluorescence. a) analyser system; b) Bruker AXS S4 Explorer.

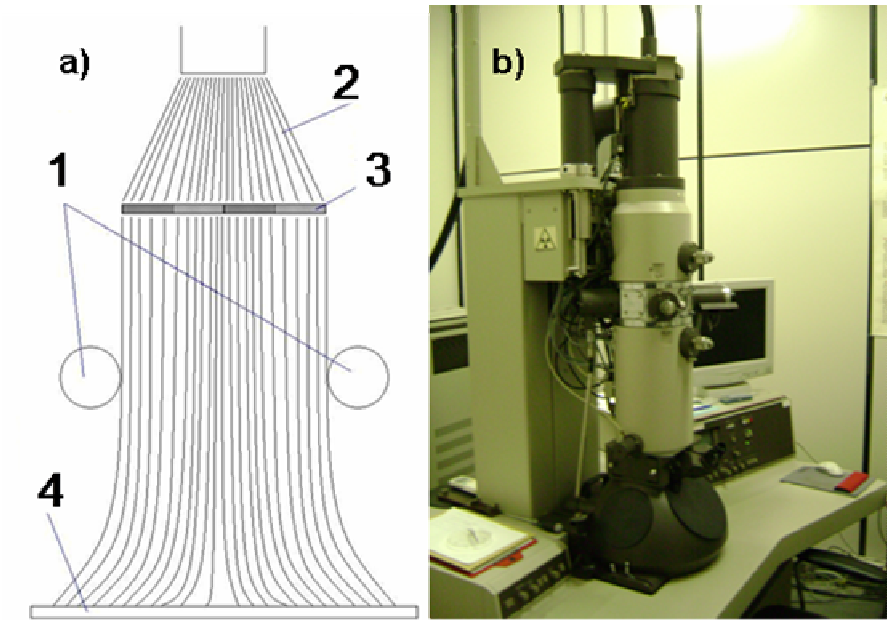

Fig. 3.3 a-b Transmission Electron Microscope. a) analyser system: 1. magnetic field; 2. electron beam; 3. sample; 4. detector; b) Philips CM12.

3.3 Electrochemical characterization

Electrodes and MEAs were prepared by as reported in Ref. [4]. Electrochemical studies were carried out in both liquid electrolyte (sulphuric acid) gas-fed half cell and in PEMFC. Half cell studies served for preliminary evaluation and screening of catalysts; whereas, PEM studies at high temperature were carried out to analyze the MEA behaviour under real high temperature conditions. For operation in sulphuric acid-based half cell (see Fig. 3.4) and PEM single cell (see Figs. 3.5-3.6), hydrophobic backing layer and hydrophilic backing layers were used, respectively. This procedure was adopted to reduce the flooding effects in liquid electrolyte half cell and to enhance humidification at 130 °C in a PEMFC. The catalytic layer for all electrodes was prepared as for a standard PEMFC, i.e. 33 wt.% Nafion ionomer, 67 wt.% catalyst with Pt loading of 0.3 mg cm^{-2}.

An evaluation of catalyst stability was first carried out in a conventional thermostated three-electrode cell consisting of the gas-diffusion electrode to be tested (working electrode), a platinum grid (counter electrode) and a reference electrode (Hg/Hg_2SO_4 sat.). A gas was fed to the electrode backing layer during the experiments. The electrode area exposed to the liquid electrolyte was 0.5 cm^2. The half cell was connected to an AUTOLAB Metrohm Potentiostat/Galvanostat equipped with FRA for AC-impedance spectroscopy and electrochemical diagnostics.

Fig. 3.4 Gas-fed half cell; a) system; b) zoom of working electrode.

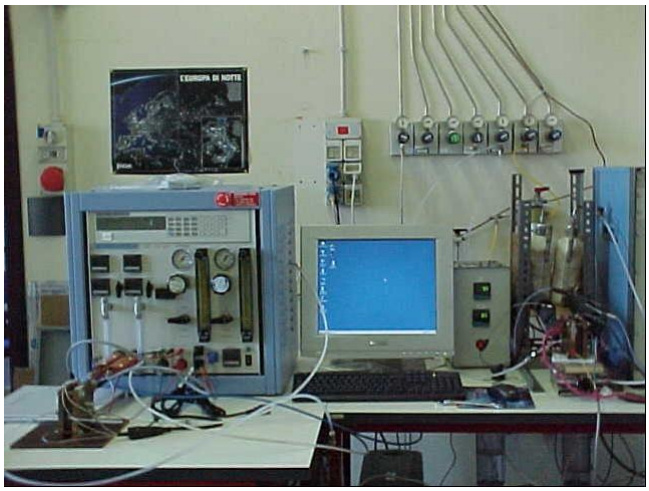

Fig. 3.5 Single cell test station.

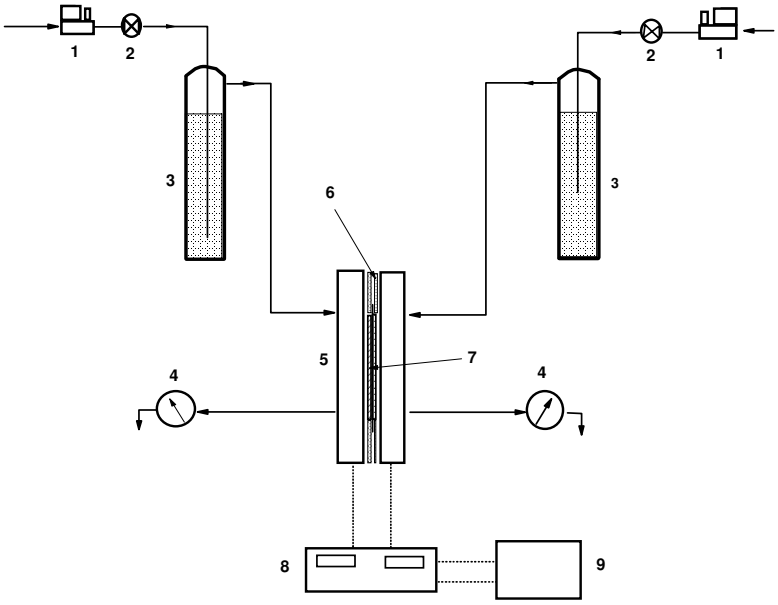

Fig. 3.6 Single cell test station layout:

1) mass flow controller;
2) shut off valve;
3) humidification bottle;
4) back-pressure regulator;
5) fuel cell;
6) gasket;
7) MEA;
8) electronic load;
9) data acquisition.

Membrane-electrode assemblies were formed by a hot-pressing procedure and subsequently installed in a fuel cell test fixture. This latter was connected to a fuel cell test station including an HP6060B electronic load and an AUTOLAB Metrohm Potentiostat/Galvanostat equipped with FRA and a 20A current booster for AC-impedance spectroscopy and electrochemical diagnostics. The gases were humidified at the same temperature of the cell i.e. 130 °C by pressurizing and heating all the pipeline from mass flow controllers to the cell (see Fig. 3.6) The humidifiers temperature were

the same of cell temperature in all experiments. The cell temperature was measured by a thermocouple embedded in the cathodic graphite plate, close to the MEA. The single cell consists in copper plates interconnected with the test station instruments, 5 cm^2 graphite flow fields, Teflon mask gaskets and MEA (see Fig. 3.7 a-b).

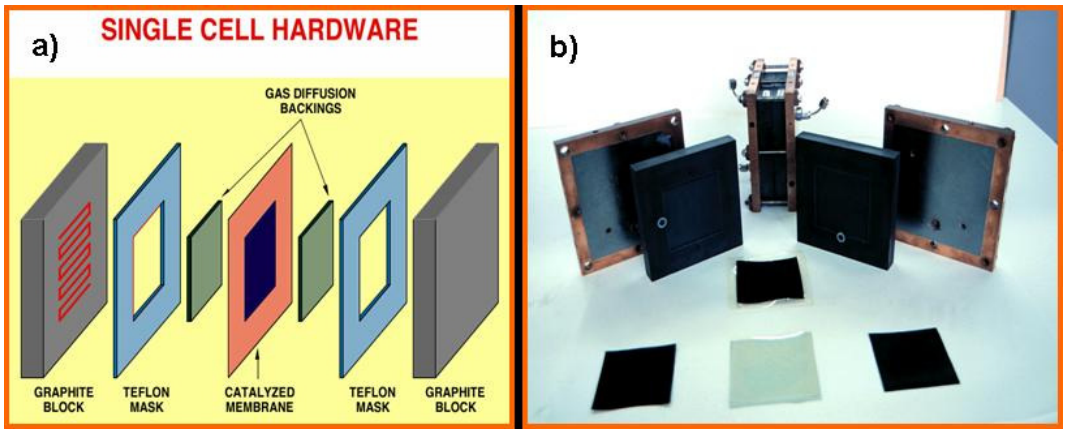

Fig. 3.7 a) Single cell explosed view; b) Single cell components.

Electrochemical studies in PEMFC were performed (polarization curves, AC-impedance) in a H_2-air and H_2-oxygen 5 cm^2 single cell at different temperature (80 – 130 °C), pressure (1 and 3 bar abs.) and a R.H. of 100%. The oxygen and hydrogen flow rates were fixed at 2 and 1.5 times, respectively, the value stoichiometry corresponding to 1 A cm^{-2}. The Pt loading was 0.3 mg cm^{-2}. Single cell performances were investigated by steady-state galvanostatic measurements. For CV studies at 80 °C under PEMFC configuration, hydrogen (1 bar. abs.) was fed to the anode that operated as both counter and reference electrode, whereas, nitrogen was fed to the working electrode. The sweep rate was 20 mV s^{-1}. The electrochemical active surface area was determined by integration of CV profile in the hydrogen adsorption region after correction for double layer capacitance. Data have not been corrected for hydrogen cross-over. Accelerated degradation tests in PEMFC were carried out at 130 °C by using the same configuration above discussed but both cell and humidifiers were pressurized and maintained at the same temperature.

3.4 Accelerated degradation tests

Catalyst stability under high temperature operation needs of proper investigation since the working conditions influence carbon black corrosion, platinum dissolution and sintering.

From a research costs point of view, it is also true that the time needed for a lifetime catalyst investigation is often unaceptable (e.g. about 5,000 h for a automotive FC stack system). Consequently, it is necessary to find proper methods to evaluate catalyst stability for high temperature applications in a reasonable limited time [5]. Among the various methods proposed in the literature [6-9], we have selected two accelerated degradation tests[1] (ADTs) carried out at high temperature to evaluate catalyst stability. The operating conditions to evaluate carbon ad platinum stability are:

- Evaluation of Pt sintering by continuous cycling between 0.6 and 1.2 V i.e. in the region where Pt is less stable. It is know that the formation of stable Pt-oxide phase at potentials higher than 1.2 V RHE stabilizes Pt, whereas at potentials smaller than 0.6 V RHE the corrosion effects are negligible.
- Evaluation of carbon corrosion on the deposited Pt nanosized particles by holding a constant potential of 1.2 V RHE for 24 hrs. At high electrochemical potentials, carbon corrosion with consequent CO_2 formation is greatly accelerated. The carbon corrosion occur by following a mechanism similar to reactions 4-6 (see section 2.3)[2].

In single cell:

- Evaluation of electrocatalysts behaviour by stability studies: constant voltage at 0.7 V for 24h; at 130 °C; 3 bar abs.; 100% RH; H_2 - O_2.

[1] Depending the system (half cell or single cell) the ADTs were conducted under different conditions. In He and at 75 °C in acid electrolyte for half cell tests. Only the Pt ADT in single cell test; H_2 - N_2 at 130 °C; 3 bar abs.; 100% RH.
[2] Test carried out only in half cell.

The verification of the decay process was carried out 'in situ' by:

- standard cyclic voltammetry: 0.02–1.2 V RHE;
- polarisation curves.

The polarization curves were carried out by using galvanostatic steady state software methods. The potential range varied from OCV up to cut-off values. After testing, the samples were characterised by 'ex situ' physico-chemical analyses of the catalytic layer to evaluate sintering and dissolution. Ohmic resistance was monitored during these experiments by AC-impedance spectroscopy (high frequency intercept on the real axis) and using Nyquist plots. The AC-impedance spectroscopy were carried out in the range of 1 MHz – 1 mHz frequency (61 point; Log scale) applying an amplitude of 10 mV. Tafel plots were calculated after IR correction.

References

1. A.S. Aricò,V. Baglio, A. Di Blasi, E. Modica, P.L. Antonucci,V. Antonucci, J. Electroanal. Chem., 557 (2003) 167.
2. V. Radmilovic, P.N. Ross Jr, J. Catal., 154 (1995) 98.
3. H.A. Gasteiger, P.N. Ross Jr, E. Cairns, J. Surf. Sci. 67 (1993) 293.
4. A.S. Aricò, A.K. Shukla, K.M. El-Khatib, P. Cretì, V. Antonucci, J. Appl. Electrochem., 29 (1999) 671.
5. J. Wu, X.Z. Yuan, J.J. Martin, H. Wang, J. Zhang, J. Shen, S. Wu,W. Merida, J. Power Sources, 184 (2008) 104.
6. P. Yu, M. Pemberton, P. Plasse, J. Power Sources, 144 (2005) 11.
7. H. R. Colon-Mercado, H. Kim, B. N. Popov, Electrochem. Commun., 6 (2004) 795.
8. R. Makharia, S. Kocha, P. Yu, M. A. Sweikart, W. Gu, F. Wagner, H. A. Gasteiger, ECS Trans., 1 (2006) 3.
9. S. C. Ball, S. L. Hudson, D. Thompsett, B. Theobald, J. Power Sources, 171 (2007) 18.

4

ELECTROCATALYSTS DEVELOPMENT FOR OXYGEN REDUCTION REACTION

4.1 Introduction

The oxygen reduction process in low temperature fuel cells is known to be enhanced on platinum alloys in relation to platinum metal [1-3]. Leaching of non-noble metals from the alloy produces a surface roughening with a corresponding increase of the Pt surface area; but, there is hardly any increase in the electrochemically active surface-area (ECSA) for the platinum alloys as compared to the state of art carbon supported Pt metal. The observed improvements for the Pt-alloys correspond to at least a doubling of the electrocatalytic activity in the Tafel region [4]. This enhancement in electrocatalytic activity has been differently interpreted, and several studies were made to analyze in depth the properties of several alloys combinations [2,5-7].

Although a comprehensive understanding of the numerous reported evidences has not yet been reached, the observed electrocatalytic effects have been ascribed to several factors (interatomic spacing, preferred orientation, electronic interactions) which play, under fuel cell conditions, a favorable role in enhancing the oxygen reduction rate (ORR) [2,7,8-12]. As example, the intrinsic electro-catalytic activity of Pt alloys (Pt-Cr, Pt-Ni, Pt-Co, Pt-Cu, Pt-Fe), with a lattice parameter smaller than that of Pt, was found to be higher than that of the base metal [5-14]. This effect has been related to the nearest neighbor distance of Pt-Pt atoms on the surface of the fcc crystals. The rate determining step was assumed to involve the rupture of the O-O bond through a dual site mechanism [3]; thus, a decrease of the Pt-Pt distance favored the dual site O_2 adsorption. In this regard, the formation of a tetragonal ordered structure upon

thermal treatment, in the case Pt-Co-Cr, was observed to lead to a more active electro-catalyst than that with a Pt fcc structure [8-12]. Besides this, an interplay between electronic and geometric factors (Pt d-band vacancy and Pt-coordination numbers) and its relative effect on the OH chemisorption from the electrolyte occurred [15]. More recently, a volcano-type relationship between the Pt d-band centre for Pt_3M alloys and the activity for the oxygen reduction reaction was derived [2]. The d-band centre appears to determine the strength of the metal-adsorbate interaction. The highest electro-catalytic activity for the Pt_3Co system in the Pt_3M alloys series appeared as a result of a balance between the adsorption of reactive intermediates and the surface coverage of blocking species [2].

It has been reported that the Pt-alloys are not surface rich in the nonnoble-metal (M) component, and are essentially all Pt [2,16,17]. Watanabe et al. reported that, after electrochemical testing of a Pt–Fe alloy, the catalyst was covered by a thin Pt skin of less than 1 nm in thickness [17,18]. Moreover, they suggested that during the adsorption step, a π orbital of O_2 interacts with empty d orbitals of Pt and consequent back donation occurs from the partially filled orbital of Pt to π^* (anti-bonding) molecular orbital of O_2. Accordingly, the increase in d-band vacancies on Pt by alloying produces a strong metal–O_2 interaction. This interaction weakens the O–O bonds, resulting in bond cleavage and bond formation between O and H^+ of the electrolyte, thus improving the ORR.

One concern with Pt alloys in PEMFCs is the dissolution of transition metals. Pourbaix diagrams indicate that most metals such as Co, Cu, Fe, Ni, etc. are soluble at a potential between 0.3 and 1 V versus SHE and at low pH values. The enhanced catalytic activity for Pt–Fe catalysts has been attributed to the presence of a Pt skin over the alloy together with an electronic effect induced by Fe on Pt, as reported by Watanabe and coworkers [17,18]. The formation of the Pt skin probably occurs because iron on the surface leaches out of the alloy during operation in acidic electrolytes, while Pt atoms are redeposited and rearranged on the surface. For what concerns the electronic effect, it was emphasized that the electronic structures of the Pt skin layers are altered by the underlying alloy substrates, which in turn facilitates the electron transfer to oxygen molecules [17,18]. On the other hand, Li et al. claimed that

the improvement in the performance of Pt–Fe/C for ORR may be partly due to the higher peroxide decomposition activity of Pt in the presence of dissolved Fe favoring the $4e^-$ transfer route [19].

A large-scale application of PEMFC systems technology requires a reduction of its high cost through a decrease of Pt loading and maximization of catalyst utilization as well as an improvement of performance and stability [1,20-22]. Various studies have shown that PtCo alloy catalysts have been recently demonstrated to be more stable to both carbon corrosion and metal area loss in PEMFCs [23-26]. This system appears a promising alternative to Pt/C catalysts for practical applications.

Then, this Ph.D activity was addressed to develop practical Pt/C anode and Pt/C or PtCo/C cathode catalysts with high metal surface. Benchmark carbon blacks with intermediate and high surface area have been selected i.e. Vulcan XC 72 with BET active area of 250 m^2/g and Ketjenblak EC with BET active area of about 850 m^2/g. The synthesis process was optimised to obtain suitable dispersion of the metal particle sizes on the support even for high metal concentration catalysts (up to 50% wt.) and a mean particle size smaller than 3 nm.

4.2 Catalysts preparation

A colloidal procedure for preparing Pt/C and PtCo/C catalysts with metal concentration ranging from 30% to 50% wt. was used [27]. Sulfite complexes of Pt, in appropriate amounts, were decomposed by hydrogen peroxide to form aqueous colloidal solutions of Pt oxides. These particles were adsorbed on carbon black. These first steps were carried out in CSTR reactors with digital stirring, thermal and pH control (see Fig. 4.1). Reactions were carried out under proper pH and temperature operating conditions. The amorphous oxides on carbon were thus reduced in a hydrogen stream to form metallic particles. The step concerning Pt reduction was performed under controlled hydrogen stream with a continuous monitoring of gas consumption by a TCD. The PtCo/C catalyst was synthesized in a similar way. Before the reduction step, cobalt nitrate was adsorbed on the amorphous Pt/C catalyst. Both

hydrogen and carbothermal reduction in inert (Ar) atmosphere were investigated for preparation of carbon supported Pt and PtCo alloy.

Fig. 4.1 CSTR for catalysts preparation.

Different pre-leaching procedures were also adopted for carbon supported PtCo alloy. Concerning with the pre-leaching treatments, these were adopted to reduce the dissolution of cobalt from the particle surface in PEMFC by favouring a Pt enrichment in the outer layers of nanosized grains. As discussed before, the dissolution of cobalt produces a contamination of the membrane electrode assembly (MEA) that gives rise to a degradation of the fuel cell [23,28-31]. The initial amount of cobalt was varied to obtain about the same metal composition (Pt:Co = 3:1) for the catalysts after the pre-leached treatment. Different temperature and acid concentration were necessary in the

Table 4.1. Catalysts and synthesis methods.

Principal characteristic of catalysts developed during the Ph.D. activity

CATALYST	ABBREVIATION	REDUCTION METHOD	Co %Wt. CONTENT
Pt/C catalysts 1st series			
30% Pt/Vulcan	30% Pt/CV 1H	H_2 stream	-
30% Pt/Ketjenblack	30% Pt/KB 2H	H_2 stream	-
50% Pt/Ketjenblack	50% Pt/KB 3H	H_2 stream	-
PtCo/C catalysts 1st series			
50% Pt_3Co_1/Ketjenblack	50% PtCo/KB 5H	H_2 stream	5
50% Pt_3Co_1/Ketjenblack	50% PtCo/KB 6C	Carbothermal	5
50% Pt_3Co_1/Ketjenblack	50% PtCo/KB 7C	Carbothermal	5
PtCo/C pre-leached and Pt/C catalysts 2nd series			
50% Pt/Ketjenblack	50% Pt/KB 4C	Carbothermal	-
50% Pt_3Co_1/Ketjenblack	50% PtCo/KB 8C-Cl	Carbothermal $HClO_4$ leaching	10[a]
50% Pt_3Co_1/Ketjenblack	50% PtCo/KB 9C-S	Carbothermal H_2SO_4 leaching	10[a]

a) Co content before pre-leaching treatment.

two leaching procedure to achieve similar final Pt/Co atomic ratios. In particular, the leaching procedure were the following: 85 °C and 0.5 M of $HClO_4$ for 50% PtCo/KB 8C-Cl catalyst; 90 °C and 2.0 M of H_2SO_4 for 50% PtCo/KB 9C-S catalyst. No efficient leaching was achieved with diluted sulphuric acid solution.

Catalysts prepared and the synthesis methods adopted are resumed in Table 4.1. In this table, they are divided in first and second series as a function of the period of development. It is pointed out that for 50% PtCo/KB 6C catalyst the carbothermal treatment was carried out at 400 °C. Insted, the other carbothermal treatments were performed at 600 °C.

4.3 Physical-chemical characterization

XRD patterns of Pt/C and PtCo/C catalysts are reported in Figures 4.2-4.4. X-ray fluorescence and CHNSO elemental analysis confirmed the nominal compositions. For the Pt/C catalysts, the carbon black support and concentration of metal phase on carbon were varied. For the PtCo/C series, concentration of metals and carbon black support were maintained constant; whereas, it was varied the reduction treatment. The high surface area carbon black was selected for the Pt-Co series to enhance the dispersion since the catalysts were treated at high temperature.

The catalysts show cubic structure for Pt and PtCo (fcc) and hexagonal structure for carbon support. XRD analyses indicate a small particle size ranging from 1.5 to 3 nm. The lattice parameter (A_0), the mean particle size, derived from XRD, and Pt/Co atomic ratio, derived from XRF, are reported in Table 4.2. For Pt/C catalysts, the particle size increases as a function of the increase of metal phase concentration and the decrease of BET surface area of carbon support. For PtCo/C catalysts a large lattice contraction corresponding to high degree of alloying was achieved only after a high temperature treatment of the alloy (600 °C).

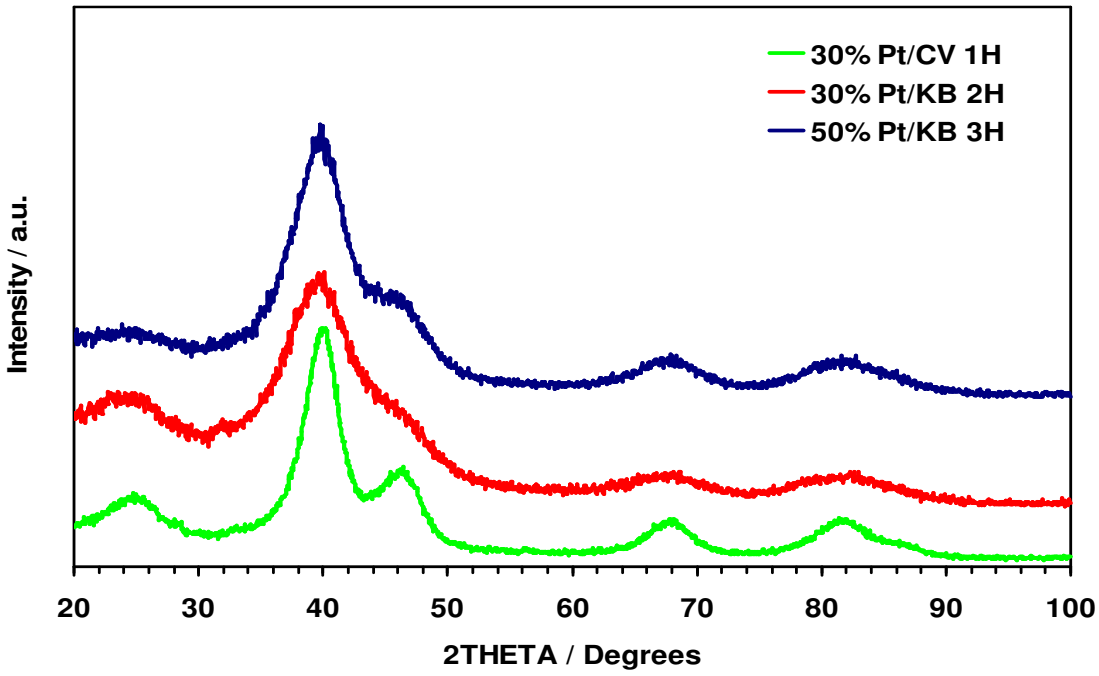

Fig. 4.2 XRD patterns of carbon supported Pt 1st series catalysts.

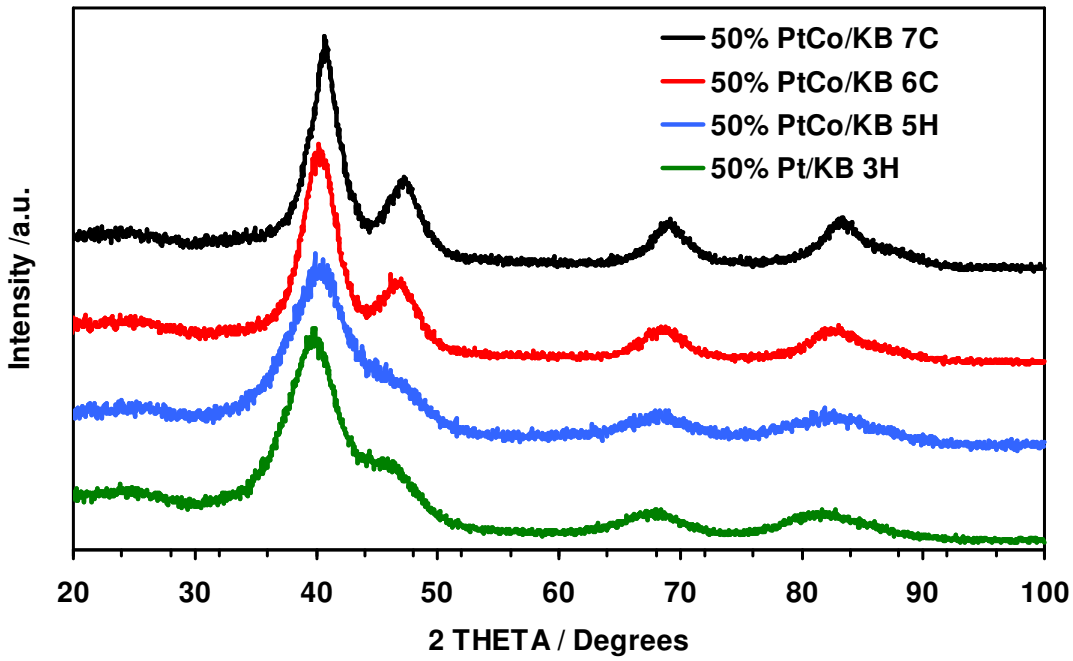

Fig. 4.3 XRD patterns of carbon supported PtCo 1st series catalysts. Note that the Pt/C catalyst is reported to highlight the peaks shift for the PtCo/C catalysts.

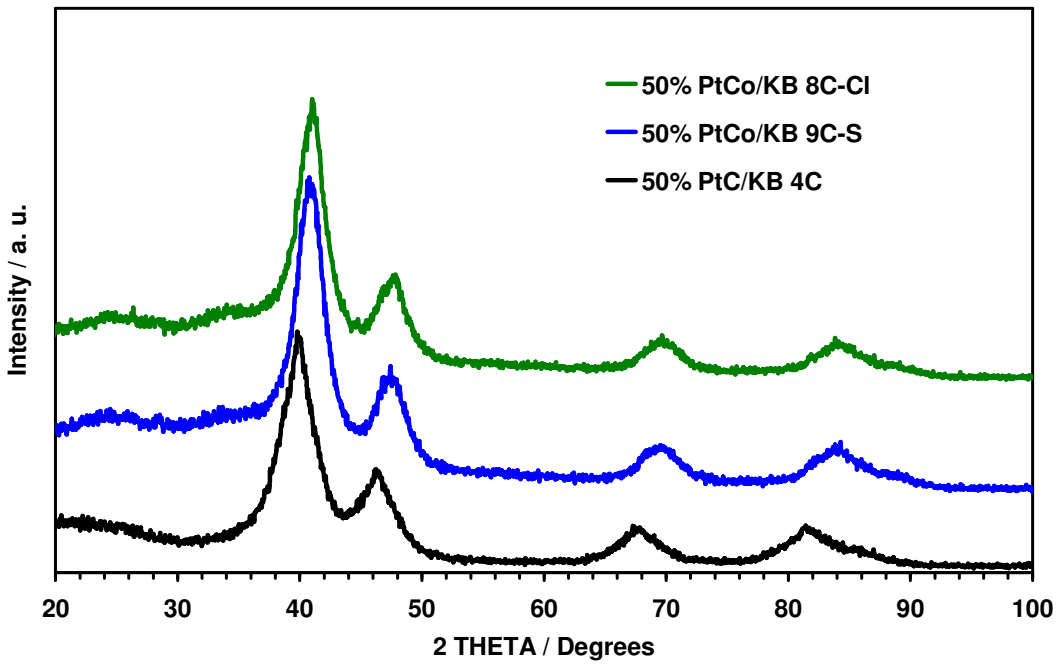

Fig. 4.4 XRD patterns of carbon supported PtCo/C and Pt/C 2nd series catalysts.

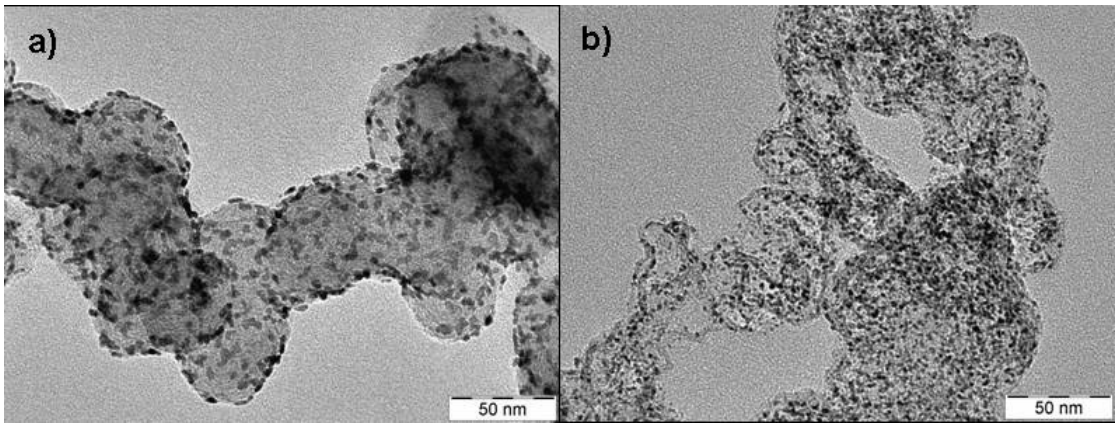

Fig. 4.5 TEM micrographs for 1st series carbon supported Pt catalysts.

a) 30% Pt/CV 1H; b) 50% Pt/KB 3H.

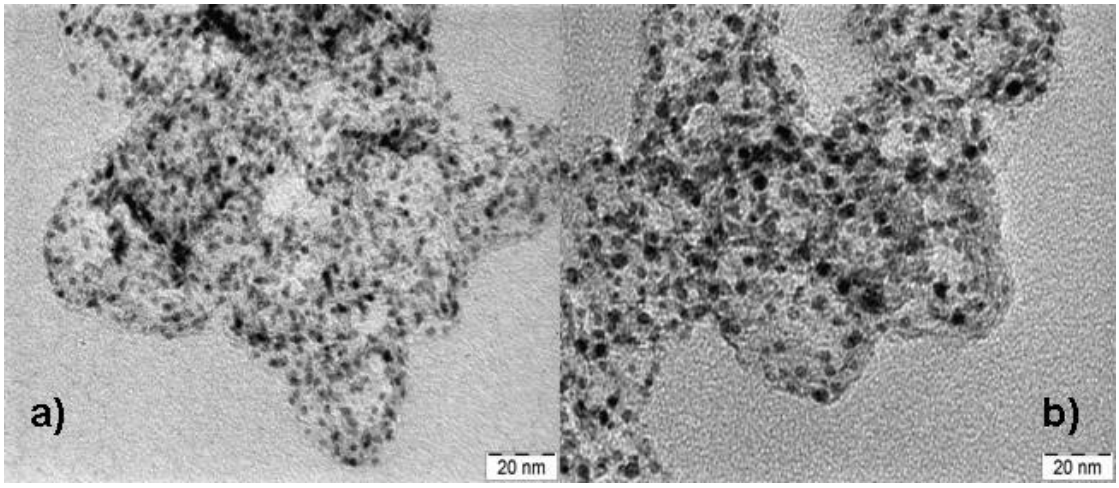

Fig. 4.6 TEM micrographs for 1st series carbon supported PtCo catalysts.

a) 50% PtCo/KB 5H; b) 50% PtCo/KB 7C.

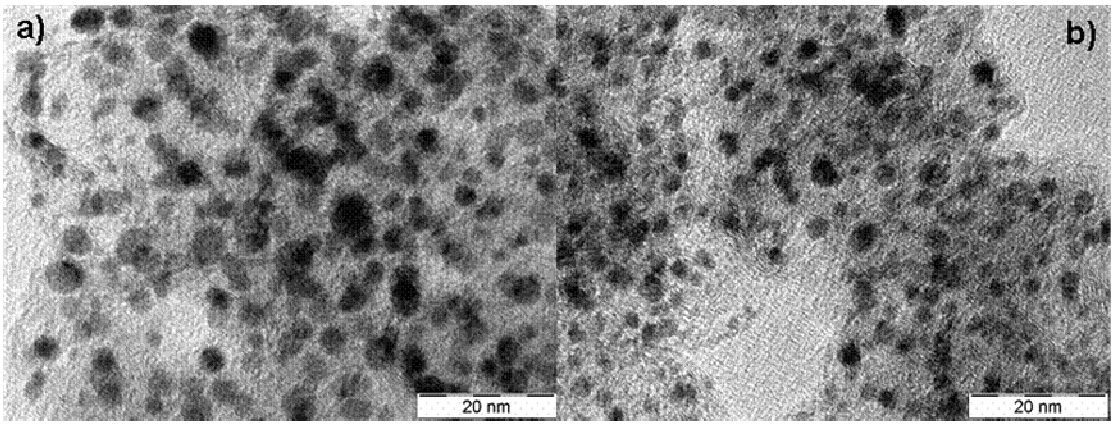

Fig. 4.7 TEM micrographs for 2nd series carbon supported Pt and PtCo catalysts.

a) 50% PtCo/KB 8C-Cl; b) 50% Pt/KB 4C.

This determines an increase of the particle size to 2.9 nm with a loss of metal surface area. An amount of about 25% of Co atomic concentration in the PtCo fcc structure was calculated from the Vegard's law for the 50% PtCo/KB 8C-Cl catalyst.

TEM micrographs of some Pt/C and PtCo/C catalysts are reported above (Figs. 4.5-4.7). TEM analyses confirmed XRD analysis for the catalyst and indicate a small particle size ranging from 1.5 to 3 nm with unimodal distribution. A good dispersion is obtained for all catalysts. Moreover, TEM analysis shown that the support BET surface area influence not only the platinum particles dimension (Table 4.2) but also the distribution of this latter. In Fig. 4.5 is evident that the metal particles on Vulcan support are homogenously distributed onto the external carbon surface (Fig. 4.5a); whereas, the Pt particles on Ketjenblack support (Fig. 4.5b) are homogenously distributed into the inner support structure despite the higher metal loading (50%).

Table 4.2 XRD and XRF catalysts characterization.

Structural and chemical characteristic of catalysts

Catalyst	Peak posit. (2θ)	A_{220} (nm)	Crystallite size (nm)	Ratio Pt/Co (XRF)	Degree of alloying (%Co)[a)]	Ratio Pt/Co (XRD)
30% Pt/CV 1H	67.660	0.391	2.4	-	-	-
30% Pt/KB 2H	67.499	0.392	1.5	-	-	-
50% Pt/KB 3H	67.595	0.392	1.8	-	-	-
50% Pt/KB 4C	67.619	0.392	2.7	-	-	-
50% PtCo/KB 5H	67.974	0.389	1.7	3.1	5.3	18.0
50% PtCo/KB 6C	68.311	0.388	2.5	2.9	10.5	8.5
50% PtCo/KB 7C	68.916	0.385	2.9	2.9	18.4	4.4
50% PtCo/KB 8C-Cl	69.370	0.383	2.9	3.2	23.7	3.2
50% PtCo/KB 9C-S	69.190	0.384	2.8	3.4	21.1	3.8

a) The degree of alloying were calculated by Vegard's law.

Among the various TGA-DSC analyses carried out on catalysts, two examples are reported in Figures 4.8a-b and 4.9a-b. For all catalysts they showed an initial weight loss up to 120-130 °C due to the water humidity samples content. Then it is possible see a complete carbon combustion is the range of 220 – 450 °C (see Figs. 4.8b and 4.9b). Above this temperature, the weight loss remaining relatively constant close to

the nominal metals load content. The CHNS-O analysis results are reported in Table 4.3. Both TGA and CHNS-O within XRF analyses confirmed the nominal compositions of the different catalysts. Finally, XRF analysis showed a decrease of the cobalt content after the leaching treatment as compared to the nominal value or with respect to the untreated catalyst (see Table 4.2).

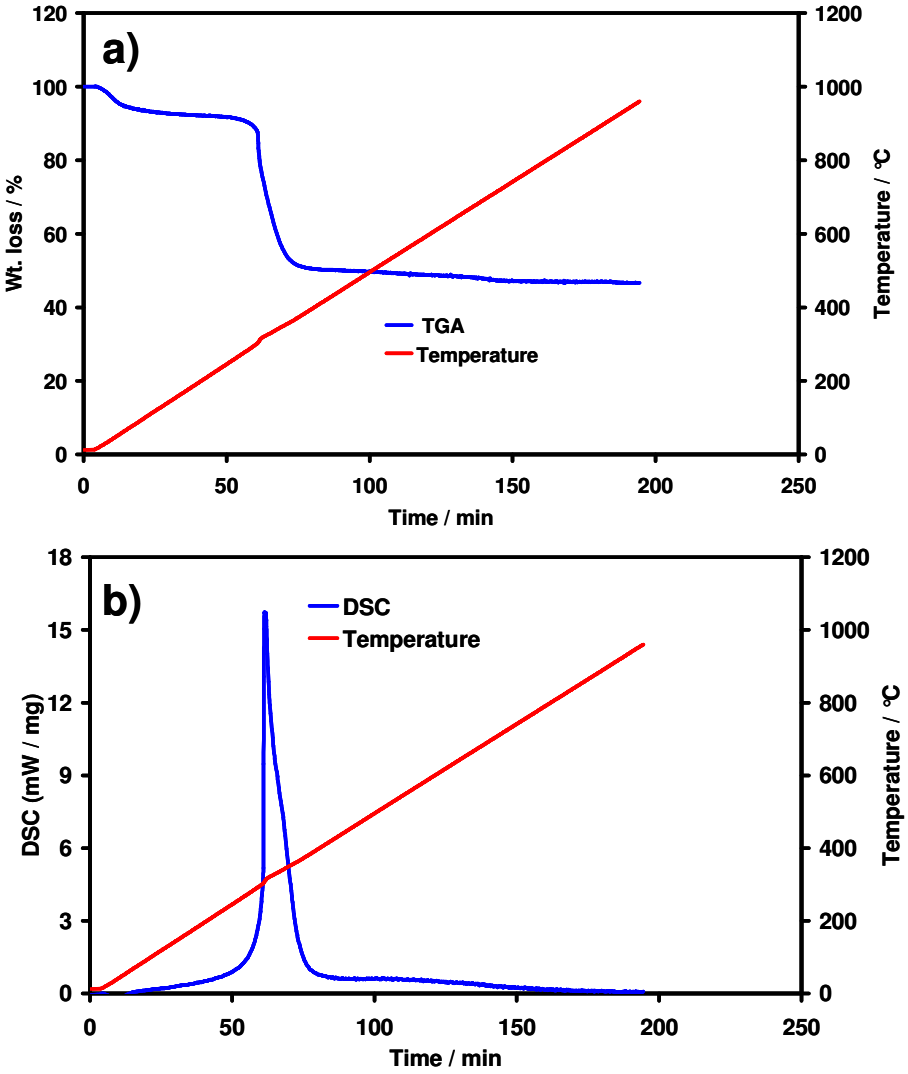

Fig. 4.8 a-b TGA-DSC analysis of 50% PtCo/KB 8C-Cl; a) TGA analysis; b) DSC analysis.

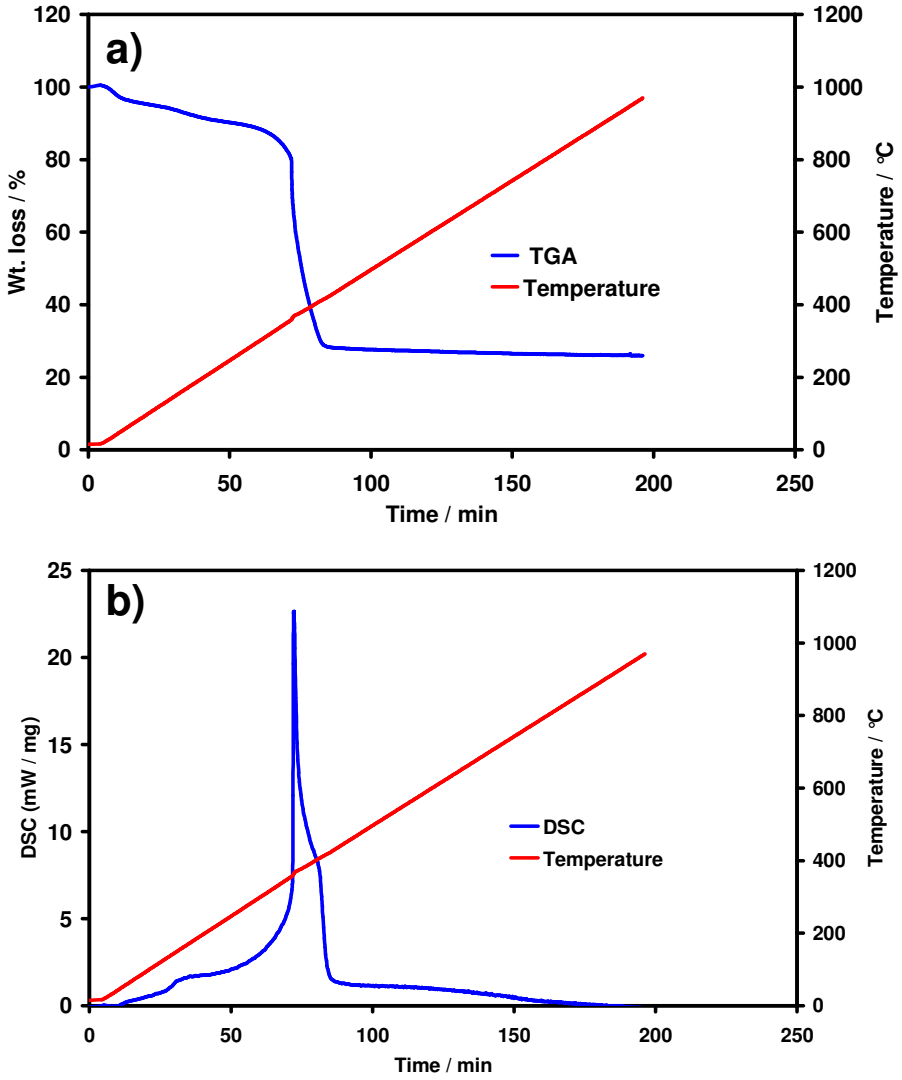

Fig. 4.9 a-b TGA-DSC analysis of 30% Pt/CV 1H; a) TGA analysis; b) DSC analysis.

Table 4.3 CHNS-O analysis. All data are expressed in %Wt.

Elementary analysis of catalysts

Catalyst	C	H	N	S	O
30% Pt/CV 1H	66.7	0.8	0.7	0.4	0.9
30% Pt/KB 2H	67.9	0.5	0.5	0.3	1.1
50% Pt/KB 3H	46.3	0.9	0.3	0.4	0.7
50% Pt/KB 4C	47.9	0.6	0.2	0.1	1.2
50% PtCo/KB 5H	45.3	1.1	0.5	0.4	0.6
50% PtCo/KB 6C	48.2	0.4	0.6	0.7	0.8
50% PtCo/KB 7C	46.8	0.7	0.3	0.6	1.1
50% PtCo/KB 8C-Cl	46.5	1.0	0.5	0.4	1.6
50% PtCo/KB 9C-S	45.7	0.8	0.4	1.3	1.4

4.4 Conclusions

Catalysts varying in terms of carbon black support, Pt particle size, metal concentration, chemistry (PtCo vs. Pt) were prepared using a colloidal procedure and benchmark support materials. The different reduction methods adopted for all catalysts could lead to a possible scale-up.

TEM analysis has shown a good dispersion for all series of catalysts. The catalyst particle size and dispersion appears to be influenced by the BET surface area of the support, metal-support interaction and concentration of the metal phase. For all catalysts, a crystalline metallic phase is obtained for Pt despite the small particle dimension (1.5-3.0 nm).

A suitable degree of alloying was obtained for the 50% PtCo/KB 8C-Cl catalyst by using a high temperature treatment and a leaching procedure while maintaining the mean particle size smaller than 3 nm.

A wide physicochemical characterization was carried out for these materials (particle size, concentration of Pt, dispersion, carbon black support) in order to provide a data-set useful to correlate such properties with the following performance and stability studies.

References

1. H.A. Gasteiger, S.S. Kocha, B. Sompalli, F.T. Wagner, Appl. Catal. B: Environ., 56 (2005), 9.
2. V.R. Stamenkovic, B.S. Mun, M. Arenz, K.J.J. Mayrhofer, C.A. Lucas, G. Wang, P.N. Ross, N.M. Markovic, Nat. Mater., 6 (2007) 241.
3. A.S. Aricò, P. Bruce, B. Scrosati, J.-M. Tarascon,W. Van Schalkwijk, Nat. Mater., 4 (2005) 366.
4. S. Mukerjee, S. Srinivasan, J. Electroanal. Chem., 357 (1993) 201.
5. M.T. Paffet, G.J. Beery, S. Gottesfeld, J. Electrochem. Soc., 135 (1988) 1431.
6. M. Watanabe, K. Tsurumi, T. Mizukami, T. Nakamura, P. Stonehart, J. Electrochem. Soc., 141 (1994) 2659.
7. A. Freund, J. Lang, T. Lehman, K.A. Starz, Cat. Today, 27 (1996) 279.
8. V. Jalan, E.J. Taylor, J. Electrochem. Soc., 130 (1983) 2299.
9. S. Gottesfeld, M.T. Paffett, A. J. Redondo, Electroanal. Chem., 205 (1986) 163.
10. B.C. Beard, P.N. Ross, J. Electrochem. Soc., 137 (1990) 3368.
11. K.T. Kim, J.T. Hwang, Y.G. Kim, J.S. Chung, J. Electrochem. Soc., 140 (1993) 31.
12. S. Mukerjee, S. Srinivasan, M.P. Soriaga, J. McBreen, J. Electrochem. Soc., 142 (1995) 1409.
13. X. Ren, T.E. Sringer, S. Gottesfeld, in Proton Conducting Membrane Fuel Cells - Second International Symposium, ed. S. Gottesfeld, T.F. Fuller, The Electrochemical Society, Pennington, New Jersey, 98-27 (1999) 341.
14. H. Dohle, J. Divisek, J. Mergel, H.F. Oetjen, C. Zingler, D. Stolten, in Fuel Cell Seminar Abstracts, 2000; October 30-November 2, Portland, Oregon, 126.
15. C.F. Zinola, A.M. Castro Luna, W.E. Triaca, A.J. Arvia, J. Applied Electrochem., 24 (1994) 119.
16. T. Toda, H. Igarashi, H. Uchida, M. Watanabe, J. Electrocehem. Soc., 146 (1999) 3750.
17. T. Toda, H. Igarashi, M. Watanabe, J. Electroanal. Chem., 460 (1999) 258.
18. H. Uchida, H. Ozuka, M. Watanabe, Electrochim. Acta, 47 (22-23) (2002) 3629.
19. W. Li, W. Zhou, H. Li, Z. Zhou, B. Zhou, G. Sun, Q. Xin, Electrochim. Acta, 49 (2004) 1045.
20. C. Jaffray, G.A. Hards, in Handbook of Fuel Cells—Fundamentals, Technology and Applications, ed..W. Vielstich, A. Lamm, H. Gasteiger, Wiley, Chichester, UK, 2003, vol. 3.
21. R.L. Borup, J.R. Davey, F.H. Garzon, D.L. Wood, M.A. Inbody, J. Power Sources, 163 (2006) 76.
22. M. Cai, M.S. Ruthkosky, B. Merzougui, S. Swathirajan, M.P. Balogh, J. Power Sources, 160 (2006) 977.
23. P. Yu, M. Pemberton, P. Plasse, J. Power Sources, 144 (2005) 11.
24. E. Antolini, J.R.C. Salgado, E.R. Gonzalez, J. Power Sources, 160 (2006) 957.
25. H.R. Colon-Mercado, B.N. Popov, J. Power Sources, 155 (2006) 253.
26. S.C. Ball, S.L. Hudson, D. Thompsett, B. Theobald, J. Power Sources, 171 (2007) 18.
27. A.S. Aricò, V. Baglio, A. Di Blasi, E. Modica, P.L. Antonucci and V.Antonucci, J. of Electroanal. Chem., 557 (2003) 167.
28. A.S. Aricò, A. Stassi, E. Modica, R. Ornelas, I. Gatto, E. Passalacqua, V. Antonucci, J. Power Sources, 178 (2008) 525.
29. A. Stassi, E. Modica, V. Antonucci, A.S. Aricò, Fuel Cells, 9 (3) (2009) 201.
30. A.S. Aricò, P.L. Antonucci, V. Antonucci, in: A. Wieckowski, E.R. Savinova, C.G. Vayenas (Eds.), Catalysis and Electrocatalysis at Nanoparticle Surfaces, Marcel Dekker, Inc., New York, 2003.

31. K. Kinoshita, Electrochemical Oxygen Technology, Wiley, New York, 1992.

5

1st SERIES ELECTROCATALYSTS
- HALF CELL CHARACTERIZATION -

5.1 Introduction

In this chapter, the gas-fed half cell studies performed on the first series electrocatalysts developed during the first two years of this Ph.D. activity, will be discussed. To accomplished the electrochemical analysis, the tests were carried out in an acid electrolyte solution (H_2SO_4 0.5 M) and at temperature of 75 °C. These operating conditions were selected to simulate a cathode side PEMFC environment. The half cell system was adopted to investigated the catalysts performance and stability and tried to correlate these latter with the physical-chemical catalysts characteristics.

5.2 Catalytic activity and degradation tests in sulphuric acid

Figures 5.1 and 5.2 summarizes the catalytic activity for oxygen reduction in half cell at 75°C in 0.5 M H_2SO_4, with pure oxygen feed. The catalysts with a mean particle size of 2.4 nm (30% Pt/CV 1H) and 2.9 nm (50% PtCo/KB 7C), respectively showed the best performance in the activation controlled region. Concernign with the Pt/C catalysts (Fig. 5.1) in the Tafel, region the performance increases as a function of the particle size in the investigated range. The Tafel slope is about 70 mV/dec for all catalysts indicating similar reduction mechanism.

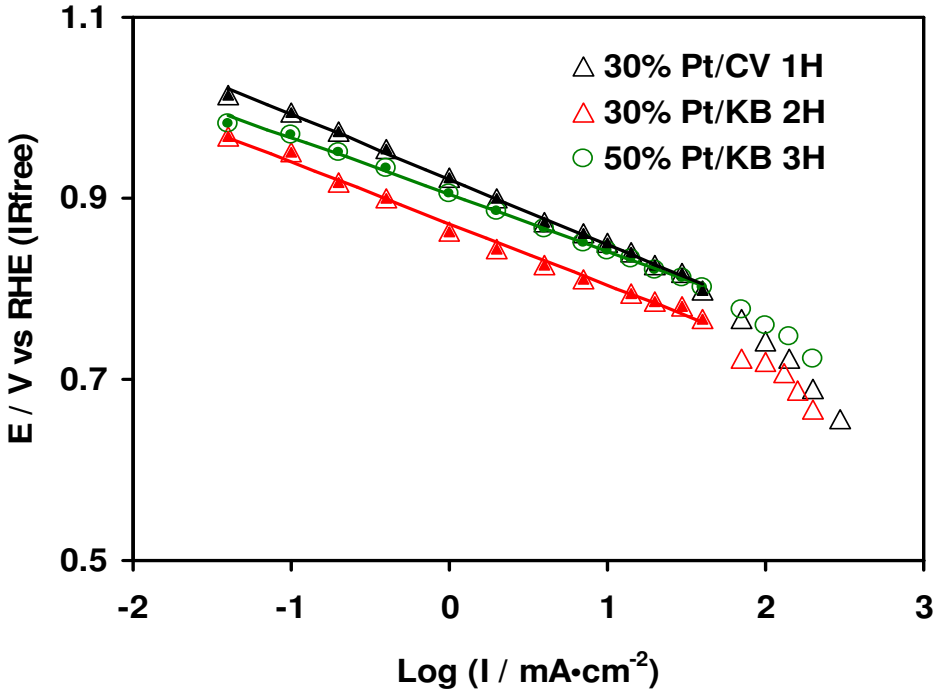

Fig. 5.1 Effect of particle size on Tafel plots for oxygen reduction for 1st series Pt/C catalysts in sulphuric acid: 0.5 M H_2SO_4; 75°C, pure O_2.

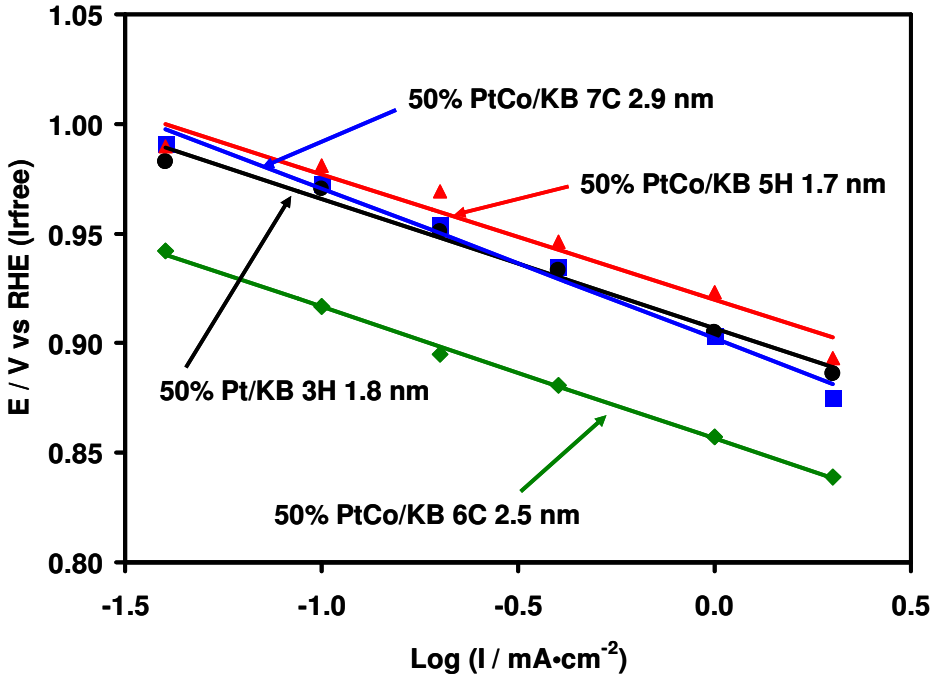

Fig. 5.2 Effect of particle size and synthesis method on Tafel plots for oxygen reduction for 1st series PtCo/C catalysts in sulphuric acid: 0.5 M H_2SO_4; 75°C, pure O_2.

We have focused our attention on small particle size catalysts characterized by strong metal support interaction [1]. It is well known that increasing the mean particle size, the mass activity for oxygen reduction passes through a maximum and then decreases [2]. The particle size of these catalysts falls in the left region of the Kinoshita volcano shape curve of mass activity vs. particle size [2].

Kinetic studies were also carried out for first series of PtCo catalysts (Fig. 5.2). The Tafel plots show that, at low current densities the best performance is achieved with the 50% PtCo/KB 7C catalysts characterized by good degree of alloying and large particle size (2.9 nm) (see Table 4.2). The performance of PtCo catalysts does not show any correlation with the particle size as opposite of Pt/C catalysts. This may be due to the different reduction procedure used for different PtCo catalysts (see Table 4.1), possibly, causing a different surface concentration of Pt and Co. A Tafel slope of about 65 mV/dec was observed for the PtCo series. A doubling of Tafel slope and a decrease of catalytic activity is envisaged at high current densities for some of the PtCo/C catalysts. However, in this region mass transport properties and flooding effects may affect the electrochemical behaviour (not shown). Thus, it is difficult to assign these effects to catalytic properties only.

As reported in Chapter 3, different accelerated test procedures have been selected to evaluate catalysts stability; these are:

a) Evaluation of Pt sintering by carrying out 1000 cycles between 0.6 and 1.2 V RHE at a scan rate of 20 mV/s with He feed in 0.5 M H_2SO_4.
b) Evaluation of carbon corrosion on the deposited Pt nanosized particles by holding a constant potential of 1.2 V RHE for 24 hrs with He feed in 0.5 M H_2SO_4.

In figure 5.3, some cycles, registered during this test for 30% Pt/CV 1H, are shown. It is clearly observed that the PtO reduction peak shifts to high potentials and decreases in intensity. This is attributed to an increase of specific activity due to the increase of particle size (sintering) and reduction of electrochemically active surface area (ECSA).

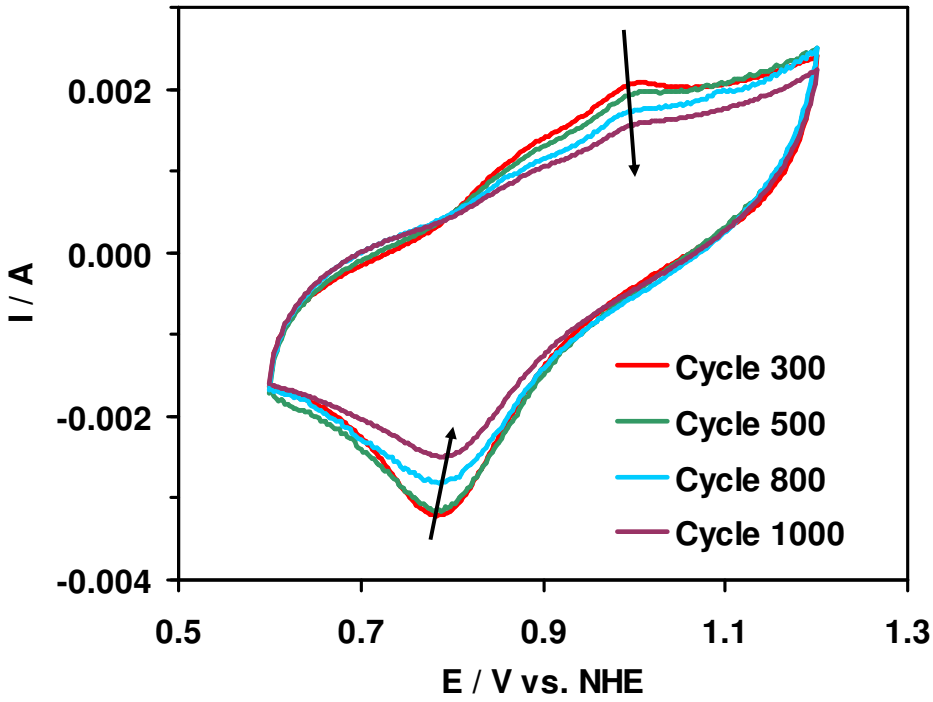

Fig 5.3 Accelerated Pt degradation for 30% Pt/CV 1H: 1000 cycles (s.r. = 20 mVs^{-1}) at 75 °C in 0.5 M H_2SO_4.

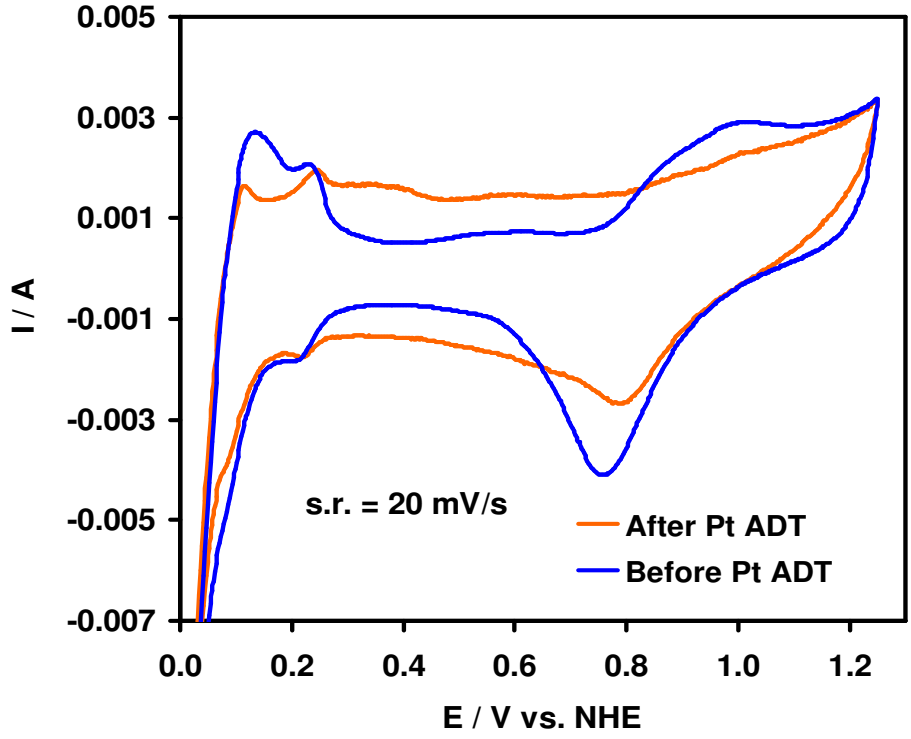

Fig. 5.4 Cyclic voltammetries of 30% Pt/VC 1H electrode before (blu line) and after (orange line) Pt degradation test (20 mVs^{-1}, 75 °C, 0.5 M H_2SO_4).

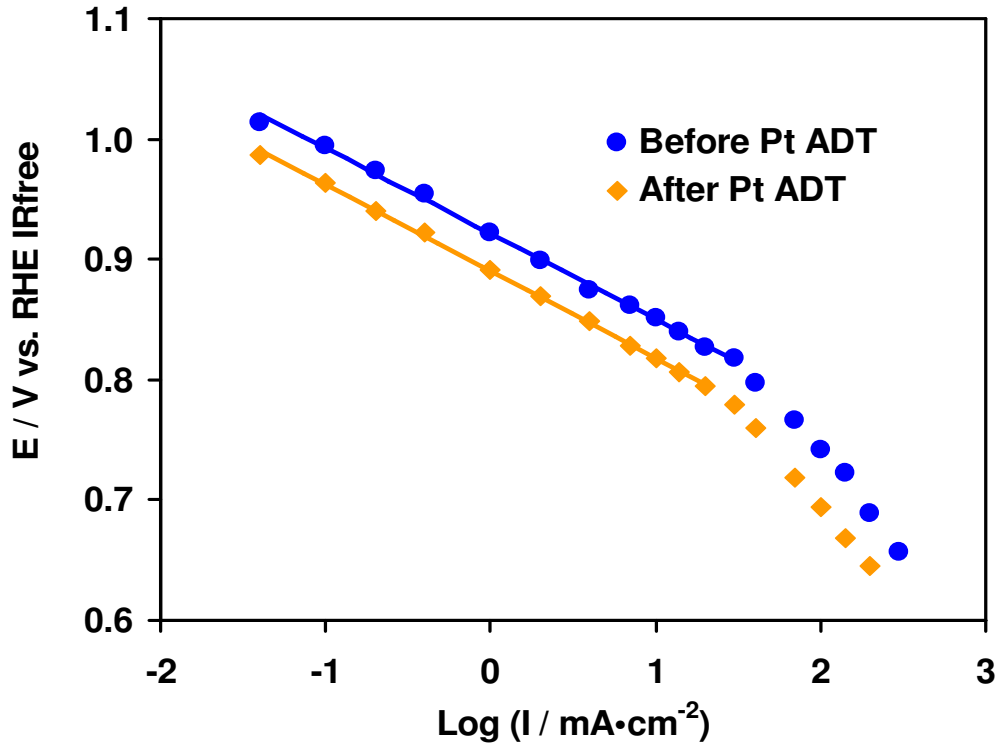

Fig. 5.5 Effect of electrode cycling on the polarization behaviour for oxygen reduction of 30% Pt/CV 1H electrode. 0.5 M H_2SO_4; 75°C, pure O_2.

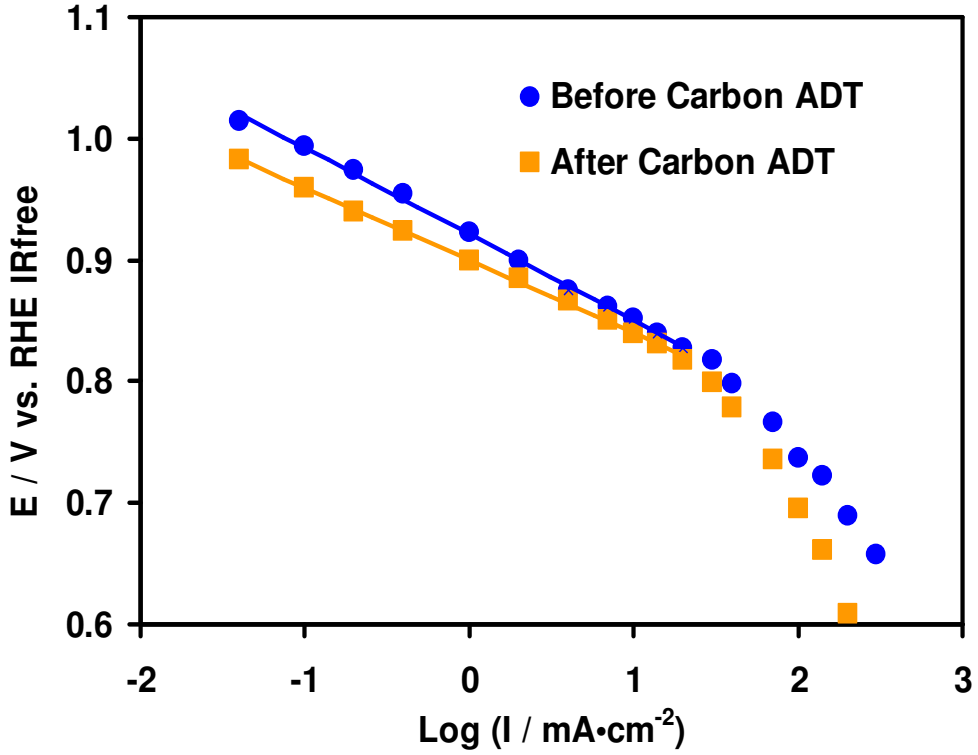

Fig. 5.6 Effect of potential holding at 1.2 V for 24 hrs on the polarization behaviour for oxygen reduction of 30% Pt/CV 1H electrode. 0.5 M H_2SO_4; 75°C, pure O_2.

The CV profile after the Pt degradation test also shows an increase of the double layer capacitance (Fig. 5.4). The active area reduction after Pt corrosion test can be observed in Figure 5.4. The ECSA decreases of about 50%. The effect of potential cycling (Pt degradation test) on electrode performance is illustrated in Figure 5.5; an average loss of 32 mV in the Tafel region is observed without mass transport losses. The effect of electrode potential holding at 1.2 V (carbon corrosion test) on the performance is shown in Figure 5.6; an average loss of about 23 mV in the Tafel region is recorded (Table 5.1).

Similar effects were observed for 30% Pt/KB 2H and 50% Pt/KB 3H in sulphuric acid half cell. Data concerning with degradation tests in sulphuric acid half cell are summarized in Table 1. In sulphuric acid half cell the Pt/VC catalyst appeared to be more stable than Pt/KB catalysts possibly due to the smaller surface area of the carbon support. It was observed that the accelerated Pt degradation test (potential cycling) causes a larger degradation of performance than the accelerated carbon corrosion test (oxidation at 1.2 V). The final particle size after the accelerated tests appears to be determined by both degradation (sintering) occurring during the experiment and initial particle size. As example, the final particle size of the 30% Pt/KB catalyst, characterized by high dispersion, is the smallest among the Pt/C series although a significant electrochemical degradation was registered for this catalyst. Thus, beside sintering, other phenomena (dissolution) may contribute to the performance loss.

The results related to the degradation behaviour of the most promising PtCo catalyst (50% PtCo/KB 7C) are reported in Figs. 5.7-5.9 and in Table 5.1. Electrode cycling show also for the PtCo catalyst an increase of the intrinsic activity and a decrease of the surface area with time as previously observed for Pt/C catalysts (Fig. 5.7). The effects of potential cycling and potential holding at 1.2 V on the performance are illustrated in Figs 5.8 and 5.9, respectively. It is observed that the carbon corrosion plays a more important effect than Pt degradation on the stability of PtCo/C catalyst on the contrary of Pt/C catalysts (Table 5.1). The increased stability of PtCo alloy versus Pt in the Tafel region probably modifies the degradation process of the bimetallic catalyst with respect to the carbon supported platinum.

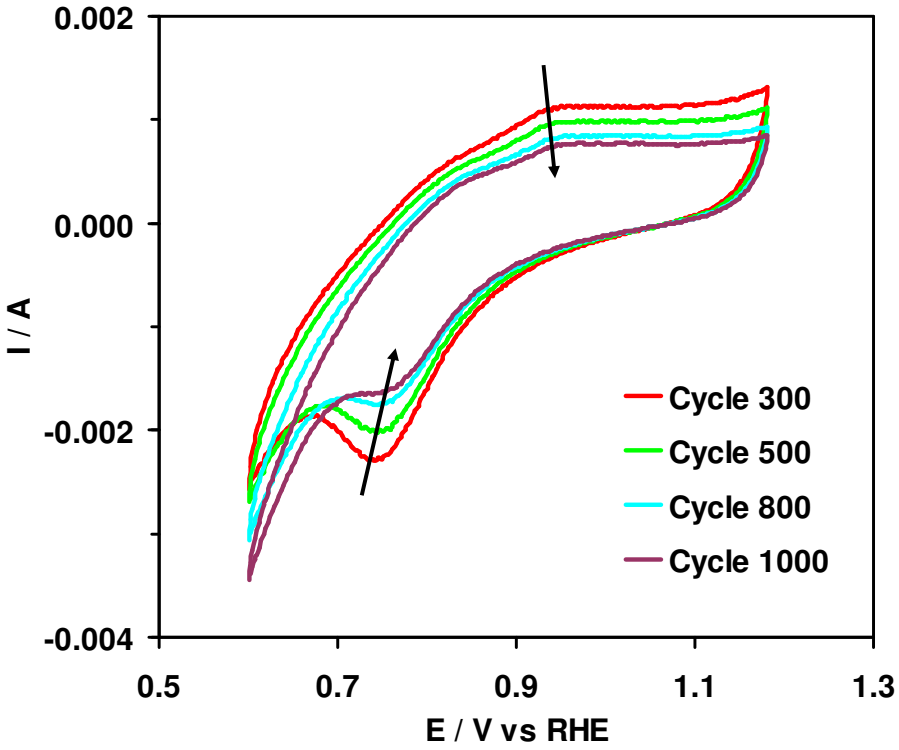

Fig. 5.7 Accelerated Pt degradation test of 50% PtCo/KB 7C: 1000 cycles at 75 °C; He feed; 0.5 M H_2SO_4.

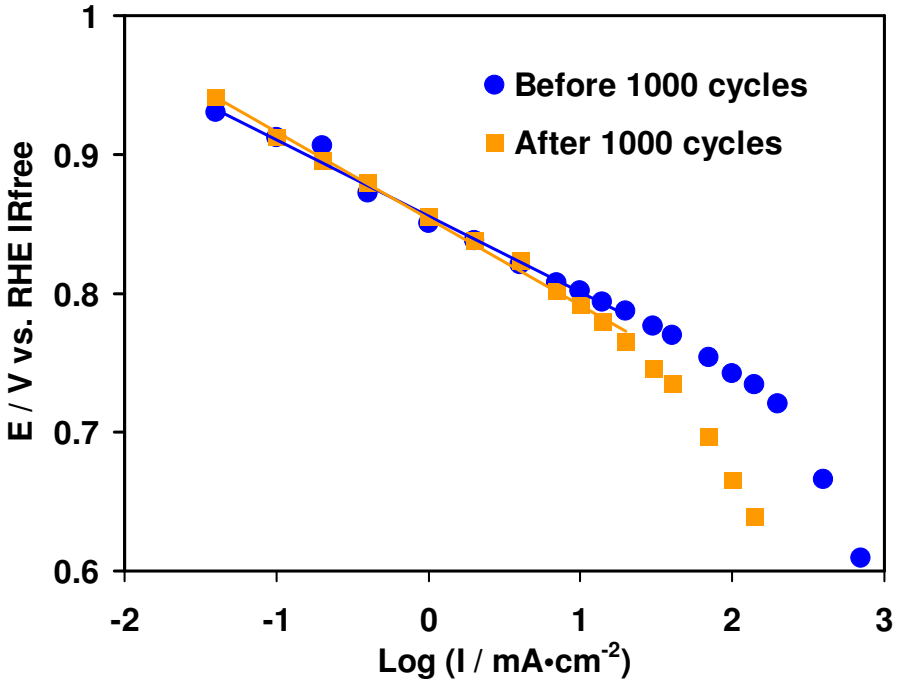

Fig. 5.8 Effect of potential cycling on the polarization behaviour of 50% PtCo/KB 7C. 0.5 M H_2SO_4; 75 °C, pure O_2.

A degradation is observed for PtCo catalyst in the mass transport controlled region, after potential cycling (Fig. 5.8); however, this effects may be due to electrode flooding with time.

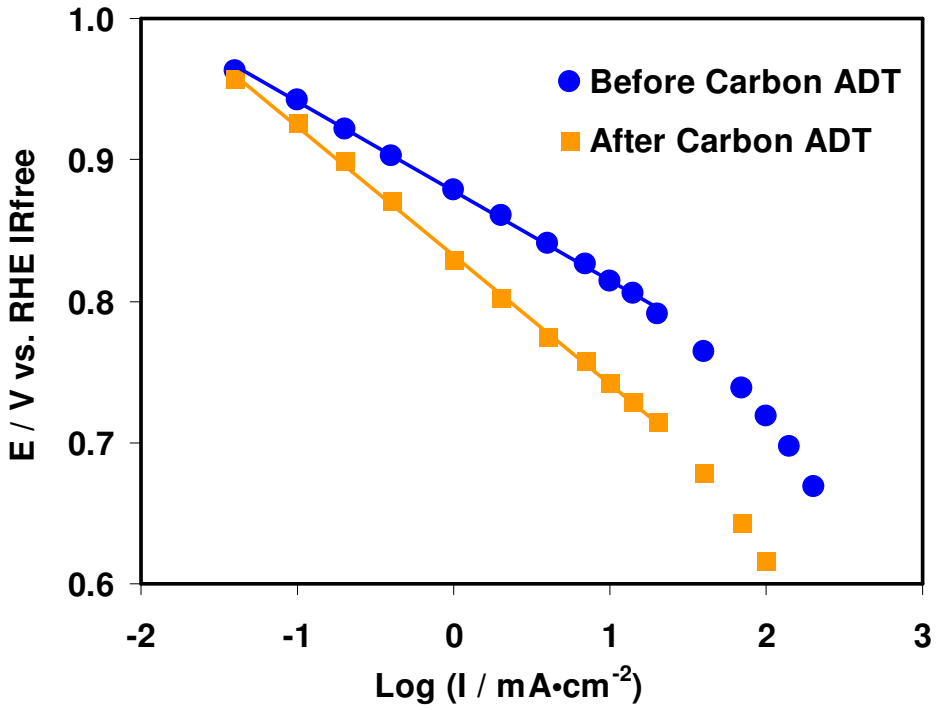

Fig. 5.9 Effect of potential holding at 1.2 V for 24 hrs on the polarization behaviour of 50% PtCo/KB 7C. 0.5 M H_2SO_4; 75 °C, pure O_2.

Table 5.1 Gas-fed half cell ADTs result.

1st series catalysts: degradation in sulphuric acid half cell

Catalyst	Potential Loss after Pt ADT (mV @ 1mAcm^{-2})	Potential Loss after C ADT (mV @ 1mAcm^{-2})	Particle Size after Pt ADT (nm)	Particle Size after C ADT (nm)
30% Pt/CV 1H	32	23	8.4	4.2
30% Pt/KB 2H	47	42	6.4	2.9
50% Pt/KB 3H	39	36	7.0	3.4
50% PtCo/KB 7C	≈0	50	5.0	7.0

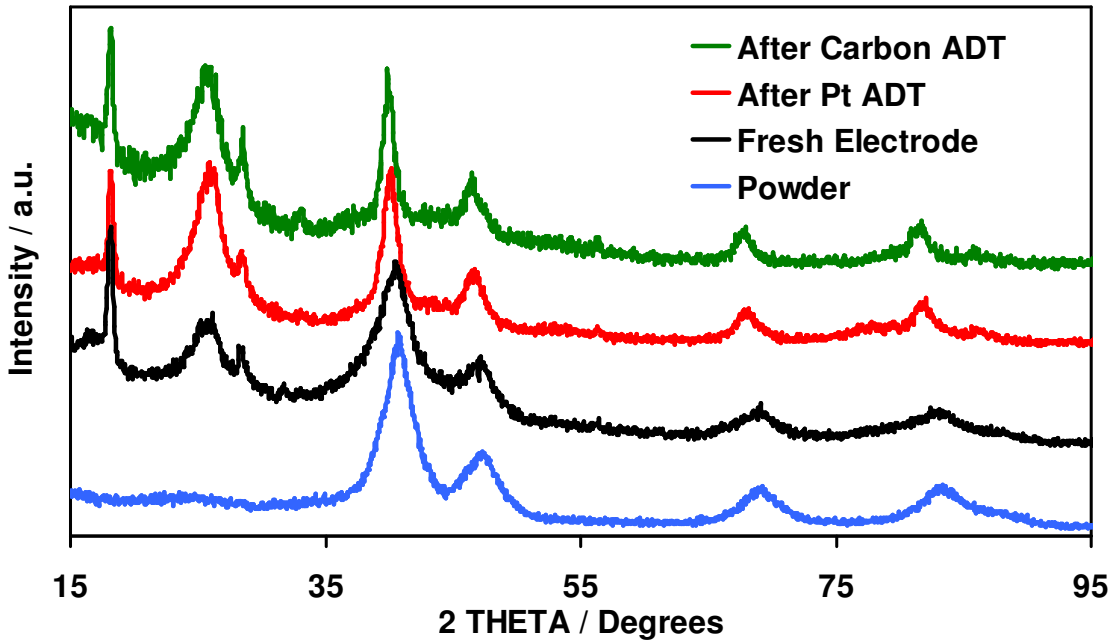

Fig. 5.10 XRD diffraction for 50% PtCo/KB 7C after electrode preparation, Pt and carbon accelerated degradation tests.

These results are confirmed by XRD analysis. An increase of particle size from 3 to 5 nm and 7 nm for 50% PtCo/KB 7C is observed after potential cycling (Pt degradation) and potential holding at 1.2 V (C corrosion) respectively (Fig. 5.10, Table 5.1). A partial dealloying occurs during Pt and carbon degradation tests as revealed by a shift in the fcc structure diffraction peaks to low Bragg angles (Fig. 5.10). Figure 5.10 also evidences that there is not a sintering effect after the electrode preparation with 50% PtCo/KB 7C (fresh electrode Fig. 5.10) on the contrary of the slight sintering effects recorded with first series of Pt/C catalysts (not shown).

5.3 Conclusions

Accelerated Pt corrosion tests for 1st series of Pt/C catalysts carried out in gas-fed half cell show that all catalysts are affected by Pt sintering; the particle size increases from two to three times after corrosion tests, Tafel analysis indicate about 30 mV loss in the activation region.

Accelerated Carbon support corrosion test for 1st series of Pt/C catalysts shows smaller potential loss with respect to Pt corrosion tests. Tafel analysis indicates in the latter case about 10-15 mV loss in the activation region.

The stability of PtCo in sulphuric acid after Pt accelerated degradation test is better than Pt/C. In fact for the PtCo catalyst, despite a sintering effect, the absence of significant degradation in the activation region results from a compensation effect between a large loss of surface area and an increase of intrinsic activity. A more higher degradation is observed only after carbon corrosion test. The stability of PtCo/KB is much better than Pt/KB but still not appropriate regarding the interaction with the support..

In order to achieve a proper stability, it would be necessary to replace the Ketjenblack with a more graphitic and lower surface area carbon black or graphite. In fact being the carbon corrosion (oxidation), the process controlling the degradation for the PtCo system this aspect can be addressed by a proper selection of the support.

References

1. A.S. Aricò, P.L. Antonucci, V. Antonucci, in: A. Wieckowski, E.R. Savinova, C.G. Vayenas (Eds.), Catalysis and Electrocatalysis at Nanoparticle Surfaces, Marcel Dekker, Inc., New York, 2003.K.
2. Kinoshita, Electrochemical Oxygen Technology, Wiley, New York, 1992.

6

1ST SERIES ELECTROCATALYSTS
- SINGLE CELL CHARACTERIZATION -

6.1 Introduction

The high temperature performance and stability of the first series catalysts in the presence of perfluorosulphonic membranes is evaluated in this chapter. The aim was to correlate these properties with the physico-chemical characteristics both in terms of electrocatalytic activity for oxygen reduction and resistance to degradation under fuel cell conditions. We have overcome the constraints related to the dehydration behaviour of the membrane at high temperature by pressurizing the PEM single cell and operating the humidifiers at the same temperature and pressure of the cell. Although, the operating conditions do not exactly reproduce those aimed by the automakers, i.e. ambient pressure and 25% relative humidity (R.H.) [1], the present approach may provide a basis to identify the high temperature degradation mechanism for conventional PEMFCs and alleviate through proper preparation procedures the performance loss.

6.2 Catalytic activity and degradation tests in single cell

It was observed in the sulphuric acid half cell studies reported in the previous Chapter that the among the Pt/C catalysts, the 30% Pt/CV 1H showed the best compromise in terms of stability and catalytic activity. The behaviour of 30% Pt/CV 1H catalyst was thus investigated in PEM-FC with hydrogen-air feed at 80 °C and 130°C (3 bar abs.) in the presence of commercial thin Nafion 112 membrane

(50 μm) and its stability was investigated by operating the PEMFC for 24 hrs at constant voltage of 0.7 V and 130 °C. During these experiments the PEM single cell was pressurized at 3 bar abs. and R.H. was 100%.

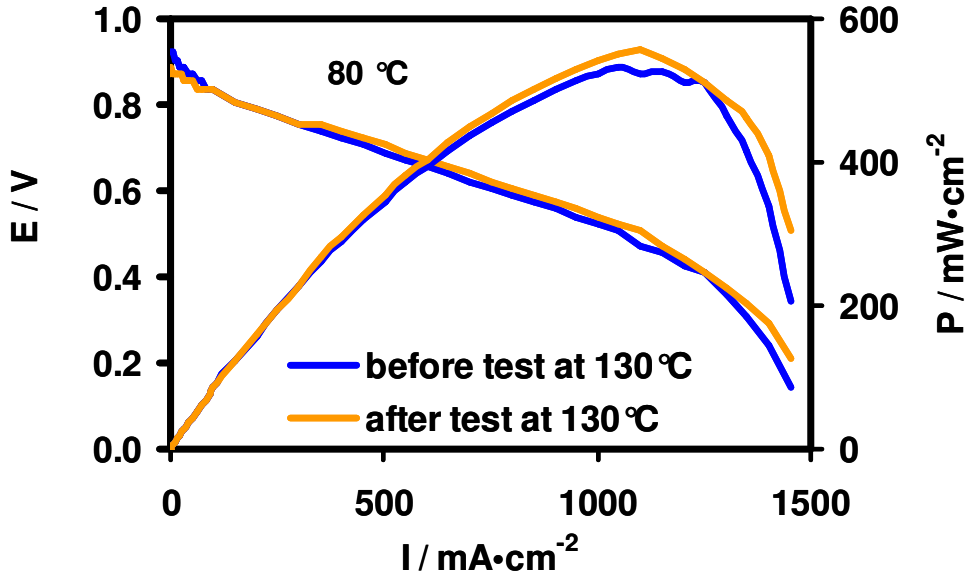

Fig. 6.1 Polarization and power density curves at 80 °C for a MEA based on 30% Pt/CV 1H, in the presence of N112 membrane, before and after operation at 130 °C for 24 hrs. Cathode: air feed, 3 bar abs..

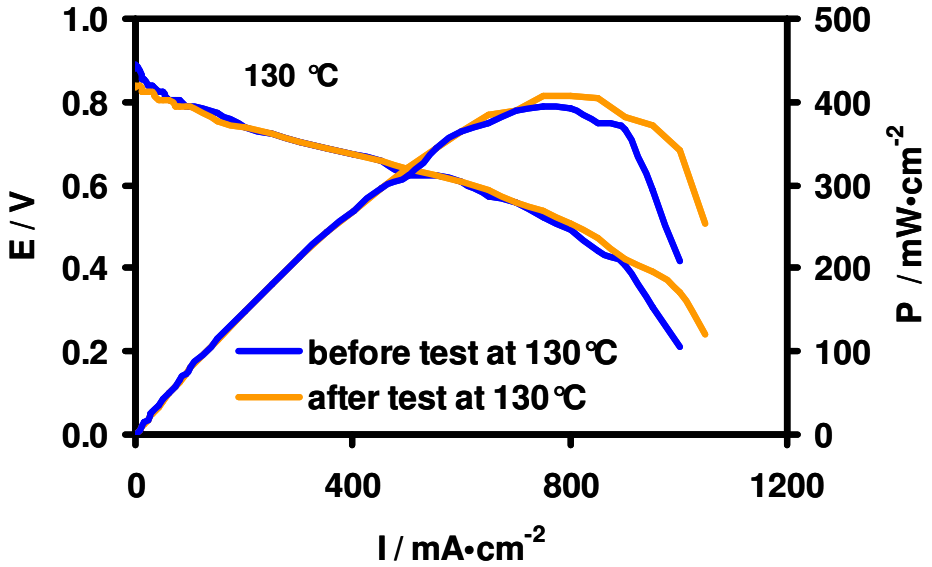

Fig. 6.2 Polarization and power density curves at 130 °C for a MEA based on 30% Pt/CV 1H, in the presence of N112 membrane, before and after operation at 130 °C for 24 hrs. Cathode: air feed, 3 bar abs..

The performances in single cell PEM FC at 80 °C (Fig. 6.1) and 130 °C (Fig. 6.2) are reported before and after a time test at 130°C for 24 hrs at a constant voltage of 0.7 V (not shown). It is observed a decrease of OCV and performance passing from 80° to 130° C. The decrease of OCV is related to the increase in membrane swelling at 130 °C. It should be also mentioned that this temperature is larger than the glass transition temperature of Nafion. The decrease of OCV is also observed at 80 °C after operation at 130 °C. A small limiting current density was recorded at 130°C than at 80 °C. Ac-impedance spectroscopy analysis (Figs. 6.3 and 6.4) did not reveal a significant increase in resistance if proper pressure and humidification conditions were selected at 130 °C. The average series resistance increased from 0.16 to 0.18 ohm cm^2 as the temperature increased from 80° to 130 °C. On the other hand, a significant increase of the charge transfer resistance at 130 °C with respect to 80 °C was recorded even at high cell potentials where mass transport is not a limiting step.

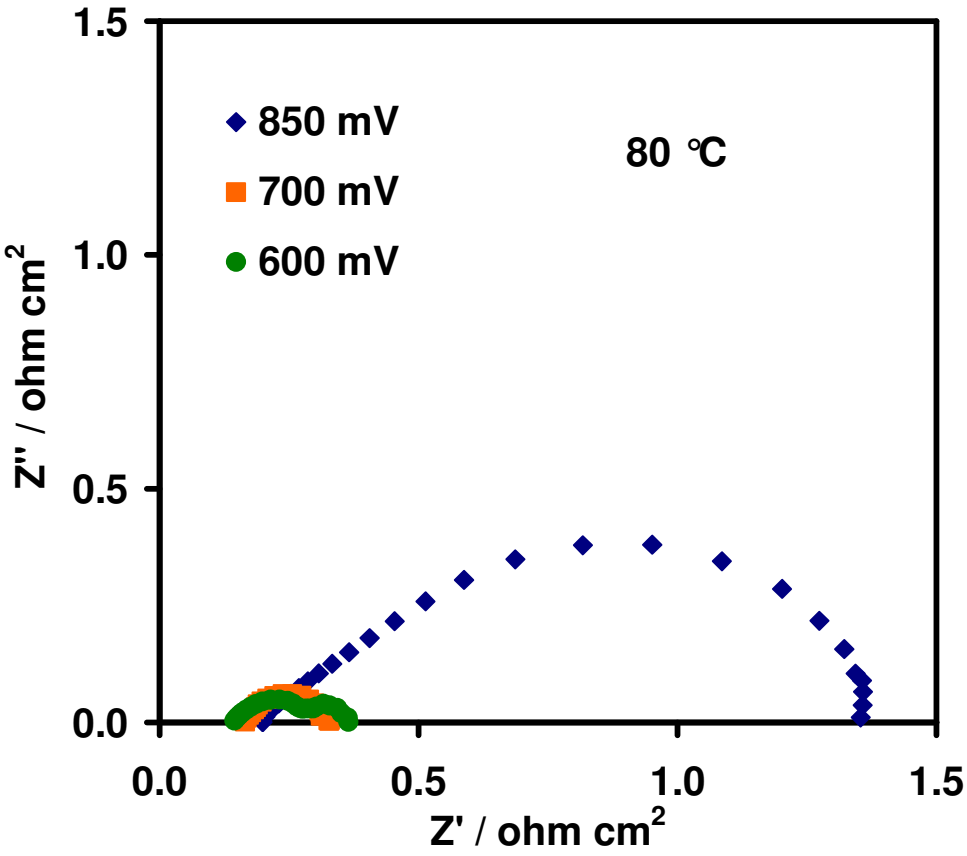

Fig. 6.3 Electrochemical impedance spectra collected during operation at 80 °C for a MEA based on 30% Pt/CV 1H, in the presence of N112 membrane. Cathode: air feed, 3 bar abs

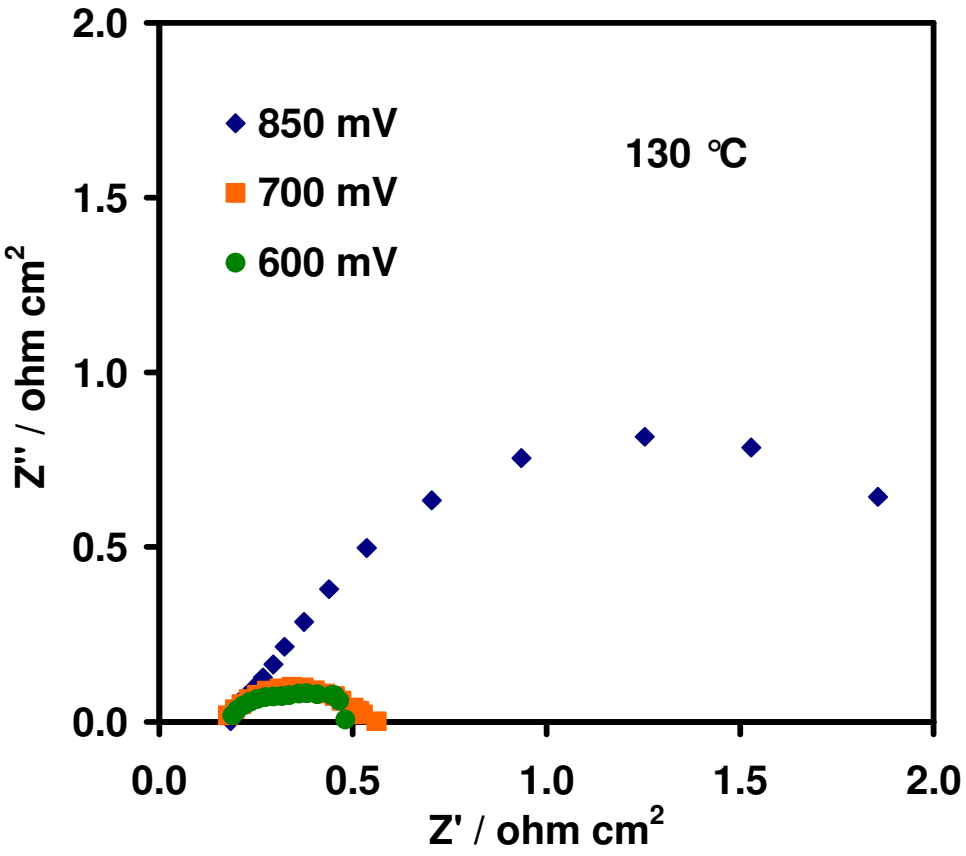

Fig. 6.4 Electrochemical impedance spectra collected during operation at 130 °C for a MEA based on 30% Pt/CV 1H, in the presence of N112 membrane. Cathode: air feed, 3 bar abs.

This indicates an increase of the activation control that is possible related to a decrease of oxygen solubility at the electrode-electrolyte interface with the temperature.

The kinetic results in sulphuric acid half cell are compared with PEM single cell (Fig. 6.5) for the 30% Pt/CV 1H. A similar Tafel slope is observed at low temperature indicating a similar mechanism. Unfortunately, at high temperature the effect of hydrogen cross over limits significantly the catalytic activity of the electrode close to 0.9 V in the PEM single cell and also causes a modification of the slope (Fig. 6.5). In order to reduce the effects of cross-over, a thicker membrane i.e. Nafion 115 (100 μm) was selected. It was observed an increase of OCV but also a significant increase of the ohmic resistance especially at 130 °C (not shown) due to humidification constraints.

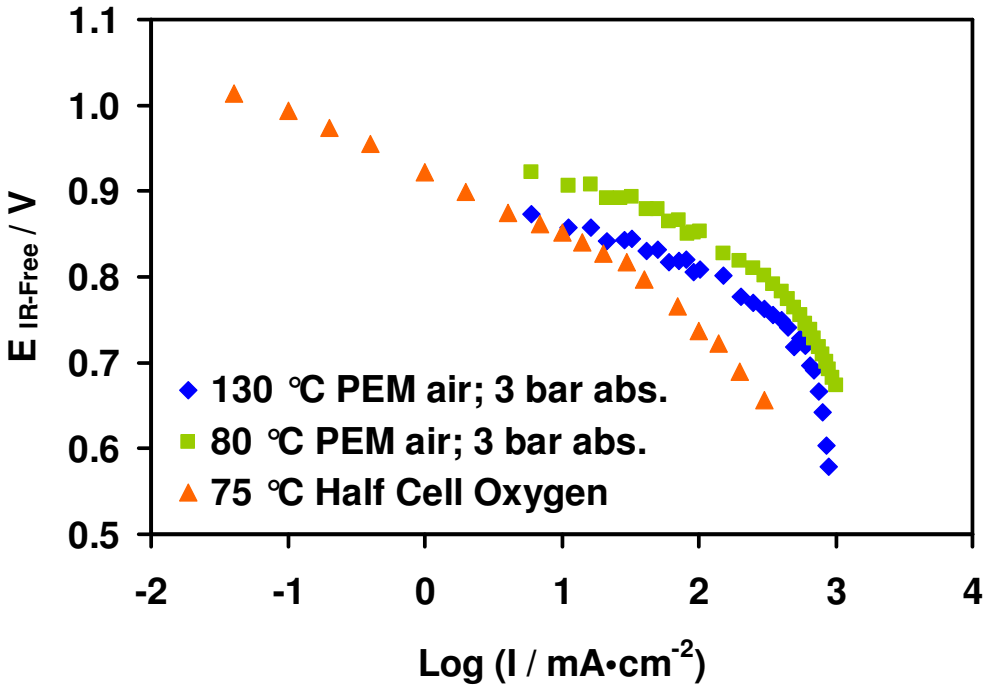

Fig. 6.5 Comparison of IR-free polarization curves for oxygen reduction in sulphuric acid half cell and PEM FC for the 30% Pt/CV 1H catalyst. Conditions are indicated in the figure.

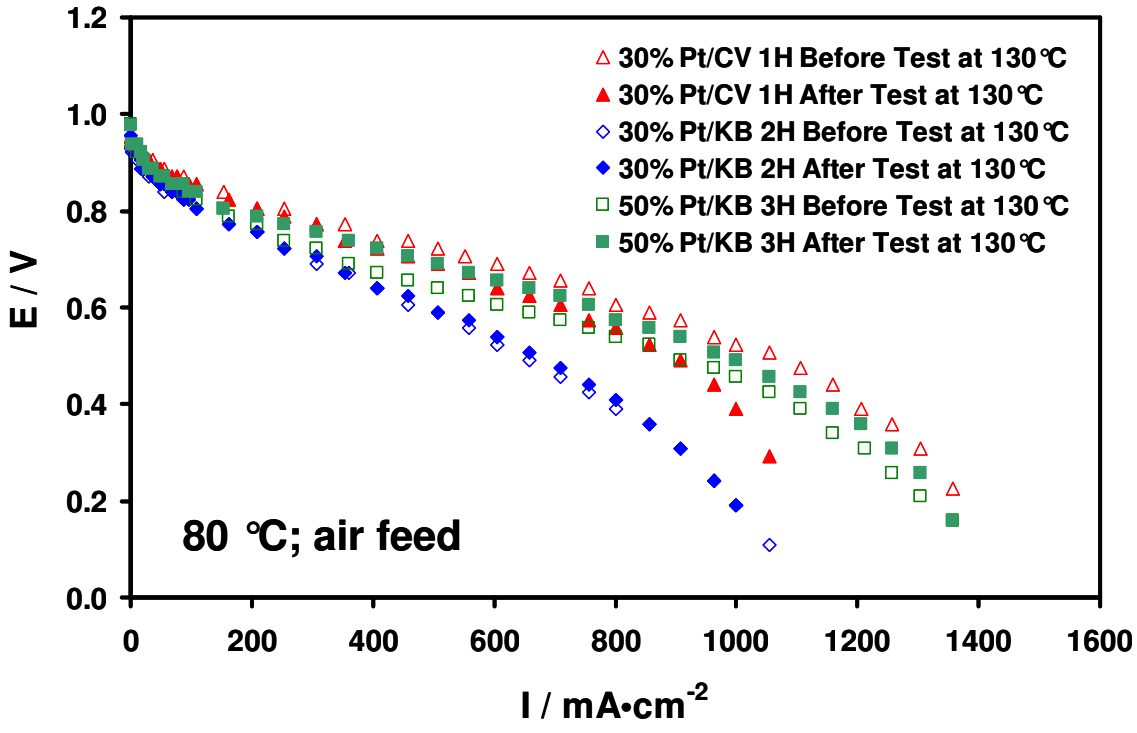

Fig. 6.6 Comparison of the polarization bevaviour for the various catalysts in the presence of Nafion 115 membrane before and after operation at 130 °C.

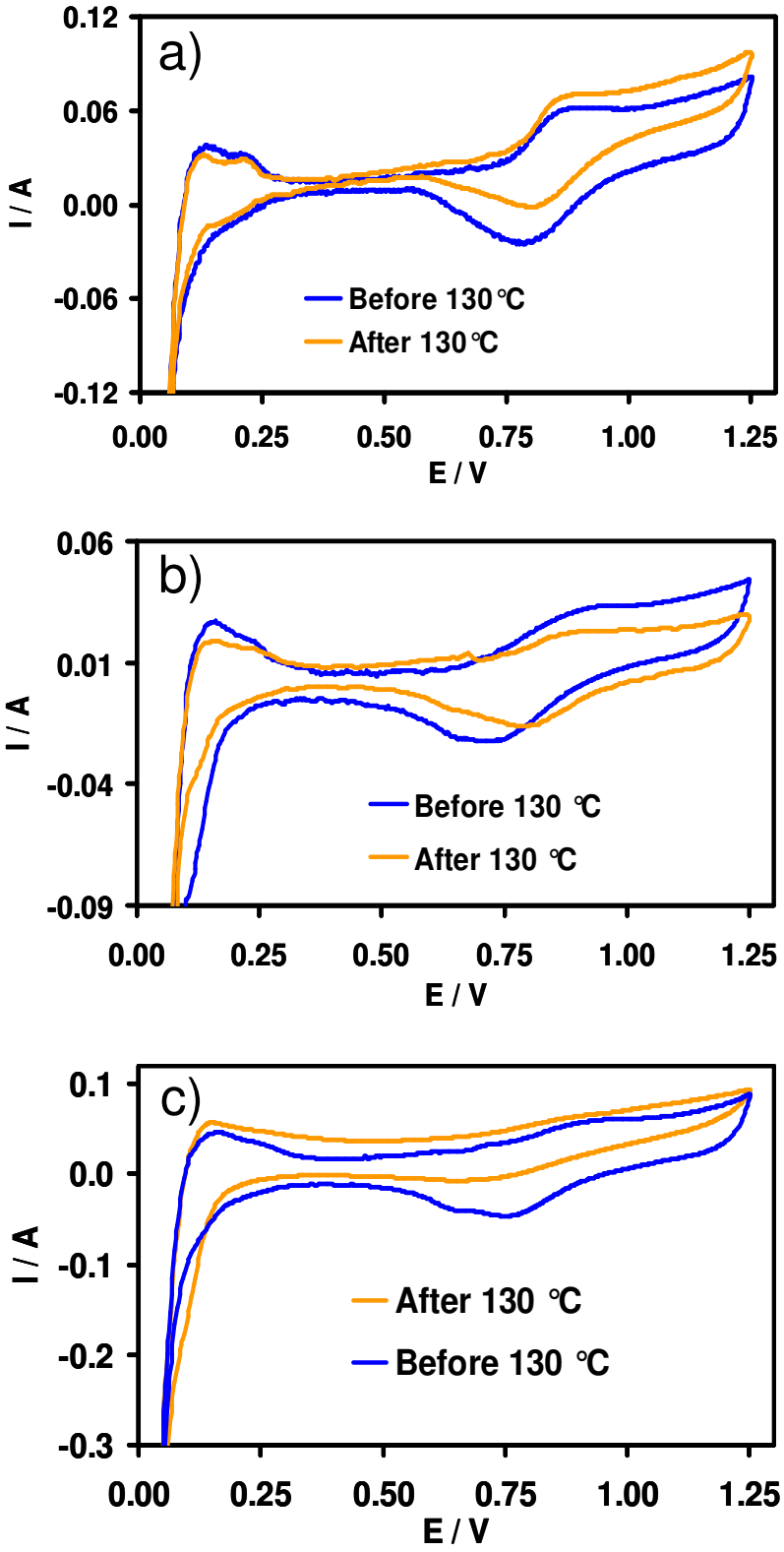

Fig. 6.7 a-c Comparison of the CV profiles (20 mV/s) for the: (a) 30% Pt/CV 1H catalyst; (b) 50% Pt/KB 3H catalyst; (c) 30% Pt/KB 2H catalyst; in the presence of Nafion 115 membrane before and after operation at 130 °C.

By comparing at 80 °C the polarization behaviour of the Pt/C catalysts before and after operation at 130 °C with Nafion 115 (Fig. 6.6), it is observed that the performance before high temperature operation follows a trend similar to that recorded in sulphuric acid in half cell. Interestingly, after operation at 130 °C, the 50% Pt/KB 3H catalyst increases its performance and surpasses that of 30% Pt/CV 1H (Fig. 6.6). The latter showed a slight decrease of activity that was not previously observed with the thin membrane. These results were interpreted on the basis of electrochemical active surface area (ECSA) changes after high temperature operation (Figs. 6.7 a-c). The CV profiles showed a shift of the Pt-oxide reduction peak towards high potentials and a positive slope as a function of the potential in the double layer region. The latter indicates the presence of strong hydrogen cross-over (no diluted hydrogen was used at the anode/counter electrode).

The ECSA decreases from 51 to 39 m^2/g for 30% Pt/CV 1H after 130 °C operation; a decrease from 72 m^2/g to 51 m^2/g is observed for 50% Pt/KB 3H; an anodic shift of the peak potential for Pt-oxide reduction to high potentials indicates an increase in specific activity after operation at 130 °C due to Pt sintering. A change in the physicochemical properties is observed in the CV profile of the 30% Pt/CV 1H. The final ECSA for this catalyst is close to 115 m^2/g. Possibly, the best compromise for these catalysts in terms of specific activity and number of Pt sites available for the reaction corresponds to a ECSA value close to 50 m^2/g. Thus, this explain why the performance of the 50% Pt/KB 3H increases when the surface area decreases from 72 to 51 m^2/g. Such analysis also explains why the performance of the 30% Pt/KB 2H is poor. This is the consequence of low specific activity for a very high surface area catalyst. It is pointed out that all data were not corrected for hydrogen cross-over; thus, the absolute value of the ECSA for these catalysts may be slightly different from those estimated. For carbon supported catalysts, mass activities slightly better than 100 A/g under air feed and without correction for hydrogen cross-over were recorded at 130°C, 0.9 V for 30% Pt/CV 1H and 50% Pt/KB 3H before and after operation at 130°C, respectively. Finally, the CVs profile (Fig. 6.7 a-c) showed a slight change of the double layer (see Fig. 6.7c) and in the profile (see Figs. 6.7 b-c; upper current line between 0.50 – 0.75 V). These could be due to a carbon corrosion effect especially for the

Ketjenblack support. The support corrosion could be attributed to operative condition (constant voltage of 0.7 V for 24 hrs at 130 °C) or to the fact that during the CVs analysis cathode side were holding above to 1.0 V for 25 s per cycle (s. r. = 20 mV s^{-1}; CV upper limit 1.25 V).

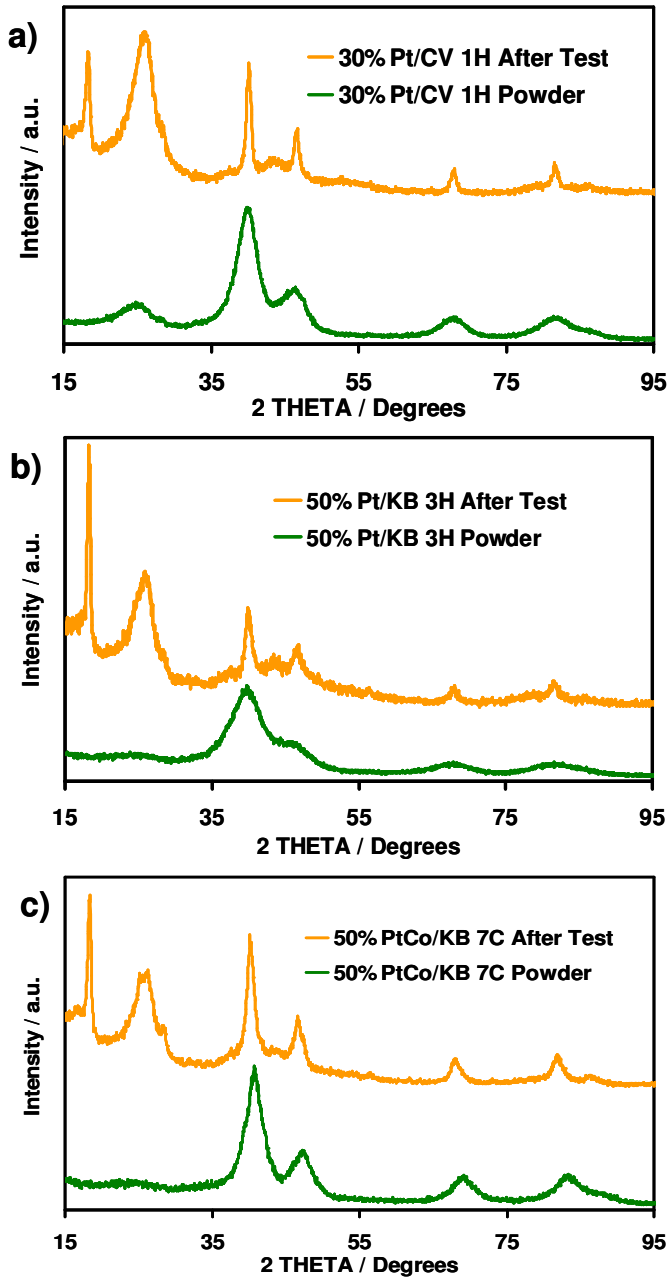

Fig. 6.8 a-c X-ray diffraction patterns of the Pt/C and Pt/Co catalysts after a Pt degradation test of 1000 cycles between 0.6 and 1.2 V vs. RHE in PEMFC at 130 °C. a) 30% Pt/CV 1H; b) 50% Pt/KB 3H; c) 50% PtCo/KB 7C.

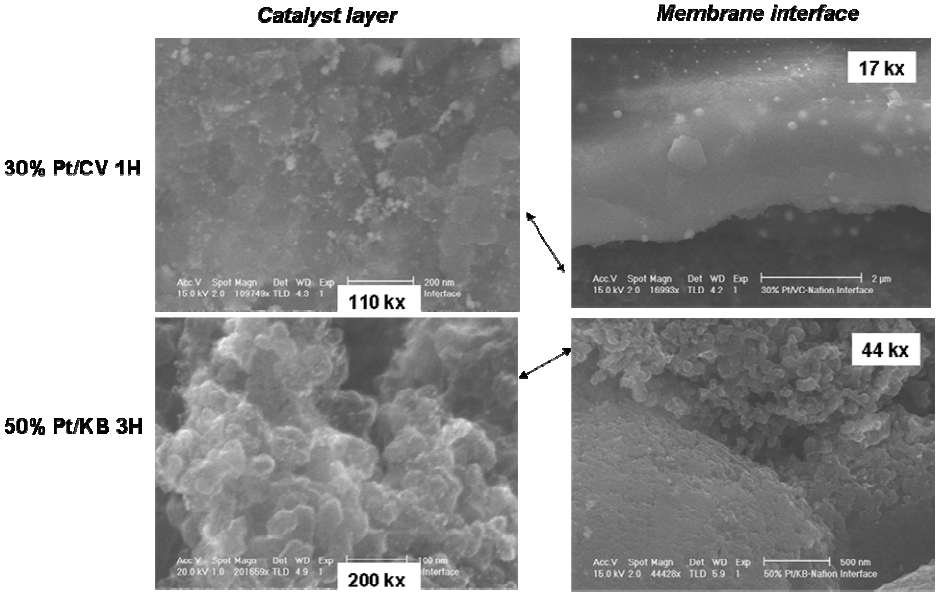

Fig. 6.9 SEM micrographs of cathode layer and cathode/membrane electrolyte interface for 30% Pt/CV 1H and 50%Pt/KB 3Hcatalysts after a degradation test of 1000 cycles between 0.6 and 1.2 V vs. RHE in PEMFC at 130°C. The magnification of the interface is larger for 50% Pt/KB 3H than 30% Pt/CV 1H.

On the contrary of sulphuric acid half cell, accelerated tests carried out in PEM single cells at 130 °C showed that the 50% Pt/KB 3H was more stable than 30% Pt/CV 1H with respect to sintering by using the same cycling procedure. This was confirmed by both XRD and SEM analyses. As an example, XRD patterns before and after 1000 cycles at 130 °C between 0.6 and 1.2 V (see Fig. 6.8 a-c), show slightly larger sintering for 30% Pt/CV 1H (see Fig. 6.8 a) than 50% Pt/KB 3H (see Fig. 6.8 b) (particle size 12 nm vs. 8 nm).

The lower degradation of the 50% Pt/KB 3H catalyst with respect to the 30% Pt/CV 1H catalysts is probably associated to the high surface graphicity index of Ketjenblack and anchoring effect of Pt particles to the support surface as a consequence of better metal-support interaction [2]. It is derived that the corrosion mechanism in sulphuric acid liquid electrolyte and in PEMFC are not exactly the same. These effects were confirmed by the investigation of the membrane-electrode interface after potential cycling at 130 °C (Fig. 6.9). It was observed a significant dissolution and growth of Pt particles in the membrane for 30% Pt/CV 1H than 50 % Pt/KB 3H. In

the latter case, observation at larger magnification indicated a much smaller amount of Pt particles in the membrane.

The performances of 50% Pt/KB 3H and 50%PtCo/KB 7C catalysts were compared in the presence of Nafion 112 membrane at 80 °C at low pressure with 1 bar abs. O_2 and at 130 °C with high pressure, with 3 bar abs. O_2 (Fig. 6.10 a-b).Oxygen feed was preferred in these test to counteract the effects of cross-over that may alter the comparison. The performance of 50% PtCo/KB 7C slightly increases passing from 80° to 130 °C as opposite of 50% Pt/KB 3H. In the latter case the performance did not vary significantly with the temperature. Whereas, it was shown above that the performance of the 30% Pt/CV 1H decreased significantly with the temperature. The increase of power density with the temperature for PtCo is possibly associated to surface modifications occurring upon high temperature operation. It should be mentioned that the PtCo catalyst was not pre-leached. Such aspects will be investigated more in-depth in the next Chapter 7.

The XRD patterns of 50% Pt/KB 3H and 30% Pt/CV 1H catalysts after 1000 cycles at 130 °C between 0.6 and 1.2 V were already compared in Figure 6.8 b-c. This figure also show the pattern of 50% PtCo/KB 7C catalyst after the same degradation test (see Fig. 6.8 c). The better stability of 50% PtCo/KB 7C catalyst over Pt/C catalysts, observed in sulphuric acid after potential cycling, was confirmed by PEM studies at 130 °C. The final particle size of 50% PtCo/KB 7C after 1000 cycles at 130 °C was 6 nm as compared to 8 and 12 nm for 50% Pt/KB 3H and 30% Pt/CV 1H, respectively.

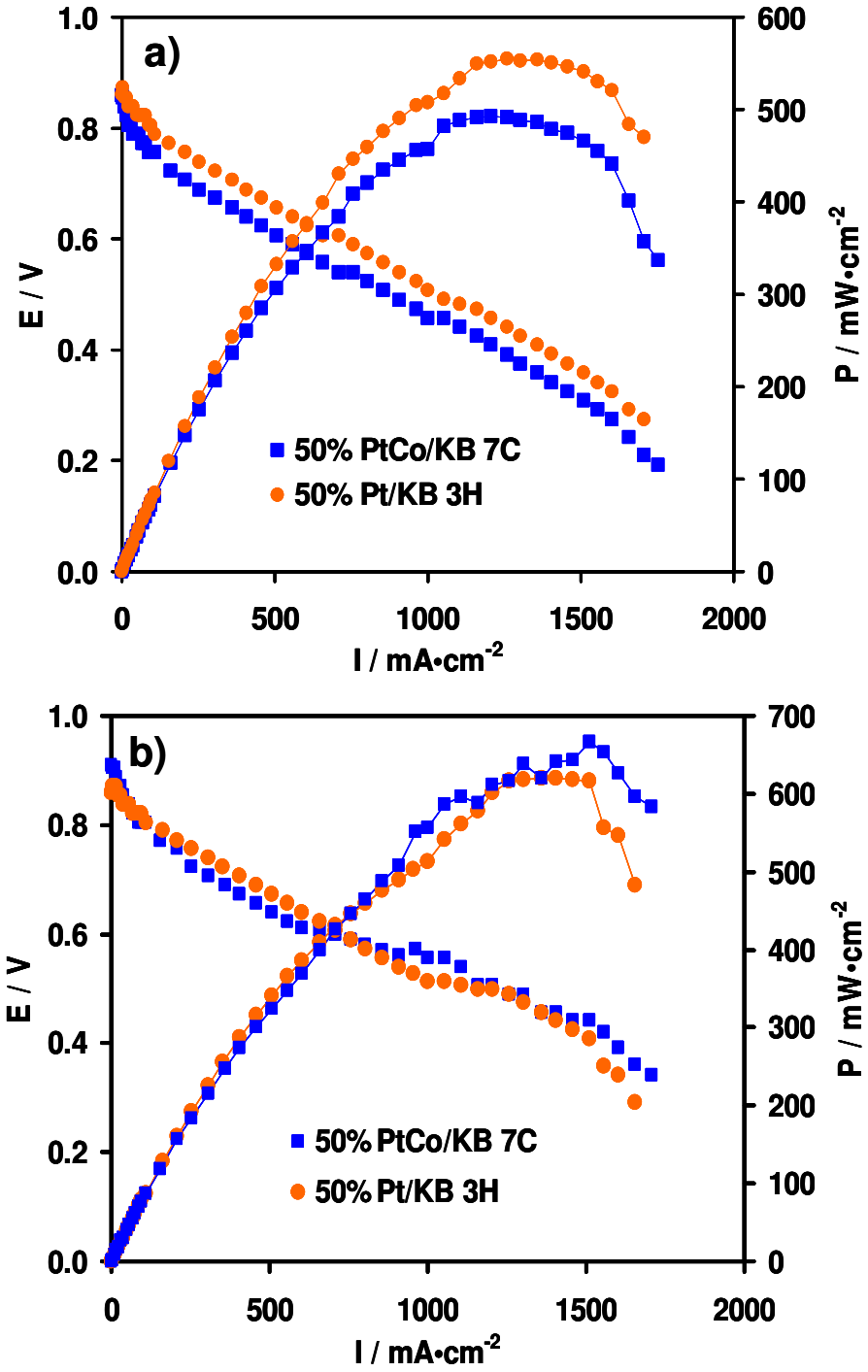

Fig. 6.10 a-b PEMFC polarization curves for 50% Pt/KB 3H and 50% PtCo/KB 7C catalysts in the presence of Nafion 112 membrane (a) at 80 °C at low pressure with 1 bar abs. O_2 pressure and (b) at 130 °C with high pressure 3 bar abs. O_2.

6.3 Conclusions

Single cell PEM analysis indicates that significant changes in the Pt electrochemical active surface area may occur after a short period of operation at 130 °C in the presence of humidification constraints. The corresponding performance changes reflect both the actual specific activity and number of sites available for the reaction. A slight sintering of nanosised Pt particles may produce an increase of performance with respect to the initial characteristics in some catalysts due to the increase in specific activity. Power densities of about 400 $mWcm^{-2}$ at 130 °C were achieved in a PEMFC with 0.3 mg cm^{-2} Pt loading, air feed and Nafion 112 for Pt/C catalysts. Mass activity of about 100 A/g Pt at 130°C, 0.9 V, air feed (3 bar abs.) has been obtained in the presence of Nafion 112 membrane without correction for hydrogen cross-over. The power density increases to about 700 mW cm^{-2} at 130 °C, 0.3 mg cm^{-2} Pt loading, in the presence of oxygen feed (3 bar abs.) and especially with PtCo catalyst.

Accelerated Pt degradation tests (cycling) show that all catalysts are affected by Pt sintering; the particle size increases from two to three times after the tests. As well as observed in tests carried out in sulphuric acid, even in PEMFC it is derived that the carbon corrosion plays the major role on the degradation of the PtCo system. The stability of PtCo in both sulphuric acid and PEM after potential cycling is better than for Pt/C catalysts.

References

1. H. A. Gasteiger, S. S. Kocha, B. Sompalli, F. T. Wagner, Appl. Catal. B Environ., 56 (2005) 9.
2. A.S. Aricò, P.L. Antonucci and V.Antonucci, in: Catalysis and Electrocatalysis at Nanoparticle Surfaces ed. by A.Wieckowski, E. R. Savinova, C. G. Vayenas, Marcel Dekker, Inc New York 2003.

7

INVESTIGATION OF PRE-LEACHING METHODS

7.1 Introduction

In this Chapter, an evaluation of the influence of pre-leaching methods is reported. The gas-fed half cell studies performed on the second series electrocatalysts developed during the third year of this Ph.D. activity, will be discussed. Accelerated degradation tests were carried out in an acid electrolyte solution (0.1 M H_2SO_4) and at temperature of 75 °C for all experiments. Both acid concentration and temperature were lower than in the pre-leaching treatments. For a proper comparison between the PtCo/KB catalysts and Pt/KB a new electrocalyst (50% Pt/KB 4C) was developed with the aim to obtain a similar particle dimension (see Table 4.1).

7.2 Catalytic activity and degradation tests in half cell

The polarization curves for the oxygen reduction at 75 °C are reported in Fig. 7.1. The catalyst pre-leached with $HClO_4$ showed the best performance in the activation-controlled region (lower current density range). The Tafel slope was about 60 mV dec^{-1} for all catalysts indicating a similar oxygen reduction mechanism. In the diffusion controlled region the untreated catalyst showed better characteristics. The wetting behaviour of the catalytic layer plays a significant role in this region due to the occurrence of flooding effects.

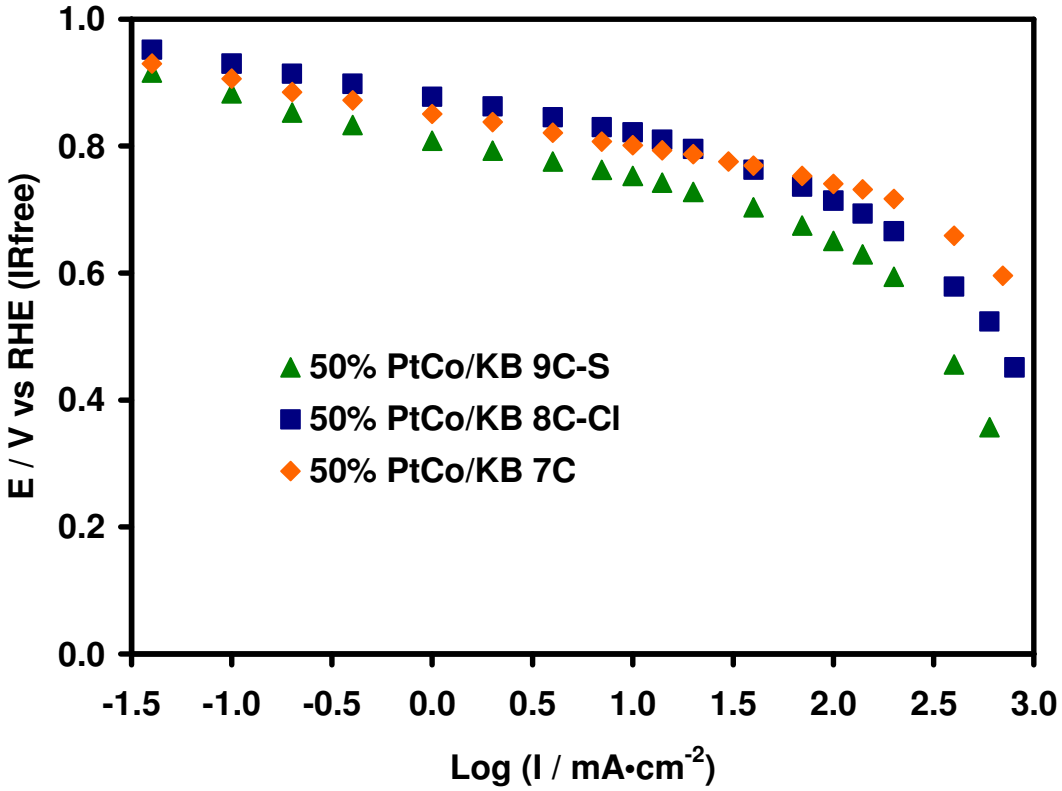

Fig. 7.1 Effect of leaching treatment on the Tafel plots for oxygen reduction of the 2nd series PtCo/C catalysts in sulphuric acid: 0.1 M H_2SO_4; 75 °C; pure O_2.

Fig. 7.2 shows a comparison of the best performing 50% PtCo/KB 8C-Cl catalyst and the 50% Pt/KB 4C catalyst with similar crystallite size in term of polarization curves. The performance of the PtCo catalyst is better in the overall range of current densities.

As discussed before (section 3.4), two accelerated test procedures were selected to evaluate catalyst stability in the electrochemical gas-fed half cell at 75 °C in 0.1 M H_2SO_4. The Pt (PtCo) sintering was investigated by continuous cycling in the presence of an inert gas between 0.6 V and 1.2 V vs. RHE.

The carbon corrosion was evaluated applying a constant potential of 1.2 V RHE for 24 hrs. For the Pt (PtCo) degradation analysis, 1000 cycles, based on triangular sweeps, between 0.6 V and 1.2 V RHE with a scan rate of 20 mV s^{-1} were carried out in He at 75 °C.

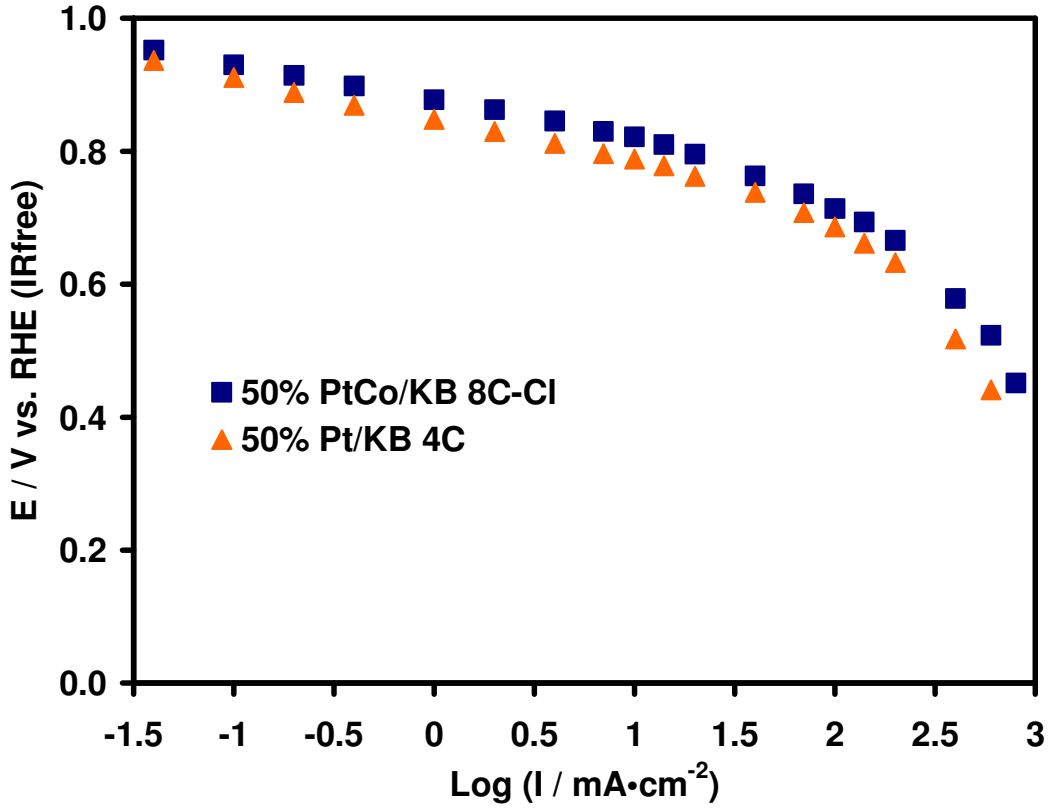

Fig. 7.2 Comparison of the oxygen reduction behaviour for the PtCo/KB pre-leached in $HClO_4$ and a 50% Pt/KB 4C catalyst: 0.1 M H_2SO_4; 75 °C; pure O_2.

Figure 7.3 shows some selected cycles registered for the 50% PtCo/KB 8C-Cl catalyst pre-leached in $HClO_4$ during this test. As recorded for the first series catalysts (see Chapter 5), it was possible to observe also for the 2nd series catalysts a shift to high potentials for the oxygen reduction peak (0.75 – 0.8 V RHE) and a decrease in intensity. These effects were attributed to an increase of specific activity for the oxygen reduction reaction due to the increase of particle size (sintering) [1] and a reduction of the electrochemically active surface area (ECSA) [2], respectively. Both properties (surface area and intrinsic activity) determine the mass activity for the oxygen reduction process [1].

In the CV profile of 50% PtCo/KB 8C-Cl (Fig. 7.4), an increase of the double layer capacitance was recorded after the Pt degradation test. This effect was clearly attributed to an increase of the functional groups on carbon black support due to a carbon surface modification.

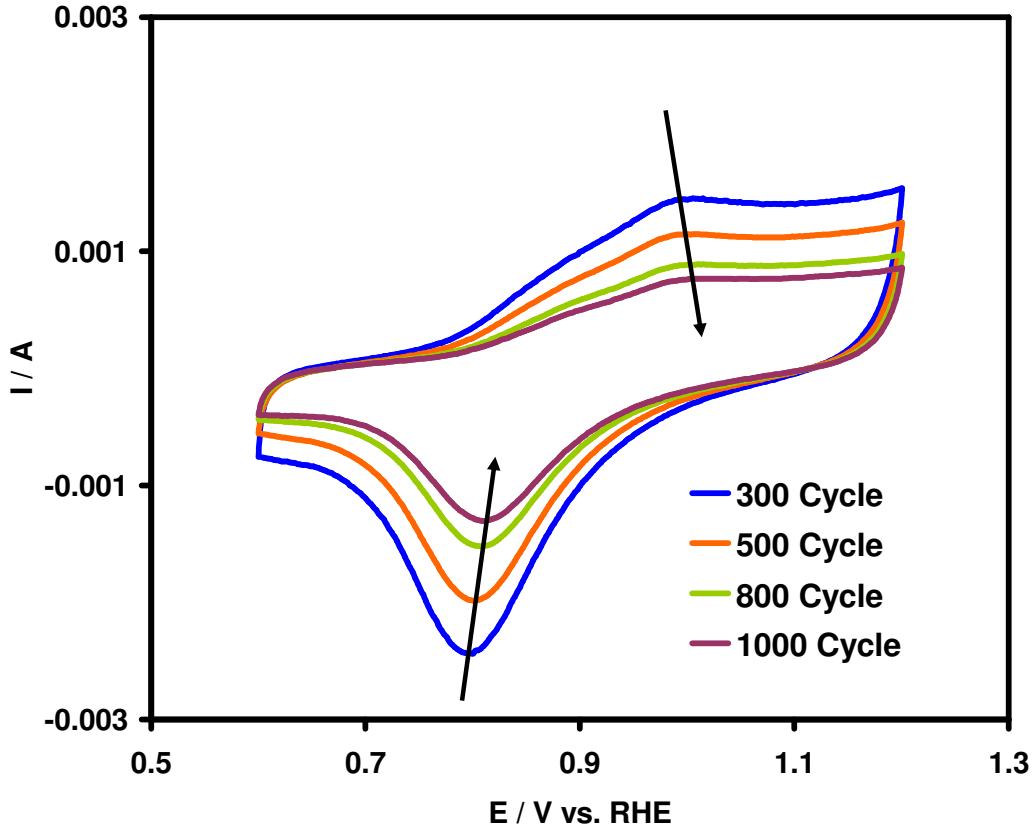

Fig. 7.3 Accelerated Pt degradation test for 50% PtCo/KB 8C-Cl pre-leached in $HClO_4$: 1000 cycles at 75 °C, He, in 0.1 M H_2SO_4.

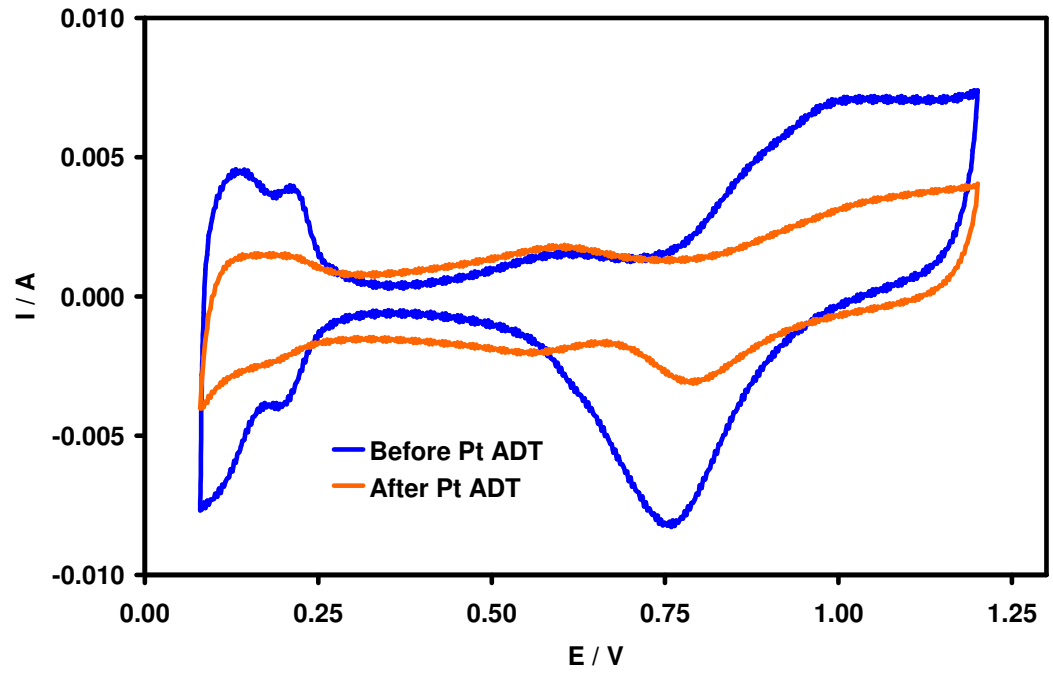

Fig. 7.4 Cyclic voltammetry of 50% PtCo/KB 8C-Cl pre-leached in $HClO_4$ electrode before and after Pt degradation test (s. r. = 50mVs^{-1}, 75 °C, He, 0.1 M H_2SO_4).

It was also possible to observe a reduction of the active area as indicated by the decrease in the intensity of the hydrogen adsorption-desorption peaks (0-0.4 V RHE). The electrochemical active surface area (ECSA) decreased of about 55% from 55 to 25 m^2/g. A similar trend was recorded with the other catalysts (not shown).

Figure 7.5 a-c shows the Tafel curves obtained before and after the Pt (PtCo) degradation test for the various catalysts. For the $HClO_4$ pre-leached and unleached catalysts no significant losses were recorded in the activation-controlled region; whereas, for the sulphuric acid pre-leached catalyst, a loss of about 80 mV was recorded at a low current density of 1 mA/cm^2. This different behaviour recorded with sulphuric acid pre-leached catalyst could be attributed to a poisoning effect due to a strong sulphate adsorption on the active sites of Pt as a consequence of the high temperature treatment in concentrated sulphuric acid (see section 4.2). However, for the other two catalysts, despite a sintering effect, the absence of significant degradation in the activation region results from a compensation effect between a large loss of surface area and an increase of intrinsic activity. At high currents a decrease of catalytic activity was recorded for all catalysts. This effect is mainly attributed to an electrode flooding with time that could increase the oxygen mass transport constraints. A similar degradation test was carried out for the 50% Pt/KB 4C catalyst (Fig. 7.6). After the potential cycling, the observed degradation was significantly larger for the 50% Pt/KB 4C as compared to the 50% PtCo/KB 8C-Cl preleached in $HClO_4$.

The effects of potential holding at 1.2 V on the performance of the 50% PtCo/KB 8C-Cl catalyst is illustrated in Fig. 7.7. The same trend was recorded for the other catalysts. It is observed that the carbon corrosion plays a more important effect than the Pt degradation (electrode cycling) on the stability of the catalysts [3,4]. Accordingly with the studies reported in Chapter 5, for the PtCo catalysts the accelerated tests (electrode cycling between 0.6 and 1.2 V and potential holding at 1.2 V) indicate that the effect of the carbon support on the degradation is predominant; thus, most of the efforts should be concentrated on this aspect to ameliorate the catalyst stability. Alternatively, since the carbon corrosion is essentially promoted by high electrochemical potentials, long time stack operation under conditions such as open circuit voltage, should be avoided. However, since an increase of cell potential at a

defined current density is associated to an improvement of electrical efficiency, the search for stable catalyst supports is mandatory.

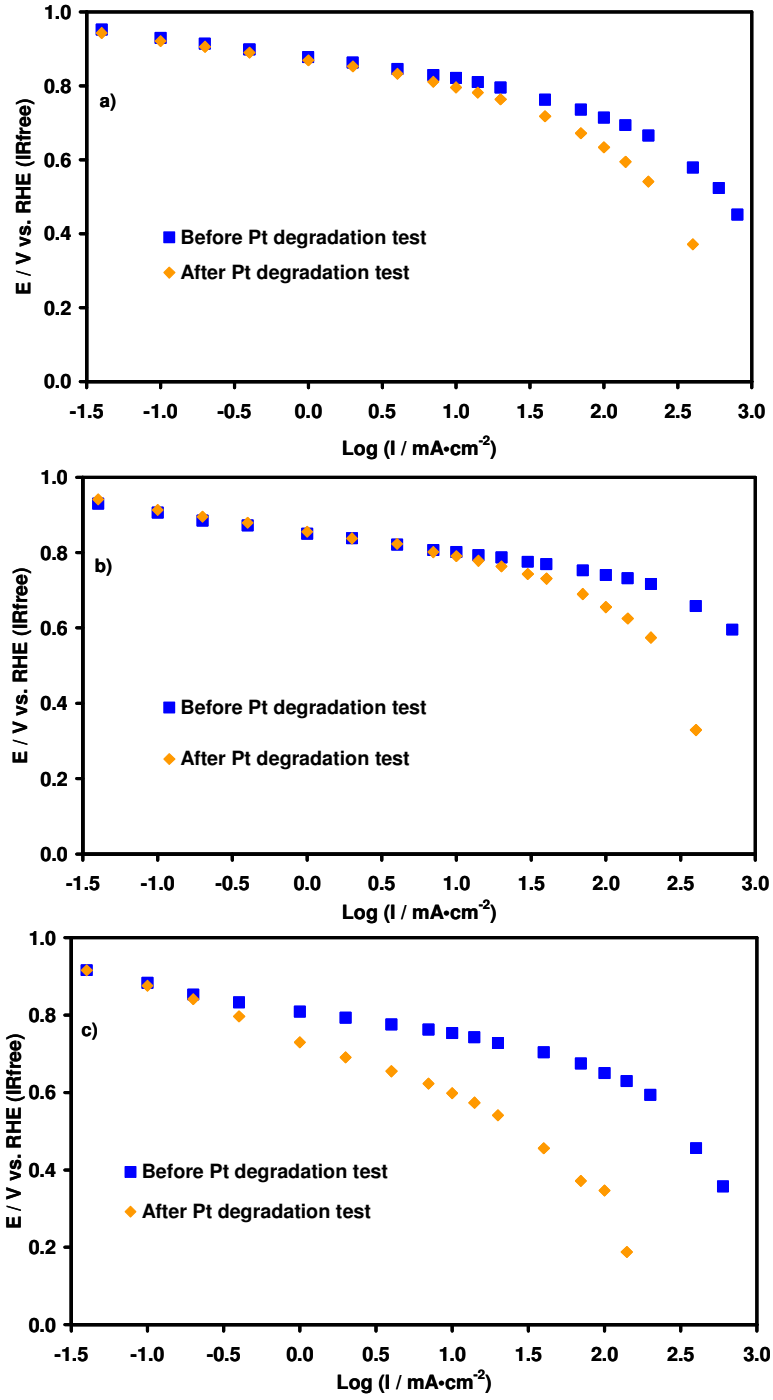

Fig. 7.5 a-c Effect of electrode cycling on the polarization behaviour for oxygen reduction of the 2nd series of PtCo/C catalysts. 0.1 M H_2SO_4; 75 °C.
a) 50% PtCo/KB 8C-Cl; b) 50% PtCo/KB 7C; c) 50% PtCo/KB 9C-S.

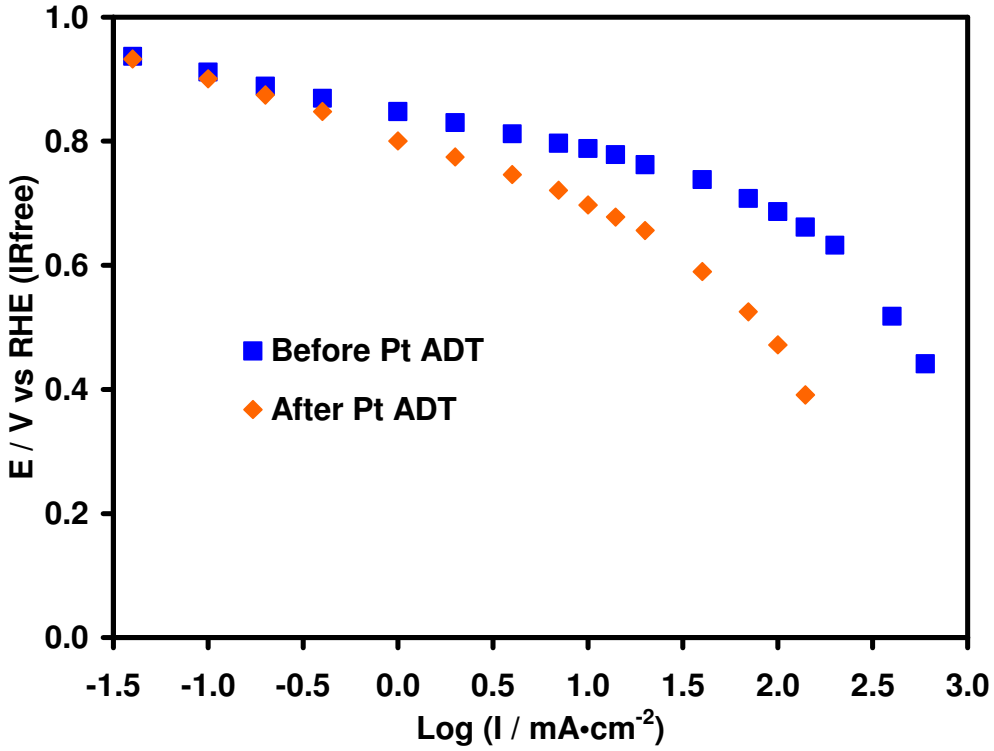

Fig. 7.6 Effect of electrode cycling on the polarization behaviour for oxygen reduction of the 50% Pt/KB 4C catalyst. 0.1 M H_2SO_4; 75 °C.

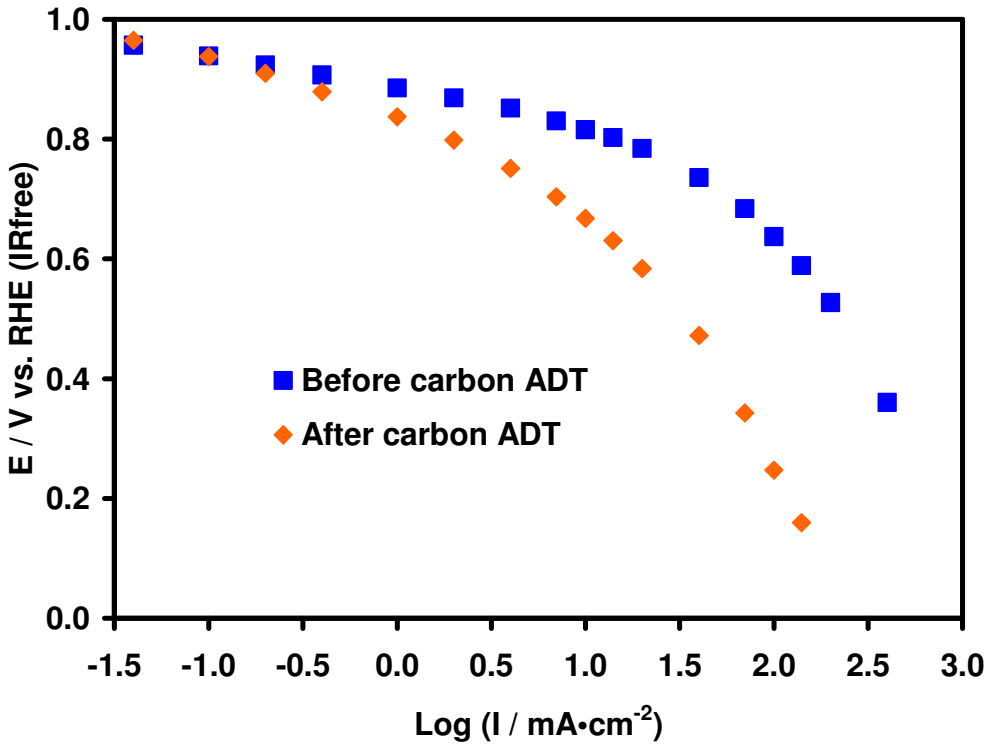

Fig. 7.7 Effect of electrode holding at 1.2 V for 24 hrs on the polarization behaviour for the oxygen reduction of the 50% PtCo/KB 8C-Cl. 0.1 M H_2SO_4; 75 °C; puro O_2.

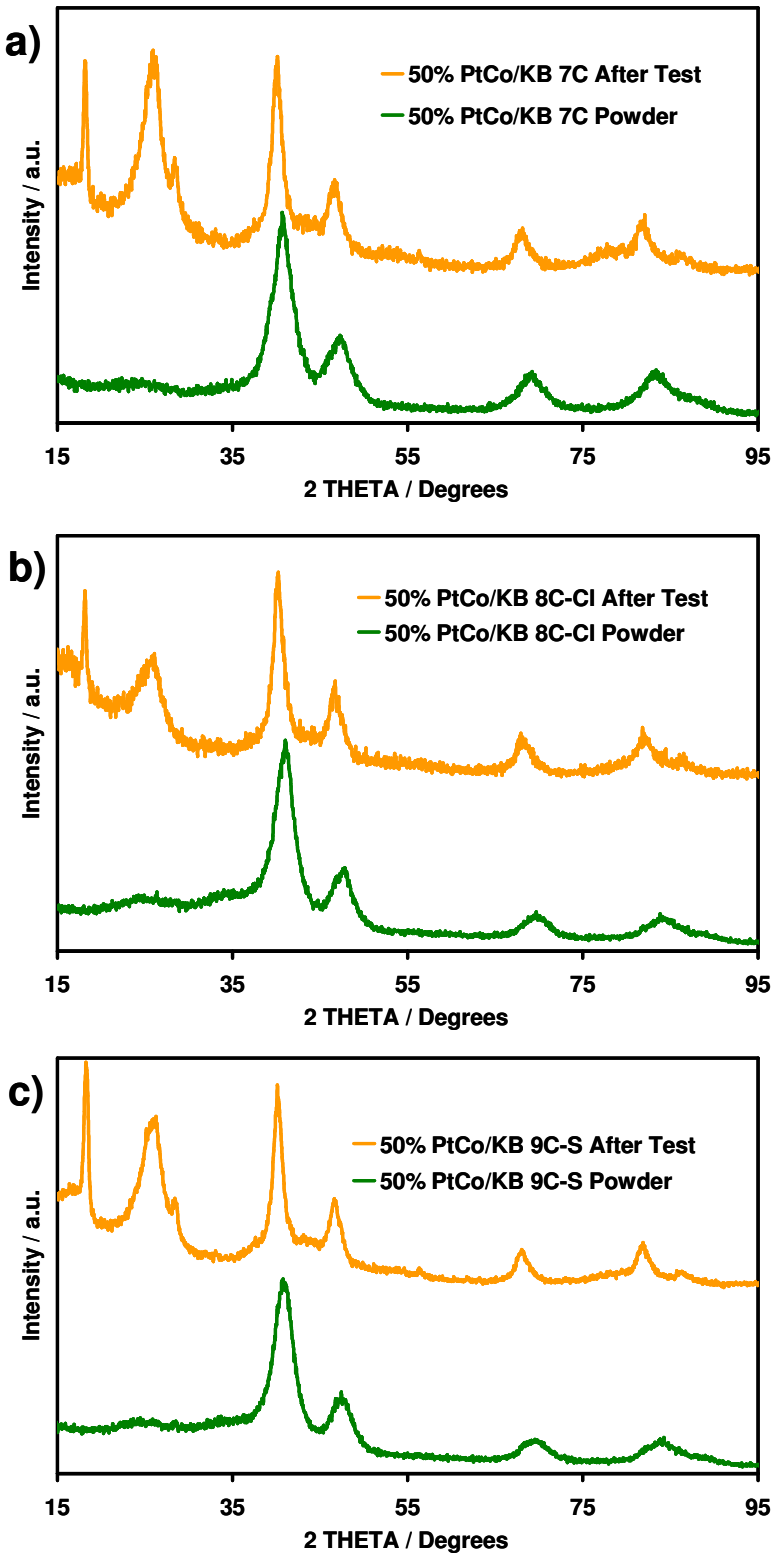

Fig. 7.8 XRD diffraction for 2nd series of PtCo catalysts after the Pt accelerated degradation test. a) 50% PtCo/KB 7C; b) 50% PtCo/KB 8C-Cl; c) 50% PtCo/KB 9C-S.

An XRD analysis was carried out on the different catalytic layers after the Pt degradation tests (Fig. 7.8 a-c). The diffraction patterns show that the catalyst pre-leached in perchloric acid (see Fig. 7.8 b) is more stable with respect to the unleached catalyst and that pre-leached in sulphuric acid (see Fig. 7.8 c). These show a larger growth of the particle size as compared to the catalyst leached in perchloric acid (Table 2.1). Such effect is usually due to the Ostwald ripening mechanism involving Pt dissolution at small particles and reprecipitation on large particles [2].

After the carbon corrosion tests the increase of particle size due to the sintering effects was about the same for all catalysts (Table 7.1). A partial dealloying occurs during carbon degradation tests as revealed by a shift of the diffraction peaks to low Bragg angles with respect to the fresh catalyst (not shown). As opposite of potential cycling, the degradation after carbon corrosion for the Pt catalyst was slightly lower than the PtCo catalysts. This was confirmed by a lower sintering effect for the Pt/C after the carbon corrosion test (Table 7.1).

Table 7.1 Gas-fed half cell ADTs result.

2nd series catalysts: degradation in sulphuric acid half cell

Catalyst	Potential Loss after Pt ADT (mV @ 1mAcm^{-2})	Potential Loss after C ADT (mV @ 1mAcm^{-2})	Particle Size after Pt ADT (nm)	Particle Size after C ADT (nm)
50% PtCo/KB 8C-Cl	≈ 0	50	4.5	6.7
50% PtCo/KB 9C-S	80	60	4.8	7.1
50% Pt/KB 4C	48	43	7.5	4.0
50% PtCo/KB 7C	≈ 10	55	5.0	7.0

An interesting in-situ leaching procedure has been recently reported for a carbon supported Pt-Cu-Co ternary alloy electrocatalyst [5]. The increase of mass activity for the partially dealloyed catalyst over a benchmark Pt/C catalyst was about fivefold in rotating disk and threefold in single cell studies [5]. In the latter case, the measured surface area was about 1.5 larger for the dealloyed catalyst than Pt. In the present case, we have compared PtCo and Pt catalysts with similar particle size (2.7 – 2.9 nm) and electrochemically active surface area (~ 55 m^2/g). The catalytic activity increase in the range 0.9 – 0.8 V passing from Pt to the PtCo catalyst preleached in $HClO_4$ was about

60%. Although, this enhancement is lower than that observed for alternative alloys [5], it appears that the ex-situ preleaching procedure here reported is promising for practical applications since it does not require an in-situ electrochemical activation step.

7.3 Conclusions

Accelerated degradation tests in sulphuric acid gas-fed half cell were carried out in order to investigate the influence of different pre-leaching treatments on the electrochemical behaviour. These analyses showed that the particle size of all catalysts increased after the tests. It was observed that after the Pt degradation test, the $HClO_4$ pre-leached catalyst showed the best performance in terms of electrochemical activity and resistance to sintering. The H_2SO_4 pre-leached catalyst showed a significant decrease in performance either before and after Pt degradation test. This behaviour was possibly due to a poisoning effect of sulphate adsorption in concentrated solution.

The carbon corrosion tests showed a similar behaviour for all first and second series PtCo catalysts. The carbon corrosion plays the major role on the degradation of the PtCo catalyst as compared to the Pt catalyst. In order to get a further increase in stability for the PtCo system, it would be necessary to replace the Ketjenblack with a more stable support. In this regard, several advancements have been achieved in the last years [6]. Among the new supports, particular interest is addressed to carbon nanotubes and Ti suboxides.

References

1. K. Kinoshita, Electrochemical Oxygen Technology, Wiley, New York, 1992.
2. A.S. Aricò, A. Stassi, E. Modica, R. Ornelas, I. Gatto, E. Passalacqua, V. Antonucci, J. Power Sources, 178 (2008) 525.
3. S.C. Ball, S.L. Hudson, D. Thompsett, B. Theobald, J. Power Sources, 171 (2007) 18.
4. M. Cai, M.S. Ruthkosky, B. Merzougui, S. Swathirajan, M.P. Balogh, J. Power Sources, 160 (2006) 977.
5. R. Srivastava, P. Mani, N. Hahn, P. Strasser, Angew. Chem. Int. Ed., 46 (2007) 8988.
6. T. Ioroi, Z. Siroma, N. Fujiwara, S. Yamazaki, K. Yasuda, Electrochem. Commun. 2005, 7, 183.

List of publications and conferences related to the thesis

During the period of my thesis, I have produced the following publications:

1. S. Siracusano, V. Baglio, A. Di Blasi, N. Briguglio, A. Stassi, R. Ornelas, E. Trifoni, V. Antonucci, A.S. Aricò; "*Electrochemical characterization of single cell and short stack PEM electrolyzers based on a nanosized IrO_2 anode electrocatalyst*"; International Journal of Hydrogen Energy 35 (2010): 5558-5568.
2. V. Baglio, A. Stassi, F.V. Matera, H. Kim, V. Antonucci, A.S. Aricò; "*AC-Impedance Investigation of Different MEA Configurations for Passive-Mode DMFC Mini-Stack Applications*"; Fuel Cells 10 (1) (2010): 124-131.
3. A.M. Castro Luna, A. Bonesi, W. E. Triaca, A. Di Blasi, A. Stassi, V. Baglio, V. Antonucci, A. S. Aricò; *"Investigation of a Pt–Fe/C catalyst for oxygen reduction reaction in direct ethanol fuel cells"*; Journal of Nanoparticle Research 12 (2010): 357-365.
4. F. Lufrano, V. Baglio, P. Staiti, A. Stassi, A.S. Aricò, and V. Antonucci; "*Investigation of sulfonated polysulfone membranes as electrolyte in a passive-mode direct methanol fuel cell mini-stack*"; Journal of Power Sources (2009) in press; DOI 10.1016/j.jpowsour.2009.11.130.
5. S. Siracusano, A. Stassi, V. Baglio, A.S. Aricò, F. Capitanio, A.C. Tavares; *"Investigation of carbon supported Pt and PtCo catalysts for oxygen reduction in direct methanol fuel cells"*; Electrochimica ACTA 59 (2009): 4844-4850.
6. A. Stassi, E. Modica, V. Antonucci, A.S. Aricò; *"A half cell study of performance and degradation of oxygen reduction catalyst for application in low temperature fuel cells";* Fuel Cells 09 (3) (2009): 201-208.
7. V. Baglio, A. Stassi, F.V. Matera, V. Antonucci, A.S. Aricò; *"Investigation of passive DMFC mini-stacks at ambient temperature"*; Electrochimica ACTA 54 (2009): 2004-2009.
8. V. Baglio, A. Stassi, F.V. Matera, A. Di Blasi, V. Antonucci, A.S. Aricò; *"Optimization of properties and operating parameters of a passive DMFC mini-stack at ambient temperature"*; Journal of Power Sources 180 (2008): 797-802.

9. A.S. Aricò, A. Stassi, E. Modica, R. Ornelas, I. Gatto, E. Passalacqua, V. Antonucci; *"Performance and degradation of high temperature polymer electrolyte fuel cell catalysts";* Journal of Power Sources 178 (2008): 525–536.
10. V. Baglio, A. Stassi, A. Di Blasi, C. D'Urso, V. Antonucci, A. S. Aricò; *"Investigation of bimetallic Pt-M/C as DMFC cathode catalysts"*; Electrochimica ACTA 53 (2007): 1360-1364.
11. G. Garcia, V. Baglio, A. Stassi, E. Pastor, V. Antonucci, A.S. Aricò; *"Investigation of Pt-Ru nanoparticle catalysts for low temperature methanol electro-oxidation"*; Journal of Solid State Electrochemistry 11 (2007): 1229-1238.
12. A. Stassi, A.S. Aricò, V. Baglio, C. D'Urso, A. Di Blasi, V. Antonucci, A.M. Castro Luna, A. Bonesi, W.E. Triaca; "*Electrocatalytic behaviour for oxygen reduction reaction of small nanostructured crystalline bimetallic Pt-M supported catalysts"*; Journal of Applied Electrochemistry 36 (2006): 1143-1149.
13. V. Baglio, A.S. Aricò, A. Stassi, C. D'Urso, A. Di Blasi, A.M. Castro Luna, V. Antonucci; *"Investigation of Pt–Fe catalysts for oxygen reduction in low temperature direct methanol fuel cells"*; Journal of Power Sources 159 (2006): 900–904.

I have contributed to the following proceedings:

1. S. Specchia, U.A. Icardi, C. Spinella, V. Baglio, C. D'Urso, A. Stassi, V. Antonucci, A.S. Aricò, G. D'Arrigo; "*Planar structure μDMFCs*"; ECS Transaction, 17 (1) (2009): 485-489
2. R. Ornelas, A. Stassi, E. Modica, A.S. Aricò, V. Antonucci; *"Accelerated degradation tests for Pt/C catalysts in sulfuric acid"*; ECS Transactions 3 (1) (2006): 633-641
3. A.S. Aricò, A. Stassi, E. Modica, R. Ornelas, I. Gatto, E. Passalacqua, V. Antonucci; *"Evaluation of high temperature degradation of Pt/C catalysts in PEM fuel cells"*; ECS Transactions 3 (1) (2006): 765-774.
4. A. Di Blasi,V. Baglio, A. Stassi, C. D'Urso, V. Antonucci, A.S. Aricò; *"Composite polymer electrolyte for direct ethanol fuel cell application"*; ECS Transactions, 3 (1) (2006): 1317-1323.

Moreover, I have contributed to the following conferences:

1. A.S. Aricò, V. Baglio, A. Stassi, V. Antonucci; *"Investigation of a Passive DMFC Mini-stack at Ambient Temperature";* CIMTEC 2010 5th Forum on New Materials, Montecatini Terme, Italy, June 2010.
2. G. Monforte, M. Lo Faro, A. Stassi, M. Minutoli, V. Antonucci, A.S. Aricò; *"A Novel Anode Based on Ni-Doped Perovskite for Direct Alcohol Solid Oxide Fuel Cells"* CIMTEC 2010 5th Forum on New Materials, Montecatini Terme, Italy, June 2010.
3. D. Sebastián, M.J. Lázaro, I.Suelves, R.Moliner, A. Stassi, V. Baglio, E. Modica, A.S. Aricò; "*Durabilidad de electrocatalizadores soportados sobre nanofibras de carbono"* ; CONAPPICE 2010 IV Congreso Nacional de Pilas de Combustible, Sevilla, Spain, June 2010.
4. M.J. Lázaro, D. Sebastián, A. Stassi, V. Baglio, A.S. Aricò, I. Suelves, R. Moliner; *"Optimized carbon nanofibers as catalyst support: effect of carbon properties on the fuel cell performance"*; CESEP'09 Carbons for Energy Storage and Environment Protection, Malaga, Spain, October 2009.
5. F. Lufrano, V. Baglio, P. Staiti, A. Stassi, A. S. Aricò, V. Antonucci; *"Sulfonated Polysulfone Membranes as Electrolytes in a Passive-mode Direct Methanol Fuel Cell Mini-stack Operating at Room Temperature"*; Spring Meeting of the European Mareials Research Society, Strasbourg, France, June 2009.
6. V. Baglio, A. Stassi, F. Matera, H. Kim, V. Antonucci, A. Aricò; *"AC Impedance Study to Evaluate the MEA Characteristics in a Passive Mode DMFC Ministack";* 215th Meeting of the Electrochemical Society, San Francisco, California, May 2009.
7. A.S. Aricò, A. Stassi, I. Gatto, E. Passalacqua and V. Antonucci; *"Surface Properties of PEMFC Catalysts and their Influence on High Temperature Performance and Degradation"*; 215th Meeting of the Electrochemical Society, San Francisco, California, May 2009.
8. S. Specchia, U.A. Icardi, C. Spinella, G. D'Arrigo, V. Baglio, C. D'Urso, A. Stassi, A. S. Aricò, V. Antonucci; *"Planar Structure Micro-DMFCs"*; Fuel Cell Seminar 2008, Phoenix, Arizona, October 2008.

9. A. Di Blasi, A. Stassi, V. Baglio, F. V. Matera, A. Di Blasi, V. Antonucci, A.S. Aricò; *"Investigation of Electrochemical Properties of a Passive DMFC Mini Stack"*; Fuel Cell Seminar 2008, Phoenix, Arizona, October 2008.
10. A. Stassi, V. Baglio, F. V. Matera, A. Di Blasi, V. Antonucci, A.S. Aricò; *"Electrochemical characterization of a passive monopolar DMFC mini-stack operating at room temperature";* Fuel Cell Science and Technology 2008, Copenhagen, Denmark, October 2008.
11. F.V. Matera, V. Baglio, A. Stassi, A. Di Blasi, V. Antonucci, A.S. Aricò; *"Design and characterization of passive DMFC monopolar ministacks for operation at room temperature"*; 17th World Hydrogen Energy Conference, Brisbane, Australia, June 2008.
12. A.S. Aricò, A. Stassi, E. Modica, R. Ornelas, I. Gatto, E. Passalacqua, V. Antonucci; *"Surface properties of high temperature polymer electrolyte fuel cell catalysts and their influence on performance and degradation"*; 3rd German-Italian-Japanese Meeting of Electrochemists, Taormina, Italy, May 2008.
13. Castro Luna A.M., Bonesi A., Triaca W., Di Blasi A., Stassi A., Baglio V. Aricò A.S., Antonucci V.; *"Investigation of Pt-M/C tolerance in presence of ethanol acid solution for the oxygen reduction reaction"*; 6th Spring Meeting of the International Society of Electrochemistry, Foz do Iguacu, Brazil, March 2008
14. Baglio V., Stassi A., Matera F.V., Di Blasi A., Antonucci V. Aricò A.S.; *"Investigation of a passive DMFC mini-stack operating at ambient temperature"*; 6th Spring Meeting of the International Society of Electrochemistry, Foz do Iguacu, Brazil, March 2008.
15. Aricò A.S., Stassi A., Modica E., Ornelas R., Gatto I., Passalacqua E., Antonucci V.; *"Electrochemical and physico-chemical investigation of polymer electrolyte fuel cell catalysts of high temperature operation"*; 6th Spring Meeting of the International Society of Electrochemistry, Foz do Iguacu, Brazil, March 2008.
16. Aricò' A.S., Stassi A., Modica E., Gatto I., Passalacqua E., Antonucci V.; *"Analisi delle proprietà elettrochimiche di catalizzatori per celle a combustibile ad elettrolita polimerico operanti ad alta temperatura"*; Gei Era 2007 – Giornate

dell'Elettrochimica Italiane – Elettrochimica per il Recupero Ambientale, Cagliari, Luglio 2007.

17. Aricò A.S., Stassi A., Modica E., Ornelas R., Gatto I., Passalacqua E., Antonucci V.; *"Performance and degradation of high temperature polymer electrolyte fuel cell catalysts"*; Polymer Batteries- Fuel Cells Conference, June 2007, Rome, Italy.
18. A. Stassi, V. Baglio, A. Di Blasi, C. D'Urso, V. Antonucci, A.S. Aricò; *"Low temperature preparation of Pt alloys with transition metal for oxygen electro-reduction in direct methanol polymer electrolyte fuel cells"*; Fuel Cell Seminar 2006, Honolulu, Hawaii, USA, November 2006.
19. A. Di Blasi, V. Baglio, A. Stassi, C. D'Urso, V. Antonucci, A.S. Aricò; *"Investigation of direct ethanol fuel cells based on composite polymer electrolytes"*; Fuel Cell Seminar 2006, Honolulu, Hawaii, USA, November 2006.
20. A. Di Blasi, V. Baglio, A. Stassi, C. D'Urso, V. Antonucci, A.S. Aricò, S. Licoccia, E. Traversa; *"Nafion-TiO2 composite DMFC membranes: Physico-chemical properties of the filler versus electrochemical performance"*; Fuel Cell Seminar 2006, Honolulu, Hawaii, USA, November 2006.
21. R. Ornelas, A. Stassi, E. Modica, A.S. Aricò, V. Antonucci; *"Accelerated degradation tests for Pt/C catalysts in sulfuric acid"*; 210th Meeting of the Electrochemical Society (ISE) Cancun, Mexico, October 2006.
22. E. Modica, P. Cretì, A.S. Aricò, A. Stassi, R. Ornelas, V. Antonucci; *"Preparation of nanosized platinum catalyst for PEM fuel cells"*; 210th Meeting of the Electrochemical Society (ISE) Cancun, Mexico, October 2006.
23. A.S. Aricò, A. Stassi, E. Modica, R. Ornelas, I. Gatto, E. Passalacqua, V. Antonucci; *" Evaluation of high temperature degradation of Pt/C catalysts in PEM fuel cells";* 210th Meeting of the Electrochemical Society (ISE) Cancun, Mexico, October 2006.
24. A. Di Blasi, V. Baglio, A. Stassi, C. D'Urso, V. Antonucci, A.S. Aricò; *"Composite polymer electrolyte for direct ethanol fuel cell application"*; 210th Meeting of the Electrochemical Society (ISE) Cancun, Mexico, October 2006.

ACKNOWLEDGEMENTS

I sincerely thank Dr. Antonino S. Aricò and Dr. Vincenzo Antonucci for their daily teaching, support, suggestion and critical evaluation on my work and my life.

I am grateful to Prof. S. Licoccia and Prof. E. Traversa for giving me the opportunity to attend to this PhD course in Materials for Environment and Energy at University of Rome "Tor Vergata".

I wish to thank Irene Gatto, Ester Modica, Rubens Ornelas and Enza Passalacqua for the synergic and kindly collaboration during the Autobrane project.

I acknowledge financial support from the European Community through the Autobrane project (FP6).

I am indebted to my double "office-wife" Laura Andaloro and Alessandra Di Blasi for their unconfinable friendship and graceful fault-finder bent.

I like mentioning here without distinction my special, past and present, colleagues of the PCE group for providing a stimulating and fun environment in which to learn and grow: Vincenzo Baglio, Pasquale Cretì, Tiziana Denaro, Claudia D'Urso, Maria Rita Girolamo, Daniela La Rosa, Massimiliano Lo Faro, Maurizio Minutoli, Giuseppe Monforte and Stefania Siracusano for their kind assistance, helpful and suggestion.

Special thanks to the wonderful team with distinction (I'm joking!): Nicola Briguglio, Giovanni Brunaccini, Giorgio Dispenza, Marco Ferraro, Giuseppe Napoli, Nico Randazzo and Francesco Sergi for the emotional time spent together inside and outside of the Institute.

I wish to thank my "chemistry family": Giacomo, Stefania, Mariagrazia, Antonio, Giampiero and Vittorio for providing anytime their boundless love.

Here I also take the opportunity to thank my entire family for their love and affection.

Last but not least thanks to all my close friends.